Lateral Torsional Buckling of Welded Wide Flange Beams

Md. Imran Kabir

A Thesis in
The Department of
Building, Civil and Environmental Engineering

Presented in Partial Fulfillment of the Requirements
for the Degree of Master of Applied Science (Civil Engineering)
at Concordia University, Montreal, Quebec, Canada

September 2016

CONCORDIA UNIVERSITY
School of Graduate Studies

This is to certify that the thesis prepared

By: Md. Imran Kabir

Entitled: Lateral Torsional Buckling of Welded Wide Flange Beams

and submitted in partial fulfillment of the requirements for the degree of

Master of Applied Science (Civil Engineering)

complies with the regulations of the University and meets the accepted standards with respect to originality and quality.

Signed by the final examining committee:

Dr. Ashutosh Bagchi *Chair*

Dr. Lucia Tirca *Examiner*

Dr. Ramin Sedaghati *Examiner*

Dr. Anjan Bhowmick *Supervisor*

Approved by _____
Chair of Department or Graduate Program Director

_____
Dean of Faculty

Date: _____

Abstract

Lateral Torsional Buckling of Welded Wide Flange Beams

Md. Imran Kabir

Lateral Torsional Buckling (LTB) can be defined as a combination of lateral displacement and twisting due to an application of load on an unsupported beam. Design specifications of Canada CSA S16-14 provides solutions for LTB of welded and rolled beams that were derived for constant moment situation. Same equations have been used over the years for design of rolled and welded shape beams. A recent study has shown that the current code equations might overestimate the capacity of the welded wide shape beams, which make them unsafe to use. Thus a detailed study is required to evaluate the existing LTB equations for welded wide flange (WWF) shapes. This thesis evaluates the performance of current equations in providing LTB capacities of WWF shape beams. A nonlinear finite element (FE) model is developed to investigate the LTB capacity of WWF shape beams. The validated FE model is used to analyze a series of simply supported WWF shape beams with varying unbraced lengths and subjected to equal end moments. Four different patterns of residual stresses and a constant initial imperfection of L/1000 are considered for the analysis. In total, 320 FE models are analyzed, and it is observed that current code overestimates the LTB capacity of WWF shape beams as much as of 37% mainly using the measured residual stress of Lehigh University.

Later, LTB capacity of WWF shape beams subjected to other loading configurations i.e. linear and non-linear moment gradient is investigated. Three types of linear moment gradient are considered i.e. end moment ratio of 0.5, 0.0, -1.0 while for non-linear moment gradient, two types of transverse loading i.e. concentrated load at mid span and uniformly distributed load along the length of the beam are considered in this research. In addition, for transverse loading, the effect of

load height is taken into account by changing the position of load at top flange, centroid and bottom flange. Thus, in total 123 and 228 FE models are developed for linear and non-linear moment gradient respectively. From the parametric study conducted for linear moment gradient, it is observed that current CSA S16-14 strength curve overestimates significantly for end moment ratio of 0.5 (40.1%) and 0.0 (34.57%) while it essentially coincides with FE results for end moment ratio of -1.0.

In the case of transverse loading, CSA S16-14 strength curve overestimates by 17% and 33% for concentrated load and distributed load respectively when the load is applied at the top flange of the beam. Unlike the top flange loading, CSA S16-14 strength curve underestimates by 64% and 44% for concentrated and distributed load applied at bottom flange respectively. However, in both cases, CSA S16-14 reasonably matches with the FE results when the load is applied at shear center of the cross-section. In addition, the mean value of equivalent moment factor, ω_2 provides good agreement with recommended values by CSA S16-14. In all cases, FE results are compared with other standards i.e. AISC, Eurocode as well as with latest equation proposed by the researchers in University of Alberta. Although, Eurocode is found to be conservative in every cases but proposed equation by the researchers at University of Alberta shows good agreement only in the case of unequal end moment and transverse loading condition. Hence, this equation can be used with a lower resistance factor for LTB strength calculation of WWF beams.

ACKNOWLEDGMENTS

It is a pleasure to convey my gratitude to numerous people who helped me in many ways for the last two years to complete my degree. Without their asistance, this thesis would not have been possible.

First and foremost, I owe my deepest gratitude to my supervisor Dr. Anjan Bhowmick for his continuous encouragement, support and guidance to pursue my graduate studies. It has been a privilege and an honor to work with and learn so many things from Dr. Bhowmick. Besides I would like to express his gratefulness for funding this research project by the Faculty of Engineering and Computer Science, Concordia University, Montreal, Canada and the Canadian Institute of Steel Construction (CISC). I would also like to gratefully acknowledge Dr. Gilbert Y. Grondin for his valuable suggestions in this project.

A special thanks goes out to my colleagues and friends especially Kallol Barua, Md. Anwar Us Sadat , Mrinmoy Nath and Manik Mia for their moral support and encouragement during my studies. Finally, I would like to thank my parents and brother whose sacrifice, financial support, and lifelong encouragement allowed me to accomplish many of my academic and personal goals.

CONTENTS

Abstract iii

ACKNOWLEDGMENTS v

LIST OF FIGURES x

LIST OF TABLES xii

List of Symbols xiii

List of Abbreviations xvi

Chapter 1 Introduction 1

1.1 General 1

1.2 Background 2

1.3 Motivation of this Research 5

1.4 Research Objectives 5

1.5 Scope and Limitations 6

1.6 Outline of the Research 7

Chapter 2 Literature Review 8

2.1 Introduction 8

2.2 Classical Lateral Torsional Buckling Solution 8

2.3 Design Approach of Different Standards 9

2.4 Factors Affecting Lateral Torsional Buckling 19

2.4.1 Residual Stress 19
2.4.2 Initial Imperfection 20
2.4.3 Effect of moment gradient 20
2.4.4 Effect of load with respect to the shear centre 21
2.4.5 Effect of supports and restraints 22
2.5 Detailed Review of Studies on Lateral Torsional Buckling of Welded Beams 23
Chapter 3 Finite Element Modeling 33
3.1 Introduction 33
3.2 Model Description 34
3.2.1 Elements and Mesh Configuration 34
3.2.2 Material Properties 36
3.2.3 Boundary Condition 37
3.2.4 Load Application 40
3.2.5 Analysis Type 41
3.2.6 Initial Geometric Imperfections 42
3.2.7 Residual Stress 46
3.3 Preliminary Validation 50
Chapter 4: Lateral Torsional Buckling of Laterally Unsupported WWF-beams Subjected to Uniform Moment 52
4.1 Introduction 52

4.2 Validation of Finite Element Model 53

4.3 Simulation Parameters 55

4.3.1 Sectional Dimension 55

4.3.2 Initial Imperfection 55

4.3.3 Residual Stress 56

4.3.3.1 Residual Stress Measured at Lehigh University 56

4.3.3.2 Residual Stress Measured by Fukumoto and Itoh (1981) 58

4.3.3.3 Residual Stress Measured by Dux and Kitipornchai (1983) 59

4.4 Sensitivity Analysis on Welded Beams 60

4.5 Summary 70

Chapter 5: Lateral Torsional Buckling of Laterally Unsupported WWF-beams Subjected to Linear and Non-linear Moment Gradient 72

5.1 Introduction 72

5.2 Evaluation of CSA Strength Curve for Welded Beams Subjected to Linear Moment Gradient 73

5.3 Validation of FE model for Non-linear Moment Gradient 77

5.3.1 Fukumoto et al (1980) 78

5.3.2 Fukumoto and Itoh (1981) 81

5.3.3 Dux and Kitipornchai (1983) 83

5.4 Evaluation of CSA Strength Curve for Welded Beams Subjected to Non-Linear Moment Gradient 85

5.4.1 Welded Beams Subjected to Concentrated Load at Mid-Span 86

5.4.2 Welded Beams Subjected to Uniformly Distributed Load 88

5.5 Equivalent moment factor, ω_2 for WWF-beams subjected to moment gradient 91

5.5.1 Equivalent moment factor, ω_2 for WWF-beams subjected to linear moment gradient 92

5.5.2 Equivalent moment factor, ω_2 for WWF-beams subjected to transverse loading 94

5.5.2.1 Welded Beams Subjected to Concentrated Load at Mid-Span 94

5.5.2.2 Welded Beams Subjected to Uniformly Distributed Load 95

Chapter 6 Conclusions and Recommendations 98

6.1 Summary 98

6.2 Conclusions 99

6.3 Recommendations for Future Work 104

REFERENCES 106

APPENDIX A 111

APPENDIX B 116

LIST OF FIGURES

Figure 1: Lateral torsional buckling 1

Figure 2: (a) The Marcy Pedestrian Bridge (Peraza, 2008), (b) Collapse of bridge girder at Edmonton, Canada 3

Figure 3: Different mode of LTB of beam 4

Figure 2.1: Moments at different position of a beam for any load configuration 11

Figure 3.1: Mesh Configuration of Finite Element Model 36

Figure 3.2: Boundary condition in finite element model 38

Figure 3.4: Longitudinal constraint for end points 40

Figure 3.5: Load Application in Finite Element Model 41

Figure 3.6: Sensitivity Analysis for initial geometric imperfection 44

Figure 3.7: Different eigen mode and associated state of failure for WWF-beams (half span only) 45

Figure 3.8: Maximum flange sweep of L/1000 for initial imperfection 46

Figure 3.9: Recommended residual stress pattern by ECCS (1984) 47

Figure 3.10: Contour map of applied residual stress in finite element model 48

Figure 3.11: Distribution of residual stress across (a) flange and (b) web from FE model 49

Figure 3.12: Effect of residual stress on LTB capacity of steel beams 50

Figure 3.13: Preliminary validation of finite element model 51

Figure 4.1: Comparison between Finite Element and Test Results 54

Figure 4.2: Residual Stress measured (a) mill plate and (b) flame cut type at Lehigh University 57

Figure 4.4: Residual Stress Measured by Fukumoto and Itoh (1981) 58

Figure 4.5: Residual Stress Measured by Dux and Kitipornchai (1983) 59

Figure 4.6: Simply Supported Beam with Equal End Moment 60

Figure 4.4. LTB resistance curves for various WWF-beams with different residual stress pattern 64

Figure 4.8: Finite element results vs CSA code values for (a) “Dux and Kiti”, (b) “Fuku and Itoh”, ... 67

(c) Mill Plate, (d) Flame Cut and (e) Zero type residual stress..... 67

Figure 5.1: Typical moment diagram for different moment gradient..... 73

Figure 5.2: Moment gradient LTB curves for (a) $\omega_2 = 1.3$, (b) $\omega_2 = 1.75$ and (c) $\omega_2 = 2.3$ 75

Figure 5.4: Test configuration and measured residual stress by Fukumoto et al (1980)..... 78

Figure 5.5: Load vs Deflection curve for 2.6 m long beam..... 80

Figure 5.6: Load vs Deflection curve for 2.0 m long beam..... 80

Figure 5.7: Load vs Deflection curve for 1.5 m long beam..... 81

Figure 5.8: Test configuration and measured residual stress by Fukumoto and Itoh (1981)..... 82

Figure 5.9: Test Loading Configuration 83

Figure 5.10: Simply supported beam under concentrated load at mid-span and uniformly distributed load acting at (a) (e) top flange, (b) (f) centroid, (c) (g) bottom flange, (d) typical moment diagram for concentrated load and (e) moment diagram for uniformly distributed load 85

Figure 5.11: CSA strength curve for LTB and FE results for concentrated load applied at (a) top flange, (b) centroid and (c) bottom flange 87

Figure 5.12: CSA strength curve for LTB and FE results for uniformly distributed load applied at (a) top flange, (b) centroid and (c) bottom flange..... 90

LIST OF TABLES

Table 2.1: Eurocode 3 LTB Curve Selection* 18

Table 2.2: Length factor for end support conditions..... 23

Table 2.3: Recommended k values for different end condition..... 23

Table 2.4: Comparison of Proposed and Current equation with test data 30

Table 4.1: Comparison of Finite Element Results with Test Results 54

Table 4.2: Details of Cross-section..... 55

Table 4.3: Finite Element Results and Comparison with CSA S16-14..... 68

Table 5.1: Mean values of material properties and comparison of FE result with test result..... 79

Table 5.2: Mean values of material properties and comparison of FE result with test result..... 83

Table 5.3: Dimension of test specimen and measured value of initial out-of- straightness 84

Table 5.4: Mean values of material properties and comparison of FE result with test result..... 84

Table 5.5: Equivalent moment gradient, ω_2 for linear moment gradient and comparison with CSA 93

Table 5.6: Equivalent moment gradient, ω_2 for concentrated load at mid-span 95

Table 5.7: Equivalent moment gradient, ω_2 for uniformly distributed load 96

List of Symbols

C_b^*	Modified equivalent moment factor
C_b	Moment gradient factor
C_w, I_w	Warping constant
F_y	Yield stress
h_o	Centre to centre distance between flanges
I_t	Torsion constant
I_y, I_z	Moment of inertia about weak axis,
k_l	Load height coefficient
k_r	Constant for weak axis restraint
k_t	Coefficient for end twist restraint
L_e	Effective span
L_p	Minimum unbraced length for attaining yielding of a member
L_u	Unbraced length of beam
M_b	Elastic buckling capacity of unbraced beam
M_{cr}	Critical lateral torsional buckling moment
M_{max}	Maximum moment capacity from test/finite element analysis
M_{max}	Absolute values of maximum moment
M_a	Absolute values of first quarter moment
M_b	Absolute values of second quarter moment
M_c	Absolute values of third quarter moment

M_n	Nominal moment capacity
M_p	Plastic moment
M_u	Moment derived from classical solution
M_y	Elastic resistance
P_{max}	Ultimate strength,
R_m	Coefficient for single curvature bending
r_{ts}	Effective radius of gyration
r_y	Radius of gyration about the y-axis
S_x	Elastic section modulus about the x-axis
W_y	Section modulus of a section
z_g	Distance between load application point and shear centre
Z_x	Plastic section modulus
α_m	Equivalent moment factor
α_s	Slenderness reduction factor
γ_{M1}	Partial safety factor for resistance to instability
$\bar{\lambda}_{LT}$	Non-dimensional slenderness parameter
ϕ_{LT}	Dimensionless parameter
d	Total depth of beam
E	Modulus of elasticity,
G	Shear modulus of elasticity,
J	Saint-Venant torsion constant
k, k_w	Effective length factors,

K_1	Factor for end fixity,
K_2	Factor for both lateral bending and warping restraint,
p	Magnitude of the concentrated load
y	Location of the applied load relative to the shear centre
β	End moment ratio
κ	Ratio of the absolute value of smaller factored moment and larger factored moment at ends of the unbraced length
λ	Modified slenderness ratio
Φ	Resistance factor
$\beta(le)$	Rotation about the longitudinal direction.
$\zeta(le)$	Displacement of the center of the cross-section along the longitudinal direction
$\eta(le)$	Displacement of the center of the cross-section along y axis (along the vertical direction)
$\xi(le)$	Displacement of the center of the cross-section along x axis (along the lateral direction)
C_1, C_2	Coefficients for loading and end restraint conditions.
ω_2	Uniform moment factor
$\bar{\lambda}_{LT,0}$	Corresponds the maximum resistance value of a given section at a plateau level
β	Constant for the shape of the strength curve

List of Abbreviations

AASHTO	American Association of State Highway and Transportation Officials
AISC	American Institute of Steel Construction
AS	Australian Standard
CISC	Canadian Institute of Steel Construction.
COV	Coefficient of Variation
CSA	Canadian Standards Association
EC	Euro Code
ECCS	European Convention for Constructional Steelwork
FE	Finite Element
FEA	Finite Element Analysis
LTB	Lateral Torsional Buckling
SSRC	Structural Stability Research Counsil
UDL	Uniformly Distributed Load
WWF	Welded Wide Flange

Chapter 1 Introduction

1.1 General

Several limit states are taken into account while designing a steel beams which includes the ultimate flexural limit states of local buckling, full section yielding, inelastic and elastic lateral torsional buckling. In addition to this failure in shear, yielding or buckling under concentrated loads, fatigue limit states and serviceability considerations for deflection and vibration need to be checked during design. Among these limit states, lateral torsional buckling (LTB) is a state of buckling where a member exhibits both lateral deflection and twisting as shown in Fig.1.

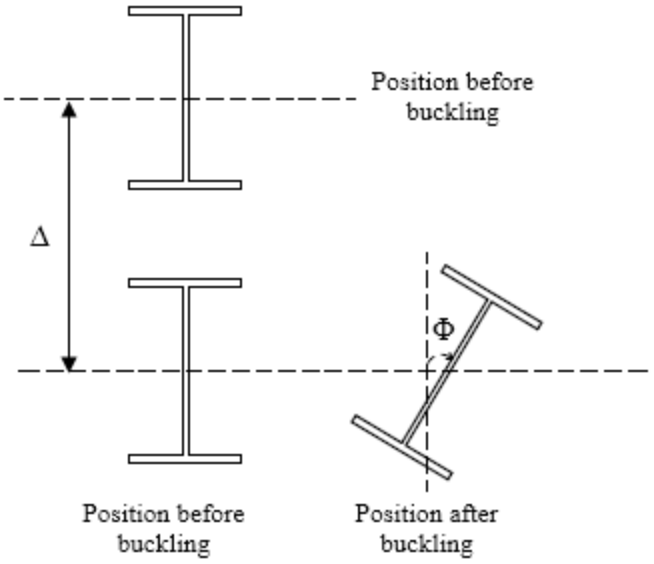

Figure 1: Lateral torsional buckling

Each steel specification has its own way of determining the strength of a steel beam that undergoes LTB and CAN/CSA is not exception to this. CAN/CSA follows same beam design formulas for both W-beams and WWF-beams and provides the flexural capacity of these members considering equal moment applied to the ends of a simply supported beam. Additionally, it recommends an equivalent moment factor for other loading configuration. However, several experimental test

results confirmed substantial reduction in flexural capacity of a welded beam due to the presence of high amount of residual stress generated from welding action. Thus, this research investigates the LTB behavior of WWF-beams in detail as well assess the performance of the current Canadian provision of determining the LTB capacity in case of WWF-beams considering various types of loading configuration. Moreover, results from finite element (FE) analysis are compared with other standards, for example AISC and Eurocode, as well as with latest equation proposed by the researchers at University of Alberta. The following sections provide the background of the research and thus delineates the motivation of this investigation. The objectives and scopes of this research are also outlined in Sections 1.4 and 1.5 respectively. An overview of the thesis contents and research investigation process is then presented in Section 1.6.

1.2 Background

Beams are frequently used in many structures in various shapes and sizes mainly because of its capability of withstanding loads by resisting bending and shear. Different types of steel sections are being produced and practiced by the designers since many years; however, I-sections are considered most popular to be chosen as a beam. Usually flexural member such as beams and girders have much greater strength about the major axis compared to minor axis. As a result of this, laterally unsupported beams and girders might fail by lateral-torsional buckling before the attainment of its full in-plane capacity. Thus, lateral torsional buckling (LTB) can be considered as a limit state of structural design where the deformation changes suddenly from in-plane bending to combined lateral deflection and twisting (Ziemian 2010). The final failure pattern involves lateral deflection and twisting in combination with various extents of yielding and flange and/or web local buckling depending on the specific member characteristics (Ziemian 2010). The consequences of such kind of premature failure is devastating particularly if it occurs during the

construction phase i.e. collapse of Marcy pedestrian bridge at New York in 2002, damage of steel bridge girder at Edmonton, Canada in 2015. Therefore, it is very important to understand and investigate the behaviour of structures and ensuring the structural stability of its members as a whole.

(a) (b)

Figure 2: (a) The Marcy Pedestrian Bridge (Peraza, 2008), (b) Collapse of bridge girder at Edmonton, Canada

Since the mid-nineteenth century, research has been performed intensively on lateral torsional buckling of beams and reported in several text books (Bleich, 1952; Timoshenko and Gere, 1961; Vlasov, 1961; Galambos T. , 1968; Trahair 1993). However, the analytical procedure of obtaining LTB strength are complex and only for the simplest cases the closed form solutions can be found. Depending on this length behaviour of LTB can be divided into three parts such as (1) elastic buckling, (2) inelastic buckling and (3) plastic behaviour. The relationship between critical moment (Mcr) and unbraced length (L) for lateral-torsional buckling can be presented graphically as shown in Figure 3.

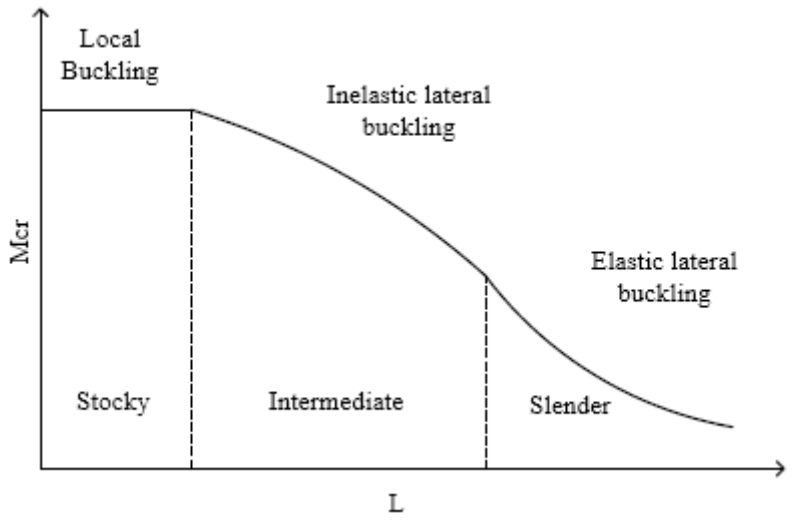

Figure 3: Different mode of LTB of beam

Different structural steel design standards (e.g., CAN-CSA S16-14 (2014), AISC-ANSI 360-10 (2010), AS 4100 (1998) , and Eurocode 3 (2005)) provide different algebric equations for estimating the LTB resistance. However, in a general sense, all of them use similar approach: staring from the calculation of elastic LTB resistance M_u and followed by a reduction of this theoretical resistance by considering various factors such as geometric imperfections, local and/or distorsional buckling, residual stress etc. (Ziemian 2010). Depending on the variables considered, nominal resistance for LTB varies considerably from statndard to standard. Australian and the European standards, AS 4100 and EC 3, provide a substantial penalty for geometric imperfections (Ziemian 2010). Another important difference between Eurocode 3 and other standards is Eurocode 3 provides two different strength curves for rolled and welded section. However, two North American standards AISC 2010 and CSA S16-14 implicitly assume that the beam has no initial out-of-straightness for long members that fail by elastic LTB (Ziemian 2010). Moreover, both AISC 2010 and CSA S16-14 make no distinction between rolled and welded beams.

1.3 Motivation of this Research

Current CSA S16-14 provisions do not make any distinction between welded and rolled shapes when dealing with the flexural strength. However, difference in behavior between these two shapes had been observed as well as the adverse effects of geometric imperfection (i.e. residual stress due to welding and initial out of straightness) had been identified by several test results. Moreover, a recent reliability study by MacPhedran and Grondin (2011) showed that current provision might overestimate the capacity of welded beams when compared against the test results of Greiner and Kaim (2001). Thus, the findings from this investigation created the motivation for a closer evaluation of the current CSA S16-14 strength curves for design of WWF-beams.

1.4 Research Objectives

The investigation of this research aims to evaluate the performance of CSA S16-14 strength curve in case of WWF-beams that undergoes lateral torsional buckling (LTB). Thus, the main objective of this research is to assess the effect of welding type residual stress on the capacity of such beams before failure using finite element analysis. Towards this goal, the key objectives are as follows:

- To investigate the LTB behavior of WWF-beams at different regions of buckling. It is done by developing a detailed finite element (FE) model that is capable of simulating accurate behavior of steel beams. The FE model is validated against four experimental test in this study.
- To investigate effects of residual stress and initial imperfection on capacity of WWF shape beams. This is done by performing a detailed sensitivity analysis considering varying unbraced lengths of several WWF-beams subjected to uniform moment gradient.
- To investigate the performance of current approach of estimating LTB capacity for other loading configuration (i.e. unequal end moment, transverse loading)

- To investigate the effect of load height with respect to shear center on LTB resistance of WWF-beams.
- To assess the performance of the equations currently used to determine equivalent moment gradient factor of WWF-beams. This is done by comparing the FE results with current recommended values in the code.
- Finally, to evaluate the current equations in different codes for design of WWF beams against LTB.

1.5 Scope and Limitations

There are several factors that affect the LTB capacity of a beam i.e. support condition, loading configuration, unbraced length, residual stress, initial out-of-straightness, etc. and thus make this research field broader. However, effect of welding type residual stress is more pronounced in inelastic range of LTB. Therefore, simply supported WWF-beams are considered subjected to several loading configuration i.e. equal end moment, unequal end moment, transverse loading of varying unbraced length with a constant initial out-of-straightness Both elastic and inelastic behavior of LTB are captured in this study. In spite of these, there are some limitations of this research which are as follows:

- Residual stresses are limited to those characteristic pattern as measured in several experiments and reported in literature.
- Sensitivity analysis is done considering a fixed initial out-of-straightness i.e. L/1000
- Class 1 and Class 2 WWF-beams are analyzed in this investigation.
- All the analyses are performed considering support at centroid of section.

1.6 Outline of the Research

This first chapter presented a short background on the importance of steel beam design and the failure mode of LTB. The scope of the investigation was discussed along with the objectives of this study.

Chapter 2 presents the literature review conducted for this study. It describes the fundamental solution of LTB as well as the contributing factors of this failure mode. A detailed discussion on the guidelines followed for beam design by four steel specifications is also presented. A brief description of previous experimental work and finite element modelling relating LTB are discussed.

Chapter 3 discusses the key assumptions and consideration made for the development of FE model in detail. It also shows a preliminary validation of FE model with code results.

Chapter 4 presents and discusses the sensitivity analysis conducted on WWF-beams considering various levels of residual stresses and initial imperfections.

Chapter 5 presents and evaluates the performance of CSA S16-14 resistance equation for different moment gradient. In addition, this chapter includes the effect of loading height on LTB capacity. Evaluation of equivalent moment gradient factor for WWF-beams concludes this chapter.

Chapter 6 concludes the thesis with a summary of the conclusions gathered throughout this study as well as recommendations for future work.

Chapter 6 is followed by appendices, which include the derivation of the elastic critical moment and FE analysis results.

.

Chapter 2 Literature Review

2.1 Introduction

The literature review in this chapter consists four parts. The general background of classical lateral torsional buckling solution is presented in Section 2.2 while section 2.3 provides a summary of the lateral torsional buckling design provisions in various standards. A brief discussion on different parameter i.e. residual stress due to welding, initial imperfection, moment gradient, load height effect, etc. which affects lateral torsional buckling capacity of a structural member is then presented in Section 2.4. A detailed review of previous studies on lateral torsional buckling of welded beams in section 2.5 concludes this chapter.

2.2 Classical Lateral Torsional Buckling Solution

In order to determine the lateral torsional buckling capacity of beams, different structural steel design standards (e.g., CAN-CSA S16-14 (2014), AISC-ANSI 360-10 (2010), AS 4100 (1998), and Eurocode 3 (2005)) provide different algebraic equations. However, in a general sense, all of them start with calculating the elastic LTB resistance M_u of a simply supported beam under uniform moments. The expression of classical lateral torsional buckling for determining the critical moment M_u is as follows,

$$M_u = \frac{\pi}{L_u}\sqrt{EI_yGJ + \left(\frac{\pi E}{L_u}\right)^2 I_y C_w} \qquad [2.1]$$

in which, M_u is the elastic moment, L_u is unbraced length of the beam, E is the modulus of elasticity, I_y is moment of inertia in weak axis, G is shear modulus of elasticity, J is Saint-Venant torsion constant and C_w is warping constant. This close formed buckling solution is well established by (Timoshenko and Gere, 1961) under the assumptions that both ends of the beam are

prevented from lateral deflection ($u=0$) and from twisting ($\varphi=0$), but they are free to rotate laterally ($u''=0$) and the end cross section is free to warp ($\varphi''=0$). However, these assumptions are based on the Vlasov theory assumptions (Vlasov 1961), i.e., throughout deformation 1) any cross-section acts as a rigid disc within its plane, and 2) shear strains within the middle surface of the beam are considered negligible. The derivation of this classical equation is shown in APPENDIX A.

The standards then apply various reduction factors to the expression to obtain the nominal resistance of the physical member according to other forms of loading and boundary conditions including other factors such as geometric imperfections, local and/or distortional buckling, residual stress, etc. (Ziemian 2010). Another significant difference between Eurocode 3 and other standards including two North American standards is Eurocode 3 provides two different strength curves for rolled and welded section. Moreover, two North American standards AISC 2010 and CSA S16-14 implicitly assume that the beam has no initial out-of-straightness for long members that fail by elastic LTB. (Ziemian 2010). In this context, a key objective of this thesis is to assess the implications of CSA S16-14 for welded wide flange beams. Towards this goal, Chapter 4 presents a detailed study on the effect of welding-type residual stress on LTB capacity of the beam. In addition, Chapter 5 reveals the impact of other factors on the performance of current guidelines of Canadian standards.

2.3 Design Approach of Different Standards

Usually, a flexural member such as beams and girders have a much greater strength about the major axis compared to the minor axis. As a result of this, laterally unsupported beams and girders might fail by lateral-torsional buckling before the attainment of their full in-plane capacity.

Therefore, lateral torsional buckling can be considered as a limit state of structural design and is governed by one of three possible modes of failure. These are 1) elastic lateral torsional buckling, 2) inelastic lateral torsional buckling, and 3) yielding of the cross-section. The standards studied in this section (CAN/CSA S16-14, ANSI/AISC 360-10, AS4100-1998, and EN 1993-1-1:2005) follow different methods to determine the resistance of a beam under each failure mode.

However, all of them use the classical lateral torsional buckling solution Eq. [2.1] for the elastic lateral torsional buckling mode, as a starting point to achieve the critical moment for a simply supported beam subjected to uniform moments. To take account, the effect of non-uniform moment distributions, each of the standards follows different ways to calculate the equivalent moment gradient factors. The moment gradient factors in the various standards fall into one of two categories, based on either 1) the ratio of end moments for linear moment distributions, or 2) moments at quarter span points of the beam for more general moment distributions.

The first category of methods is used to calculate the equivalent moment gradient factor of beams subjected to unequal end moments only. This equation was developed by Salvadori in 1955 using the Rayleigh- Ritz method to determine interaction curves for I-beams simply supported in the weak plane under thrust and unequal end moments (Salvadori, 1955). The moment gradient factor C_b can be represented by a general expression as shown in Equation 2.2

$$C_b = 1.75 + 1.05\kappa + 0.3\kappa^2 \leq 2.3 \qquad [2.2]$$

where the term κ is the ratio of the absolute value of smaller factored moment and larger factored moment at ends of the unbraced length and is taken as positive and negative for double curvature and single curvature respectively.

The second category of methods, developed by Kirby et al. (1979) is more versatile and is applicable to calculate a moment gradient factor for any moment distributions. The proposed equation by Kirby et al. (1979) can be expressed as follows.

$$C_b = \frac{12\ M_{max}}{2\ M_{max} + 3M_A + 4M_B + 3M_C} \qquad [2.3]$$

Equation 2.3 is known as the quarter-point method, where M_{max} , M_a , M_b , M_c represent absolute values of maximum, first, second and third quarter moment along the unbraced length of a section for a given load configuration, as shown in figure 2.1.

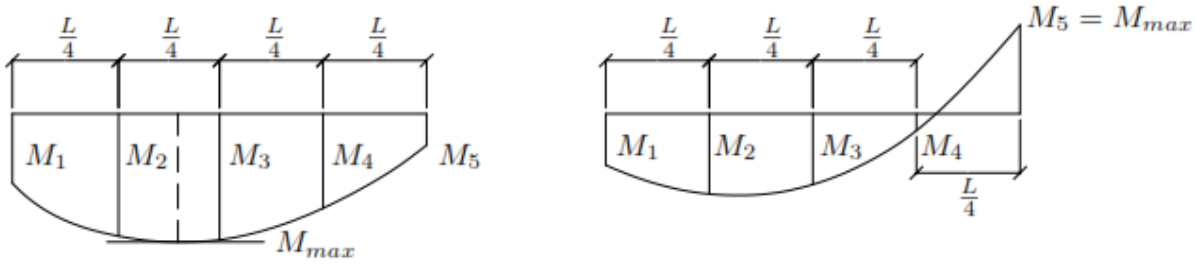

Figure 2.1: Moments at different position of a beam for any load configuration

Considering the yielding strength of beams, all standards divides beam cross-sections into three distinct parts: 1) those that are thick enough (compact) to attain their plastic resistance prior undergoing buckling, 2) those of moderate thickness (or non-compact) and thus exhibit local buckling after achieving their yield moment strength but before developing their plastic moment resistance, and 3) those that are too thin (slender) to develop their yield moment capacity prior exhibiting local buckling (Rusul 2013). However, each standard uses their set of names for recalling the classes or categories. For example, while the ANSI/AISC 360-10 and AS 4100-1998 use the terms Compact/ Non-Compact/Slender, the equivalent terms in CAN/CSA S16-14 and EN 1993-1-1:2005 are Class 1 or 2/Class 3/ Class 4. In all design standards, the inelastic lateral

torsional buckling resistance of a member is determined using the specified equations by corresponding design standard which mainly depends upon on both flexural yield strength and elastic lateral torsional buckling resistance of the member.

CAN/CSA S16-14

To determine the flexure-resistance for a laterally unsupported beam of doubly symmetric cross-sections, CAN/CSA S16-14 provides the following procedure.

Based on the section class, the yield resistance of a member is taken either equal to the plastic moment $M_p = Z_x F_y$ or the elastic resistance $M_y = S_x F_y$, in which Z_x and S_x are the plastic and elastic section modulus taken about the x-axis respectively, and F_y is the specified minimum yield stress while the elastic critical lateral torsional buckling moment is determined by multiplying the classical lateral torsional buckling moment for the case of the uniform moment as determined from Eq. [2.1] by a moment gradient factor ω_2 given by,

$$M_{cr}=\omega_2 M_u= \omega_2 \frac{\pi}{L_u}\sqrt{EI_y GJ+\left(\frac{\pi E}{L_u}\right)^2 I_y C_w} \qquad [2.4]$$

The Canadian CAN/CSA S16-14 Standard allows designers both of the methods for determining the moment gradient factor ω_2. The general equation provided to obtain moment gradient factor for any moment distribution is a quarter point method which was introduced by Wong and Driver (2010). The solution is given as

$$\omega_2 = \frac{4\,M_{max}}{\sqrt{{M_{max}}^2+4\,{M_a}^2+7{M_b}^2+4{M_c}^2}} \leq 2.5 \qquad [2.5]$$

where M_{max}, M_a, M_b, M_c represent absolute values of maximum, first, second and third quarter moment along the unbraced length of a section for a given load configuration. The standard also supports the use of the solution as shown in Eq. 2.2. However, it gave very conservative results for many common cases (Driver et al., 2010). Therefore, in CAN/CSA S16-14, a slightly higher value of 2.5 is suggested as an upper limit, i.e.,

$$\omega_2 = 1.75 + 1.05\kappa + 0.3\kappa^2 \leq 2.5 \quad [2.6]$$

If $M_{cr} < 0.67\, M_p$ for Class 1 or 2 sections or $M_{cr} < 0.67\, M_y$ for Class 3 sections, the nominal resistance of the member will be referred to elastic lateral torsional buckling as determined by,

$$M_r = \Phi M_{cr} \quad [2.7]$$

in which Φ is a resistance factor and taken as 0.9. If $M_{cr} > 0.67\, M_p$ for Class 1 or 2 sections or $M_{cr} > 0.67\, M_y$ for Class 3 sections, the nominal resistance of the member will be referred to inelastic lateral torsional buckling or full plastic capacity as determined by,

$$M_r = \Phi 1.15 M_p \left(1 - \frac{0.28 M_p}{M_{cr}}\right) \leq \Phi\, M_p \quad [2.8]$$

while for Class 3 sections, M_p is replaced by M_y in Equation 2.8 to determine the resistance capacity of a particular section.

ANSI/AISC 360-10

ANSI/AISC 360-10 provides a resistance calculation method by which the LTB resistance curve is clearly divided into three distinct part. It uses two limiting spans L_p and L_r to fix the failure mode where the span L_r

$$L_r = 1.95 r_{ts} \frac{E}{0.7F_y} \sqrt{\frac{J}{S_x h_o} + \sqrt{\left(\frac{J}{S_x h_o}\right)^2 + 6.76\left(\frac{0.7F_y}{E}\right)^2}} \quad [2.9]$$

where h_o is centre to centre distance between flange and r_{ts} is the effective radius of gyration which can be calculated by the following expression,

$$r_{ts} = \frac{\sqrt{I_y C_w}}{S_x} \quad [2.10]$$

The minimum unbraced length for attaining yielding of a member, L_p is determined by

$$L_p = 1.76 r_y \sqrt{\frac{E}{F_y}} \quad [2.11]$$

in which r_y is the radius of gyration about the y-axis.

When $L_u > L_r$, where L_u is the unbraced length of the section, the failure mode of buckling is termed as elastic lateral torsional buckling which is calculated by the expression as follows.

$$M_n = C_b M_u = C_b \frac{\pi}{L_u} \sqrt{EI_y GJ + \left(\frac{\pi E}{L_u}\right)^2 I_y C_w} \leq M_p \quad [2.12]$$

where, C_b is the ANSI/AISC 360-10 moment gradient factor given by,

$$C_b = \frac{12.5\, M_{max}}{2.5\, M_{max} + 3M_A + 4M_B + 3M_C} \leq 3.0 \quad [2.13]$$

Eq. 2.13 is a slightly modified form of Eq. 2.3 which was proposed by Kirby and Nethercot (1979).

When $L_p < L_u < L_r$, the mode of failure is governed by inelastic lateral torsional buckling and the nominal moment capacity of beam is determined using the following equation 2.14

$$M_n = C_b \left[M_p - \left(M_p - 0.7 F_y S_x \right) \left(\frac{L_u - L_p}{L_r - L_p} \right) \right] \leq M_p \quad [2.14]$$

When $L_u < L_p$, the mode of failure is termed as fully yielded and the nominal moment capacity is determined by $M_n = Z_x F_y$ for compact section while $M_n = S_x F_y$ for non-compact sections.

AS 4100-1998

The Australian Standard AS 4100 (SAA, 1998) provides the following equation for the compact section to determine the nominal LTB resistance of structural member.

$$M_n = \alpha_m \alpha_s M_p \leq M_p \quad [2.15]$$

where M_p is the plastic moment capacity, that is, the moment capacity of a fully braced member, α_m is an equivalent moment factor, which is in concept similar to moment factor as calculated in CSA and AISC and is calculated by the following equation

$$C_{AUS} = \frac{1.7 M_{max}}{\sqrt{M_A{}^2 + M_B{}^2 + M_C{}^2}} \leq 2.5 \quad [2.16]$$

And α_s is termed to as the slenderness reduction factor and accounts for the reduction in strength due to the global slenderness of member. This parameter can be calculated from the next equation.

$$\alpha_s = 0.6 \left[\sqrt{\left[\left(\frac{M_p}{M_o} \right)^2 + 3 \right]} - \left(\frac{M_p}{M_o} \right) \right] \quad [2.17]$$

in which M_o is a slightly altered version of the classical lateral torsional buckling solution given by M_u as follows

$$M_o = \frac{\pi}{L_e}\sqrt{EI_yGJ + \left(\frac{\pi E}{L_e}\right)^2 I_y C_w} \qquad [2.18]$$

where, $L_e = k_t k_l k_r L_u$ is an effective span, k_t accounts for end twist restraint, k_l is a coefficient which considers the effect of load height with respect to the shear centre, k_r is a constant for weak axis restraint and L_u refers the length of the member. The values of all constants k_t, k_l, and k_r for general end restrains is given by AS 4100-1998.

EN 1993-1-1:2005

EN 1993-1-1 provides two methods such as the general case and the special case of determining the lateral buckling resistance of a beam. Unlike the general case, the special case is specifically used for rolled I-section beams and equivalent welded beams of standard dimensions. Regardless of the case, this code guides to determine the elastic lateral torsional buckling moment Mu for the case of the uniform moment as a starting point. But this standard does not provide any explicit equation for determining Mu. However, NCCI (2008) states the following formula 2.19 to calculate elastic critical moment which is derived from the buckling theory.

$$M_{cr} = C_1 \frac{\pi^2 EI_z}{(kL)^2}\left\{\sqrt{\left(\frac{k}{k_w}\right)^2 \frac{I_w}{I_z} + \frac{(kL)^2 GI_t}{\pi^2 EI_z} + (C_2 z_g)^2} - C_2 z_g\right\} \qquad [2.19]$$

where E is the Young modulus, G is the shear modulus, I_z is the second moment of area about a weak axis, I_t is the torsion constant, I_w is warping constant, L is the length of the beam, k and k_w is the effective length factors, z_g refers the distance between load application point and shear centre and C_1, C_2 are coefficients for loading and end restraint conditions.

In case of ideally simply supported beams, k and k_w are taken equal to 1. In addition to, when the moment gradient is linear along the unbraced length of a member or when the transverse load is

applied to the shear centre, $C_2 z_g$ becomes zero. As a result, equation [2.19] turns into a simplified form of equation 2.20 which is identical to the earlier expression for calculating elastic lateral torsional buckling of beam Mu as stated in equation 2.1.

$$M_{cr} = C_1 \frac{\pi^2 E I_z}{L^2} \left\{ \sqrt{\frac{I_w}{I_z} + \frac{L^2 G I_t}{\pi^2 E I_z}} \right\} \quad [2.20]$$

C_1 is a moment gradient factor for which no expression is given in this standard rather specified values for both end moment and transverse loading or any combination of loading as enclosed in NCCI (2008). In both cases, the non-dimensional slenderness parameter $\bar{\lambda}_{LT}$ is then calculated by using the following equation 2.21

$$\bar{\lambda}_{LT} = \sqrt{\frac{W_y F_y}{M_{cr}}} \quad [2.21]$$

Where W_y represents the modulus of the section. For class 2 section, plastic section modulus Z_x is used while for class 3 sections this plastic section modulus is replaced by elastic section modulus of section S_x. Given the slenderness parameter, the dimensionless parameter ϕ_{LT} is then calculated by using the following expression

$$\phi_{LT} = 0.5[1 + \alpha_{LT}(\bar{\lambda}_{LT} - \bar{\lambda}_{LT,0}) + \beta \bar{\lambda}^2{}_{LT}] \quad [2.22]$$

Where the coefficient $\bar{\lambda}_{LT,0}$ corresponds the maximum resistance value of a given section at a plateau level and it is taken as 0.2 and up to 0.4 for general and special case respectively. Whereas β, a constant which accounts for the shape of the strength curve is taken as 1.0 and reduced up to 0.75 for general and special case respectively. Eurocode 3 also recommends distinct strength curve

based on the shape and type of section i.e. wide and narrow, rolled and wide by incorporating an imperfection factor α_{LT} into equation 2.22. The values of α_{LT} is summarised in Table 2.1.

Table 2.1: Eurocode 3 LTB Curve Selection*

Cross section	Limits	General Case		Rolled or Equivalent Welded-Case	
		Buckling Curve	α_{LT}	Buckling Curve	α_{LT}
Rolled I-section	$d/b \leq 2$	a	0.21	b	0.34
	$d/b > 2$	b	0.34	c	0.49
Welded I-section	$d/b \leq 2$	c	0.49	c	0.49
	$d/b > 2$	d	0.76	d	0.76
Other cross-sections		d	0.76	d	0.76

*Zeiman (2010)

Next step is to determine the reduction factor χ_{LT} by using the equation [2.23] based on the calculated value of slenderness parameter $\bar{\lambda}_{LT}$ and the dimensionless imperfection parameter α_{LT}.

$$\chi_{LT} = \frac{1}{\phi_{LT} + \sqrt{\phi_{LT}{}^2 - \bar{\lambda}^2{}_{LT}}} \leq 1.0 \qquad [2.23]$$

The corresponding nominal flexure resistance of a section in then calculated by equation 2.24

$$M_n = \chi_{LT} W_y F_y \qquad [2.24]$$

in which W_y is either taken as Z_x, plastic section modulus for Class 1 and 2 section or S_x, elastic section modulus for Class 3 section. The factored resistance, M_r is then obtained by dividing the nominal resistance by the partial safety factor for resistance to instability γ_{M1} which is taken as 1.0.

$$M_r = M_n = \frac{\chi_{LT} W_y F_y}{\gamma_{M1}} \qquad [2.25]$$

2.4 Factors Affecting Lateral Torsional Buckling

There are several contributing factors that change the resistance of a member due to lateral torsional buckling i.e. residual stress, initial imperfection, moment gradient effect, load-height effect, support and restraint, etc. In this section, effects of these factors are briefly described.

2.4.1 Residual Stress

In general, it is expected that there is no stress or strain in a structural element initially i.e. during the no load phase. But, in practical, both stresses and strains remain in a structural element due to the manufacturing process of these elements. During the manufacturing process, steel members are usually subjected to massive thermal expansions which consecutively results in a high level of strains i.e. yield level strains within the member. As the subsequent cooling is not uniform throughout the element, self-equilibrating internal stress patterns are formed. These stresses are known as residual stresses.

Both the distribution and magnitude of residual stresses depend on the manufacturing process for instance hot rolling, welding and flame cutting. The residual stresses due to cold straightening usually present in some areas of the member and thus it can be neglected in most of the cases (Galambos, 1968). But it is essential to note that, as soon as the yielding is initiated by the presence of residual stresses, it starts to spread gradually over the cross section as the moment is increased. However, it shows no effect on the value of plastic moment capacity, M_p and thus the plastic range is virtually unaffected (Kirby et al., 1979).

High amount of compressive residual stress can be found at the flange tip of a beam, especially in hot-rolled and mill plate type residual stress. This scenario is more pronounced in beams where flange to web area ratio is very high, and thus the inelastic buckling is initiated comparatively early

in these beams. However, welded beams manufactured from the flame cutting exhibit a significant amount of tensile stress at the flange tips and the distribution of such residual stress pattern gives area under the compressive stress to area under the tensile stress ratio is as unity. Thus it compensates the adverse effect of compressive stress. In spite of these matters, presence of residual stress in beams somewhat imply a negative effect on the lateral torsional buckling capacity of a steel beam (Fukumoto (1976), Fukumoto and Kubo (1977), Fukumoto et al. (1980), Fukumoto and Itoh (1981), etc.).

2.4.2 Initial Imperfection

Geometric imperfection influences the LTB resistance capacity of a beam. This effect is even more significant for thin-walled structure. Imperfections are unintentionally introduced due to the mistake in the manufacturing process and may significantly decrease the load-carrying capacity of a structure (Cook et al., 2002). Both lateral deflection and twist of an imperfect beam tend to increase as soon as the commencement of loading and continue until the applied moment turns into the critical moment, Mcr. After this, both of this quantity decrease sharply due to the considerable reduction in stiffness which indicates that the beam is no longer able to carry any load further. So, additional deformations caused by the presence of imperfection incorporates other stresses and thus it affects the stability of a member by minimising the load carrying capacity of it (Kirby et al., 1979).

2.4.3 Effect of moment gradient

In a practical situation, a wide range of different loadings is applied to a beam, which consecutively yields a set of different moment gradient. According to many researchers including Kirby et al. (1979), the constant moment distribution can hardly be originated in the site, which is usually

considered as a worse case of loading. However, beams subjected to two equal point loads is frequently found in practice and thus constant moment distribution exists between the two point loads. As the effect of a non-uniform moment distribution is less severe, most of the design specification adopts an equivalent moment factor commonly known as C_b and approximates the critical moment for this case by multiplying the equation 2.1 with a value of this factor greater or equal to one (Driver et al., 2010).

2.4.4 Effect of load with respect to the shear centre

When transverse loads are applied to a beam, the LTB resisting capacity of a beam is dependent on both the arrangement and position of the load i.e. top flange, shear centre and bottom flange along the span of the beam. The runway for a crane girder can be said of as a common example of top flange loading of a beam, while a runway beam with the hoist suspended from the bottom flange can be taken as an example of bottom-flange loading (Kirby et al., 1979).

In the case of the top flange loading i.e. position of the load above the shear centre, it generates an extra torsional moment within the member which consecutively accelerates the cross-sectional rotation of beam even more. Thus it decreases the LTB resistance of a beam, and the opposite is also true when the load is applied to the bottom flange of a beam which works against the rotation of the beam to decrease the effect of LTB. To take account this effect, different design standard follows different ways depending on the position of load. However, recommended Helwig et.al. (1997) recommended a modified form of an equivalent moment factor C_b^* which accounts the effect of loading that is not applied at the shear centre and can be expressed by,

$$C_b^* = C_b\left(1.4^{\frac{2y}{h_o}}\right)R_m \qquad [2.26]$$

in which y refers the location of the applied load relative to the shear centre of the doubly symmetric cross section and taken negative & positive for loading above or below the shear centre and h_o refers the distance between flange centroids. In addition, the parameter R_m is made equal to 1.0 for unbraced lengths subjected to single curvature bending.

2.4.5 Effect of supports and restraints

The classical lateral torsional buckling solution for determining Mcr as expressed in equation 2.1, the supports are assumed to prevent both lateral deflection and twisting as a lowest possible measure of lateral restrain. Thus, equation 2.1 provides the lowest value of Mcr. However, in reality, three deformations i.e. twisting, lateral bending, and warping might occur at the time of LTB and hence there is a possibility to have a more or less beneficial support condition. For example, a completely fixed beam at both ends while subjected to a uniform moment forms two inflexion points at quarter points of its unbraced segment and thus becomes identical to the Euler buckling of a strut (Timoshenko et al., 1961). Therefore, it is suggested to replace the length of the beam by the half of its length when calculating its flexural resistance using the equation 2.1. Nethercot et al. (1971) extended the study of Timoshenko to investigate the effect of end restraints on LTB resistance of a beam by considering four types of support conditions and came up with an analogous solution as Timoshenko suggested.

At first, Nethercot et al. (1971) proposed two different length factor for a beam subjected to constant moment gradient i.e. factor for end fixity, K_1, and factor for both lateral bending and warping restraint, K_2 as shown in Table 2.2.

Table 2.2: Length factor for end support conditions

Type of end condition	K_1	K_2
Simply Supported	1.0	1.0
Warping Fixed	0.92*	0.48*
Completely Fixed	0.5	0.5

*Approximate Value

However, it was difficult to fix the values of these two factors K_1 and K_2 for other types of load configuration as it is not constant rather varies with proportions of the beam. As a consequence, Kirby et al. (1979) suggested a single length factor, k by replacing these two factors which were then adopted in BS 449 as expressed in following equation 2.27

$$l = kL \qquad [2.27]$$

where k refers to effective length factor and the values of it is listed in Table 2.3

Table 2.3: Recommended k values for different end condition

End Condition	k
Ends unrestrained against lateral bending	1.0
Ends partially restrained against lateral bending	0.85
Ends practically fixed against lateral bending	0.7

It is essential to note that to take account the effect of various types of loading the tableted value of k is a conservative choice. Also, in practical, it is impossible to get a fully fixed end supports against rotation and warping. (Kirby et al., 1979).

2.5 Detailed Review of Studies on Lateral Torsional Buckling of Welded Beams

Dibley (1969)

Dibley (1969) conducted a series of tests on universal I-beams of high strength steel subjected to four-point loading to verify the proposed design stresses. Two point loads are applied vertically

downwards at a certain distance from the supports so that the centre unbraced segment of the beam carries a uniform bending moment. In order to record the incremental loading, two types of load cell were with a range of 50 tonne and 5 tonnes. In this research, tensile tests were done for six full-scale specimens while the residual stress measurements were carried out on one section of each series. A similar trend in magnitude and distribution of residual stress were obtained from the measurement as found from the previous test in case of the lower strength steel section. (Dux and Kitipornchai (1983)). Moreover, vertical deflection of the ends of the beam was recorded including the lateral deflection and rotation at the mid-span of the beam using two dial gauges.

In order to investigate both inelastic and elastic LTB behaviour of selected sections, the lengths were fixed accordingly. In this study, for determining the equivalent length factor, a method was also proposed in order to use the same expression for various loading and end restrain condition. Maximum moment from the experiment carried by those sections was then summarised and also compared with the theoretical moment calculated from the latest equation of till date which was found satisfactory with an adequate level of safety. It was also concluded that the effect of residual stress is smaller in high strength steels and higher design stresses could be achieved resulting greater economy.

Fukumoto (1976)

Fukumoto (1976) experimented twenty-one welded beams including nine annealed beams with SM 50 steel and fifteen welded beams including three annealed beams with HT 80 steel to compare the test result considering the effect of residual stress and initial deformation on lateral buckling with theory. The test specimens were not braced between two ends except the both ends of the specimens were connected with heavy box cross section using high strength bolts in order to apply

loads and thus the support condition was both laterally and torsional restrained. The experiment was carried out for two types of moment gradient i.e. uniform moment gradient and moment gradient with the end moment ratio of 0.5. The measurement of initial imperfection was done for each beam in flanges and web plates at mid span of its effective length after setting the specimen at perfect position for testing and just before loading. In addition to this, welding was done manually for both types of steel and the typical pattern of measured residual stress were reported with magnitude. However, the author attempted to set the annealing condition only to relieve the welding residual stress which was also reported in this study.

In this test, lateral deflection of both flanges and vertical deflection at mid span of a beam and a girder in HT 80 were recorded. However, the ultimate moment from the experiment was collected for all specimen in both cases i.e. SM 50 and HT 80. The test points were then non-dimensionalized and plotted. From the graphical presentation, it was apparently found that corresponding test points of HT 80 steel were less scattered as compared to SM 50 steel. In addition to this, comparison was made between the annealed beams and as-weld beams of same sizes in terms of lateral strength and it was observed that annealed beams gained at least 11% more strength that that of as-weld beams in the case of SM 50 steel whereas it was only 6% for HT 80 steel in inelastic range of buckling. In other words, it can be said that welding residual stress may decrease the lateral buckling strength of about 11% for SM 50 and 6% for HT 80 as opposed to the beams without residual stress. Thus, it was clear that the effect of welding residual stress for higher yield strength steel was less than that of low yield steel, and this effect was more dominant in inelastic range of buckling.

Fukumoto and Kubo (1977)

Fukumoto and Kubo (1977) gathered information on the experimental strength of both laterally supported and unsupported that failed by lateral torsional buckling during the test. However, the primary intension was to collect the experimental results which were done intensively in this area and published in Japanese papers. Apart from that, in this survey in total 43 references were presented that were released in the preliminary and final reports of Liege Colloquium. While assembling experimental data, several parameters were kept in consideration such as steel grade, the dimension of cross-sections, loading conditions, support conditions and fabrication process. In addition to this, results from experiments was categorized into three groups: slender beams, stocky beams and beams with intermediate slenderness whose resisting strength due to LTB is mostly limited by elastic buckling strength, plastic strength and inelastic buckling strength respectively. Thus, in total 159 rolled beams and 116 welded beams were reviewed including 28 welded plate girders. However, among them, 87 rolled beams and 112 welded beams selected from several experiments that were done in Japan. The scattered test points were then statistically evaluated in terms of mean M, M-2S and the coefficients of variation. In addition to this, test results were compared with proposed design formulas which were available till date based on these statistical parameters. Form the review of all experimental results; authors concluded that welded beams have a lower lateral buckling capacity as opposed to rolled beams since they observed significant scattering of test points in the case of the welded beams.

Fukumoto et al. (1980)

Fukumoto et al. (1980) presents an experimental investigation of laterally unsupported beams to acquire a broad range of data on initial imperfection in form of residual stress in beam-type hot rolled sections including initial crookedness and thus evaluate the effect of such imperfections on

lateral resistance of beams using identical parameter i.e. loading, supports and cross-sectional dimension.

In this experiment, a number of twenty-five I-shape beams with a length of 7m were prepared. It is important to note that, the cross-sectional dimension of each beam was kept same i.e. I-200mm ×100 mm × 5.5 mm × 8 mm. After that, three beams were cut out from each of the 7m beams with a length of 2.6 m, 2.0 m, and 1.5 m. Thus, in total 75 beams were prepared for the buckling test under a concentrated load applied at the mid-span of the beam. All of the test specimens were restrained at their supports against torsion rather warping. However, the strain reading along the test specimen during a preliminary test confirmed the successful implementation of simply supported end condition.

Apart from this, two other short beams were cut out for the tension coupon test and residual stress measurement. In total, tension coupon tests were done at four locations of beam among them two were done for top and bottom flanges, and other two were done on the web for each of the 25 beams. However, residual stresses measurements were done by the sectioning method, and initial measurements of the crookedness of 75 beams are taken at equally-divided five points about the major and minor axes and in the angle of rotation.

The variations of the geometrical and material imperfections were measured and reported by histograph. In addition, the ultimate strength, P_{max} of all beams were summarized including the load-deflection curves i.e. horizontal and vertical deflection curve for a selected beam of three different lengths. Moreover, the effect of these imperfections on lateral buckling were reviewed with existing test data and design formula by plotting the test results as a ratio of M_{max}/M_p against

modified slenderness ratio $\lambda = \sqrt{\frac{M_p}{M_u}}$, in which M_{max} is obtained from experimental results, M_p and M_u refer the sections full plastic moment and classical lateral torsional resistance of the corresponding beam respectively. It was concluded that presence of compressive residual stress at the flange tip always reduced the ultimate strength of test specimen, however, the relationship of the initial crookedness with ultimate strength was not revealed appropriately since the measured of it was less than 1/5000 of the span length.

Fukumoto and Itoh (1981)

Later, in 1981 Fukumoto and Itoh conducted an experimental investigation of laterally unsupported welded beams. In this test, in total thirty-four welded beams with identical cross-sections i.e. I-250×100×6×8 mm were prepared and categorised into two groups with different lengths of 1.8 m and 2.6 m. Thus, in total 68 beams were tested under the same loading and boundary condition similar to an earlier study (Fukumoto et al. 1980). However, it is essential to note that, to examine the effect of welding on LTB resistance, welded sections which are geometrically similar to those section used in Fukumoto et al. (1980) were selected.

Moreover, a small beam had been cut out for residual stress measurement and tension coupon test as well. Measurement of residual stress was done following same way as it was done in Fukumoto et. al (1980) and results showed that the residual stress patterns in welded beam-type sections were significantly different in the flange, as compared to both the patterns for the column-type sections (McFalls and Tall 1969, Nagaraja Rao et al. 1964) and 25 rolled beams (Fukumoto et al. 1980).

In addition, the ultimate strength, P_{max} of all 68 beams were recorded including the resulting mean M, standard deviation S, and coefficient of variation. Thus, the change of strength was presented graphically by plotting the test results as a ratio of M_{max}/M_p in ordinate and modified slenderness ratio $\lambda = \sqrt{\frac{M_p}{M_u}}$, in abscissa where M_{max} is obtained at mid-span of the beam from test results, M_p and M_u refer the sections full plastic moment and classical lateral torsional resistance of the corresponding beam respectively. Authors concluded from this test was, welded beams tend to have a lower strength resistance and large coefficient of variation as opposed to rolled beams due to the considerable variation in the compressive residual stress and the initial out of straightness

MacPhedran and Grondin (2009)

MacPhedran and Grondin (2009) conducted a reliability analysis and proposed a single-part alternative equation for strength calculation of laterally unbraced structural steel beams. A similar format of present steel column design curve was used as a replacement of existing three-part strength equation. A modified slenderness ratio, $\bar{\lambda}$ derived from the braced (maximum) moment capacity, M_b was used in proposed equation along with the unbraced (elastic buckling) capacity, M_u which makes it equivalent of column strength curve. The proposed equation is as follows:

$$M_n = M_b(1+\bar{\lambda}^{2n})^{-1/n}, \quad \bar{\lambda}^2 = M_b/M_u \qquad [2.28]$$

The presence of a coefficient "n" makes the expression more convenient to use it on particular situation for all laterally unsupported length. ECCS (European Convention for Constructional Steelwork, 1976) recommendations the value of n = 2.5 for designing laterally unbraced beams. However, in this research, a suitable value for n is determined through a reliability analysis to apply the same equation to account the various contributing factors such as residual stress or

geometric imperfections. Thus, Equation [2.28] can be rewritten accordingly for the design of class 1 or 2 beams and expressed as follows.

$$M_r = \phi M_p (1+\bar{\lambda}^{2n})^{-1/n}, \quad \bar{\lambda}^2 = M_p/M_u \qquad [2.29]$$

in which, M_p refers the full plastic moment resistance before local buckling of a section before local buckling. The proposed equation was then calibrated against the experimental data of Greiner and Kaim (2001), as summarized in Eurocode 3. The gathered data were separated into two groups: rolled and welded section. In total 144 tests data represent rolled shape beams while 71 test data were collected representing welded shape beams. For both type of section, coefficient of variation, test to predicted ratio were determined using both proposed equation and S16-09 equation. The details of these data are presented in the following Table 2.4.

Table 2.4: Comparison of Proposed and Current equation with test data

Type of Equation	Rolled Beam		Welded Beam	
	Test to predicted ratio	Coefficient of Variation	Bias co-efficient	Coefficient of Variation
Proposed Equation*	1.015	0.066	1.011	0.109
CSA S16-09	0.983	0.060	0.916	0.111

*Proposed equation is derived using n = 3.1 and 1.9 for rolled and welded beam respectively.

From the above comparison, it was observed that existing design equation was somewhat overestimating the resistance of welded beams. Therefore, the authors conducted a reliability analysis to evaluate the performance of current and proposed equation against experimental test results of Greiner and Kaim (2001). From the analysis, it was found that in the case of the welded beams, current strength equation of CSA S16-09 provides a resistance factor of 0.9 with the corresponding reliability index of 1.6 instead of 3.0. The analysis also indicated that to confirm a

reliability index of 3.0, as it was suggested in the benchmark reliability study on this equation by (Kennedy and Gad Aly 1980), would require a resistance factor of approximately 0.82. At the same time, the existing equation was found to be entirely satisfactory with an overall reliability analysis of about 3.0 for a resistance factor of 0.9.

Unlike the current formula, the assessment of proposed laterally unsupported beam strength curve (Eq. [2.28]) showed that it achieves at least a reliability index of 2.7 with n = 3.1 and 1.9 for rolled and welded shape beams respectively using the same resistance factor of 0.9. However, it is essential to note that, the proposed equation offered a reliability index of 3.0 or greater for a resistance factor of 0.9 in the case of the rolled sections only. For class 3 sections, the same equations can be used by replacing the braced moment with the yield moment of the cross section. Nevertheless, the shortcomings of this study were not to consider several factors that might affect the LTB strength of a member namely height of loading, strain hardening, beam stockiness, another mode of failure, effective length and moment distribution along the unsupported span of a particular member.

Subramanian and White (2015)

Subramanian and White (2015) evaluated the performance of AISC/AASHTO LTB resistance equations by means of typical FEA test simulations. However, it is significant to note that FEA simulations are likely to be conservative for many reasons i.e. use of idealized boundary conditions, assumed nominal residual stresses and geometric imperfections. Therefore, the authors conducted extensive sensitivity analyses with different magnitudes of imperfections and different residual stress patterns on members with simply supported boundary conditions of twist restrained, lateral bending and warping free at ends of the member. Hence, the sensitivity analyses were done on selected experimental tests with compact and non-compact web members subjected to uniform

bending and having more general boundary conditions. Based on these studies, the authors recommended nominal residual stresses and geometric imperfections which were then used to do further FEA simulations. Thus the simulations became more representative of the mean experimental strengths captured by the AISC/AASHTO resistance equations.

While developing the FE model, several parameters were taken into consideration for example appropriate size of element, selection of material properties, the magnitude of initial imperfection, selection of residual stress pattern, boundary condition and so on. Aspect ratio of each element was kept as 1.0 while the material was modelled considering stain hardening. The magnitude of imperfection and the typical pattern of residual stresses were selected from several literatures. Moreover, the simply supported boundary conditions were enforced into FE model. From the sensitivity analysis performed on rolled beams, for all cases of residual stress AISC/AASTHO LTB resistance equation over predicted except the imperfection magnitude of L/2000 with one-half of the Lehigh residual stresses pattern which provided best correlation with the AISC/AASHTO LTB resistance curve. As a part of this study, sensitivity analysis was also performed on welded plate girders to evaluate the AISC/AASHTO LTB resistance curve for this type of members and it was observed that like the rolled beams AISC/AASHTO LTB resistance curve overestimated the LTB strength by at least 20% although the imperfection magnitude of L/2000 with half Best-Fit Prawel residual stresses pattern showed the best fit with AISC/AASHTO LTB resistance equation. However, in this study, the proposed model by Kim (2010) was evaluated for welded plate girders and found the conservative maximum of 13% in the elastic region of buckling. In other sense, proposed model predicted 30% more strength relative to test simulations. Further investigations were also recommended such as non-uniform bending by the authors.

Chapter 3 Finite Element Modeling

3.1 Introduction

The main purpose of this chapter is to present and discuss the development of finite element model (FEM) in order to study the behavior of a simply supported beam that undergoes LTB. The failure of a steel beam by LTB can be considered as a limit state of structural design. Although this topic has been studied intensively for many years by several researchers, still there are many areas that need to be addressed including the effect of welding on capacity. Therefore, a comprehensive study using finite element analysis (FEA) was conducted to explore the lateral torsional buckling behavior of simply supported W-shape welded beams.

With the aid of powerful computers and comprehensive software packages, this type of failure can be investigated in detail. To date, many researchers have used finite element analysis to predict the ultimate load capacity of steel beams and compared this to the results obtained from different steel codes. However, very few of these models have been developed for W-shape welded beams. Hence, the goal of this section is to develop an FE model in order to investigate the behavior of a welded beam subjected to various bending moment distributions by using the software package Abaqus. Abaqus is a general-purpose FEA program for use in the numerical modelling of structural response.

This chapter will describe the detailed modelling techniques and assumptions i.e. element type, material properties, and boundary conditions which were adopted to develop a suitable FE model. Furthermore, the inclusion of initial imperfections is presented along with a sensitivity study of these imperfections as well as the modelling of residual stresses. This chapter concludes with a preliminary validation of the numerical model to assist in the further investigation.

3.2 Model Description

The deformation of beams that undergo in lateral torsional buckling mode is very complex, particularly when approaching towards the final stage of failure. Therefore, three-dimensional finite elements must be used as it is capable of simulating the real structural behavior including global behaviors of structure and various load effects.

In this research, simply supported WWF-beams were modelled using shell elements because it is suitable for incorporating both geometric and material nonlinearities preciously. Besides, shell elements are sufficiently capable of predicting the effect of geometric imperfections i.e. initial out-of-straightness and residual stresses. Also, effects of loading and support conditions can be investigated in greater detail. The subsequent sections will present the description of the model adopted in this study in detail.

3.2.1 Elements and Mesh Configuration

In order to investigate the non-linear lateral torsional buckling failure, shell elements are considered as a promising modelling building block as they can provide required degrees of freedom to capture the real buckling deformations and spread of plasticity effects. There are various commercial finite element analysis packages that can perform the second-order inelastic analysis. Among them, ABAQUS (HKS, 1998) was found to be the most appropriate and hence a nonlinear FE model was developed using the commercial finite element software package ABAQUS (ABAQUS 2010).

Due to the simplicity of the geometry of W-section beams, 4-noded shell elements are selected in this study. Three types of 4-noded shell elements are available in default element library of ABAQUS Standard version of 6.11 (S4, S4R, and S4R5). Among them, S4R5 element is a thin,

shear flexible, isoparametric quadrilateral shell with four nodes and five degrees of freedom per node, utilizing reduced integration and bilinear interpolation schemes. This element imposes the Kirchhoff constraint numerically which makes them inappropriate to use in large-strain analysis. Whereas, both S4 and S4R elements are doubly curved general-purpose, finite membrane strain shell elements where "R" refers to reduced integration with hourglass control. These two elements are usually selected for shell structures whose thickness is larger than 1/15 of the element length for which transverse shear deformation is important and Kirchhoff constraint is satisfied analytically. In comparison with S4R5, both S4 and S4R elements have six degrees of freedom per node and have multiple integration locations for each element. As a result of this, these two elements are significantly more computationally expensive and also able to provide more accurate result than the S4R5 element. However, the S4R element also uses reduced integration to form the element stiffness which makes it suitable for providing accurate results in comparison to the general fully integrated S4 shell. Apart from that, running time of the analysis can be reduced significantly, especially in three dimensions using S4R element. Therefore, S4R element was selected for the analysis of all the models.

Selection of mesh density depends on the geometrical characteristics of the structures and CPU speed. The simplicity of the geometry of this model makes mesh configuration very easy. However, in order to achieve an optimal aspect ratio, minimize the localized stress concentrations at the beam supports and also to keep the computer run time manageable a mesh sensitivity analysis was conducted as shown in Figure 3.1 (a). From this analysis, adequate mesh density has been achieved for the section with 8 elements across the width of the flange and 32 elements along the height of the web with quad-dominated element shape as shown in Fig 3.1 (b). In addition, total 300 elements were created along the length of each model.

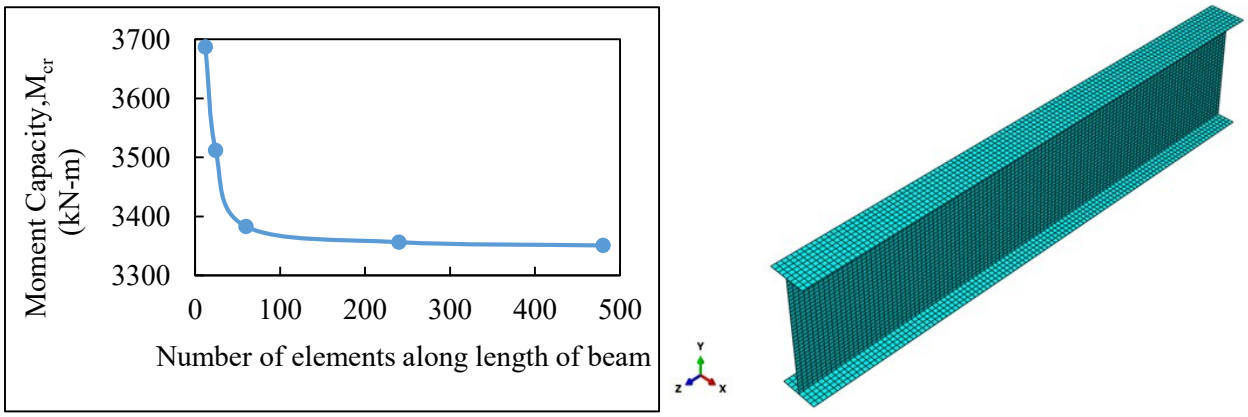

(a) (b)

Figure 3.1: Mesh Configuration of Finite Element Model

3.2.2 Material Properties

The ABAQUS classical metal plasticity rule was adopted in all the analyses. This rule implements the von Mises yield surface to define isotropic yielding and associated plastic flow theory i.e. as the material yields, the inelastic deformation rate is in the direction of the normal to the yield surface. This model is widely acceptable for most calculations with metals.

A bilinear elastoplastic stress versus strain curve was assumed for all the model. Structural steel elements usually exhibit strain hardening and it may affect the capacity of members. Therefore, the strain-hardening behavior was incorporated into the models. A strain hardening of 2% of the elastic stiffness was considered for all analyses since the post-yield stiffness of steel is approximately equal to 0.5–5% of the elastic stiffness (Saatcioglu M and Humar J.). The reasons for this assumption are: strain-hardening data is not readily available and the aim of this research is to verify the current code capacities which are based on the experimental result. In ABAQUS, both isotropic and kinematic strain hardening can be included in the finite element analysis. However, in this research, a nonlinear isotropic hardening model was used. The nominal value of

yield stress for both web and flanges was taken as 350 MPa. The elastic modulus and the Poisson's ratio were taken as 200000 MPa and 0.3, respectively.

3.2.3 Boundary Condition

The most critical load case in lateral-torsional buckling research is simply supported beam with uniform end moment. The empirical equations in current design specifications are in general based on testing of simply supported beams under this load case. It should be noted that both load and boundary conditions have very significant effects on the inelastic lateral torsional buckling failure mode. Nonetheless, in this section, an attempt was made to achieve the idealized boundary condition proposed by Trahair (1993) for simply supported beam with constant moment gradient. According to Trahair (1993), the beam is assumed to be simply supported at both ends relative to the strong axis bending, weak axis bending, and twist. It is essential to confirm that idealized boundary conditions adopted in modelling are as close as possible to theoretical buckling analysis. Hence, these assumptions have been replicated into to FE model by means of the following criterion.

1. Simply supported in plane: centroids of both ends were restrained against in-plane y-axis deflection ($U_2 = 0$) but unrestrained against in-plane rotation($UR_1 \neq UR_2 \neq 0$), also one end was restrained against z-axis displacement ($U_3 = 0$). (Figure 3.2)
2. Simply supported out-of-plane: all web nodes including the centroid of both ends were restrained against out-of-plane x-axis deflection ($U_1 = 0$) and only centroids of the both ends were restrained against z-axis rotation ($UR_3 = 0$), but unrestrained against minor axis rotation and warping displacement (Trahair 1993). (Figure 3.2)

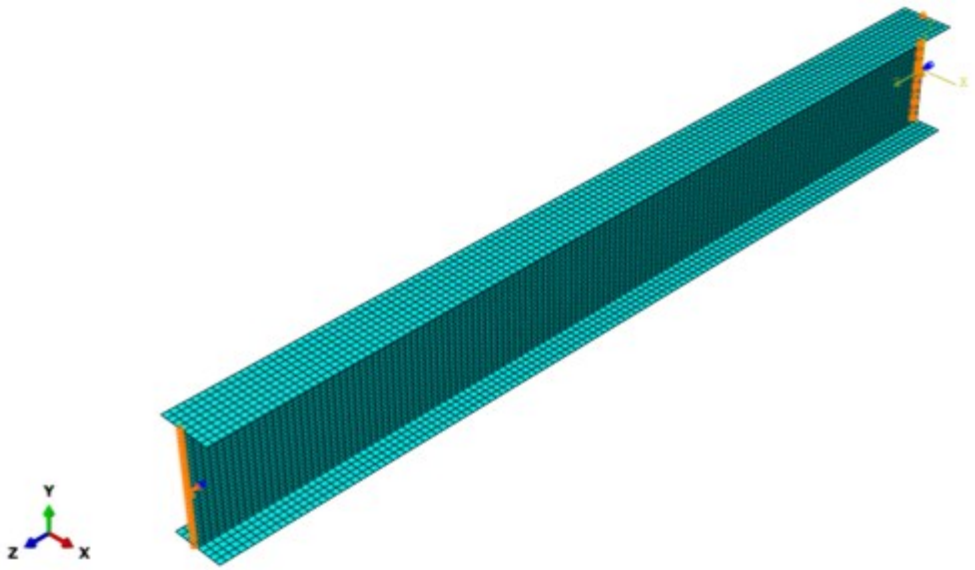

Figure 3.2: Boundary condition in finite element model

In conjunction with the above criterion, a type of constraint also needs to be applied to all nodes of end cross section such that those points follow the beam kinematics of Vlassov. Also, it is necessary to ensure the theoretical simply supported boundary condition as close as possible at both ends. According to Vlasov theory, longitudinal displacement w for a generic point (x, y) at both beam ends (l_e=0 and l) is given by,

$$w(le, y, x) = \zeta(le) - \xi'(le)x - \eta'(le)y - \beta'(le)xy \qquad [3.1]$$

where, $\zeta(le)$ refers the displacement of the centre of the cross-section along the longitudinal direction, $\xi(le)$ is the displacement along x axis (along the lateral direction), $\eta(le)$ is the displacement along y axis (along the vertical direction), $\beta(le)$ is the rotation about the longitudinal direction.

Hence, Equation 3.1 was applied to the corner points of each end and the following equation can be achieved for the longitudinal displacement of corner points

$$\begin{Bmatrix} w_1 \\ w_2 \\ w_3 \\ w_4 \end{Bmatrix} = \begin{bmatrix} 1 & x_1 & y_1 & x_1y_1 \\ 1 & x_2 & y_2 & x_2y_2 \\ 1 & x_3 & y_3 & x_3y_3 \\ 1 & x_4 & y_4 & x_4y_4 \end{bmatrix} \times \begin{Bmatrix} \zeta(le) \\ \xi'(le) \\ \eta'(le) \\ \beta'(le) \end{Bmatrix} \quad [3.2]$$

In which $(x_1,y_1),(x_2,y_2),(x_3,y_3),(x_4,y_4)$ refer the coordinates of corner points and w_1, w_2, w_3, w_4 refer the corresponding longitudinal displacement of those points. Solving Equation 3.2 for vector $(\zeta(le) \quad \xi'(le) \quad \eta'(le) \quad \beta'(le))^T$, Equation 3.3 has been obtained

$$\begin{Bmatrix} \zeta(le) \\ \xi'(le) \\ \eta'(le) \\ \beta'(le) \end{Bmatrix} = \begin{bmatrix} 1 & x_1 & y_1 & x_1y_1 \\ 1 & x_2 & y_2 & x_2y_2 \\ 1 & x_3 & y_3 & x_3y_3 \\ 1 & x_4 & y_4 & x_4y_4 \end{bmatrix}^{-1} \times \begin{Bmatrix} w_1 \\ w_2 \\ w_3 \\ w_4 \end{Bmatrix} \quad [3.3]$$

From equation [3.3] into [3.1] gives,

$$w(le,y,x) - (1 \quad x \quad y \quad xy)^T \begin{bmatrix} 1 & x_1 & y_1 & x_1y_1 \\ 1 & x_2 & y_2 & x_2y_2 \\ 1 & x_3 & y_3 & x_3y_3 \\ 1 & x_4 & y_4 & x_4y_4 \end{bmatrix}^{-1} \begin{Bmatrix} w_1 \\ w_2 \\ w_3 \\ w_4 \end{Bmatrix} = 0 \quad [3.4]$$

Equation [3.4] calculates the longitudinal displacement w at any generic point (le, x, y) on end le in terms of the longitudinal displacements of corner points (Xiao 2014). Therefore, corresponding longitudinal displacement of four corner points for all nodal points (except the center node of web of both end) of end cross-section of both ends are calculated and then applied to FE model using the multi-point equation constraint feature of ABAQUS as shown in Figure 3.4

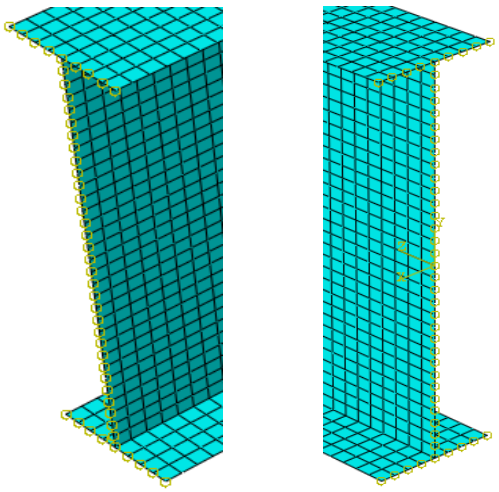

Figure 3.4: Longitudinal constraint for end points

3.2.4 Load Application

In this section, the primary focus was to develop a simply supported beam subjected to equal end moments. However, other loading configuration will also be discussed in subsequent chapters according to the requirement. Therefore, the uniform moment condition was obtained by applying two pairs of equal concentrated force at corners. The force was applied along the longitudinal direction of the beam and both of the pairs is opposite to each other as shown in Figure 3.5. Thus, the loading scheme created a coupling situation with zero longitudinal resultant, weak axis moments, and bi-moments which in turn confirming the application of load at shear center. Also, the magnitude of each concentrated force was fixed in a way so that the magnitude of applied moments remains as 1.0 kN-m using Equation 3.5. A similar method for applying uniform moment was followed earlier by several researchers in the different analytical model (Xiao 2014; Hassan 2013; Amin Mohebkhah 2012; Sharifi 2015 etc.).

$$4p \times \left(\frac{d}{2}\right) = 2pd \qquad [3.5]$$

where p is the magnitude of the concentrated load and d is the total depth of beam (Figure 3.5).

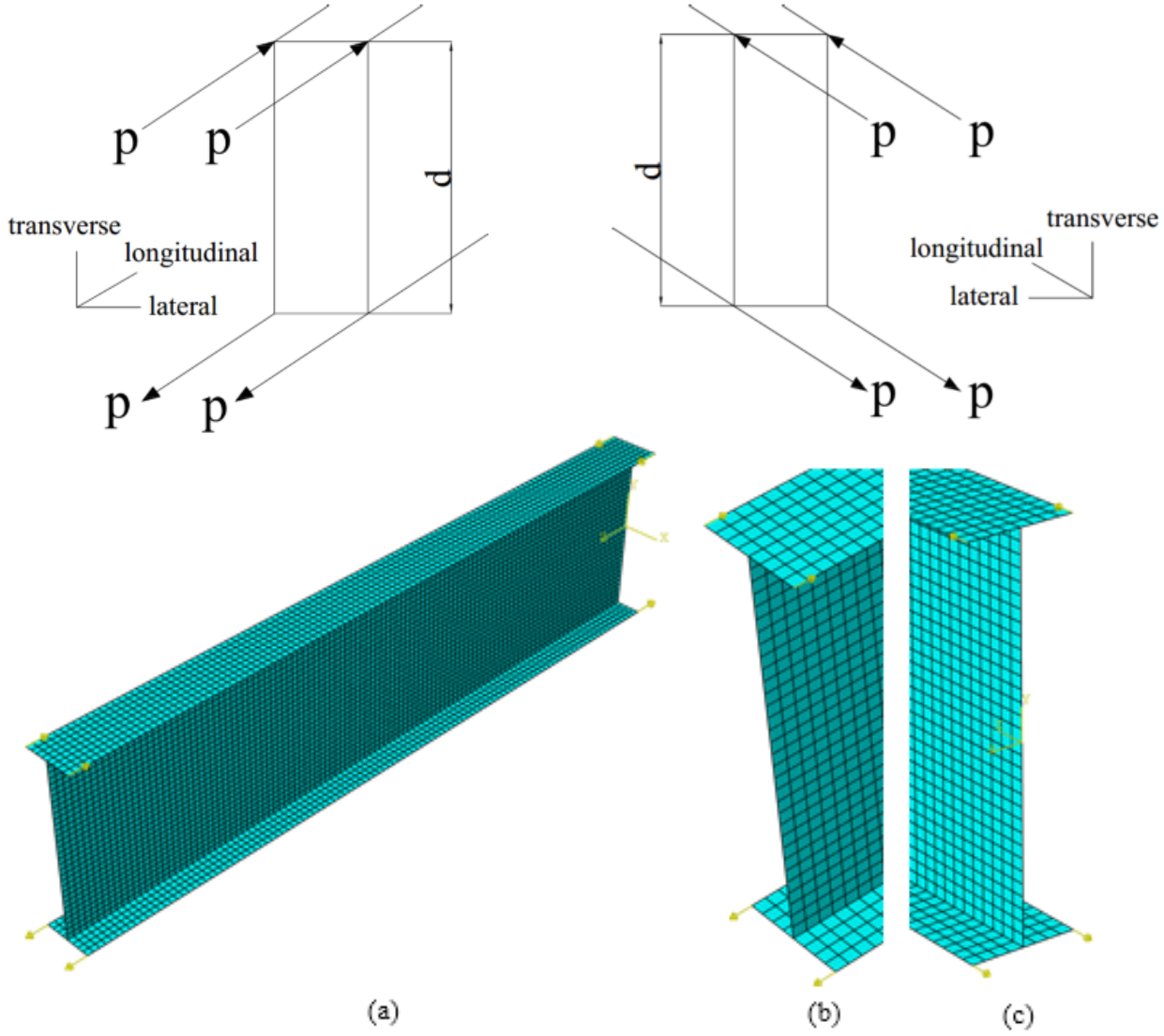

Figure 3.5: Load Application in Finite Element Model

3.2.5 Analysis Type

Two types of analysis i.e. elastic buckling analysis and non-linear analysis were conducted to estimate the ultimate load carrying capacity of beams subjected to all loading configuration i.e. equal end moment, point load at mid-span, uniformly distributed load etc. Firstly, an eigenvalue analysis was performed for elastic buckling analysis in which eigenvalues of corresponding eigenmodes are requested using the linear perturbation buckling analysis. In this study, four

eigenvalues for each run were extracted. The main purpose of eigen value buckling analysis was to achieve a suitable pattern of imperfection which will be incorporated into nonlinear analysis later.

It is essential for this research that, the post-buckling response of beam be captured accurately, in order to predict the capacity of the beams. The Modified Riks method can be used for this purpose since this technique is usually suitable for predicting the instability as well as for understanding the non-linear behavior of geometric collapse (Simulia 2013). This method is also useful for problems with material nonlinearity and for obtaining solutions to limit load problems. The Modified Riks method uses proportional loading and relies on the smooth response of the system (i.e. no bifurcation behavior). Although it follows the basic algorithm of Newton-Raphson method to solve the equilibrium equations, however, it incorporates an additional parameter called arc length procedure in providing solutions concurrently for load and displacement. Hence, it is essential to limit the increment size in order to obtain the correct equilibrium path. So, the initial increment size needs to be fixed by the user, but it is automatically adjusted by the algorithm implemented in ABAQUS for subsequent increments depending on the convergence rate and the minimum increment size specified by the user**.**

3.2.6 Initial Geometric Imperfections

It is very obvious that every steel built up section has some form of geometric imperfection due to the production process and even by the handling of these members. Unfortunately, adequate data are not available on these imperfections. Also available data do not represent the effect of imperfection on LTB accurately. But generally, two aspects of geometric imperfections i.e. shape of the imperfection and magnitude are considered to have a direct effect on ultimate capacity.

However, imperfections in steel beams are random and therefore it could be said that these random imperfections only initiate the buckling deformation. At this stage, it would be significant to mention that, buckling mode shapes do not predict the actual deformation magnitudes rather they are normalized to provide the maximum displacement value as 1.0 at mid-span of the beam. So, the correct mode of buckling must be selected and hence scaled with a suitable factor to take account the effect of imperfection on LTB preciously. According to Trahair (1993), the lowest positive eigenvalue refers the load which initiates the buckling of a structure and associated eigenvector refers the related buckling shape or buckling mode of that structure. In order to justify this theory and get a clear understanding of the behavior of a beam, a sensitivity analysis was performed following the modeling techniques as discussed in sections 3.2.1 to 3.2.5 with different magnitude of imperfection and shape. All the analysis was done for WWF-700×175 section with a length of 8m under uniform moment gradient. Also, the residual stress was not incorporated into those models to get a better understanding of the effect of initial geometric imperfection.

Thus, the ultimate capacity of the beam was determined from non-linear buckling analysis using two different eigen mode with varying degree of imperfection. Figure 3.6 plots the ultimate moment capacity of beam against the imperfection magnitude. From the results in Figure 3.6, it is clearly evident that the lowest positive eigen mode dictates the ultimate capacity of the beam and has a significant effect on LTB capacity for varying degree of imperfection.

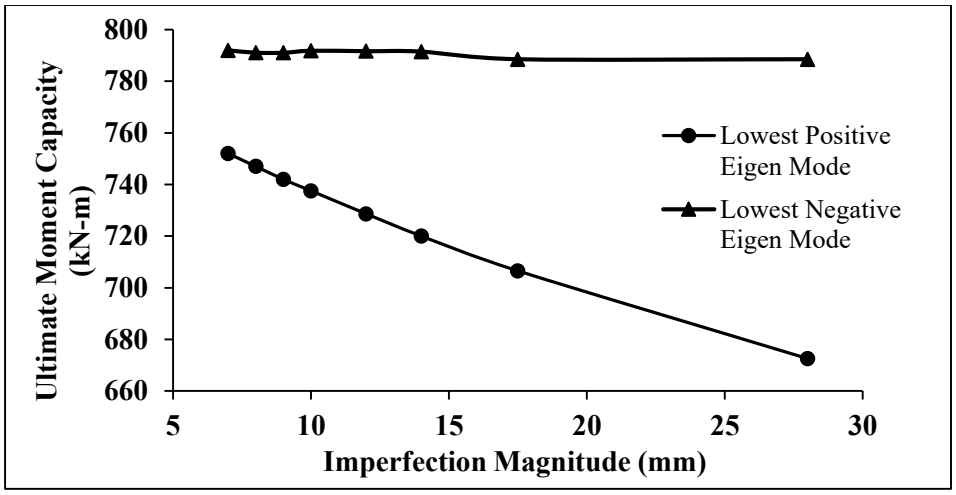

Figure 3.6: Sensitivity Analysis for initial geometric imperfection

Another important outcome of this sensitivity analysis was that even though the non-linear analyses was performed for different imperfection shapes or modes, at the final stage of failure, the member always exhibited similar failure pattern as shown in Figure 3.7. It should be noted that only half of the span is shown in Figure 3.7 for illustration purpose.

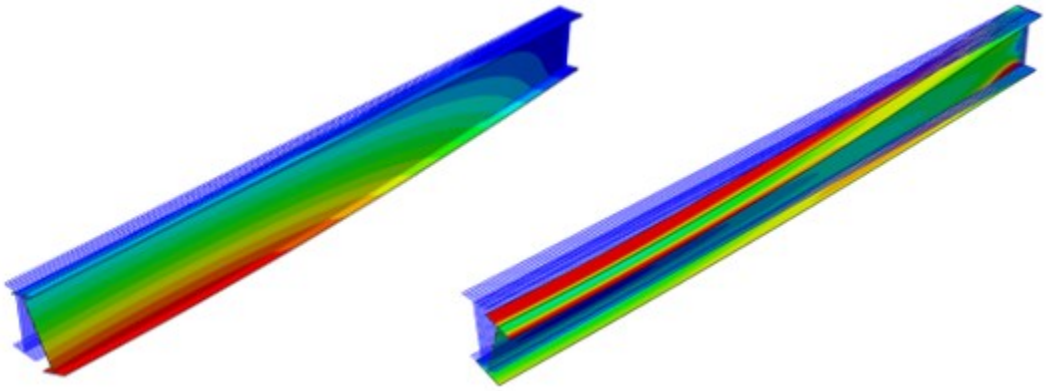

(a) Lowest positive eigen mode (left) and final state of failure (right)

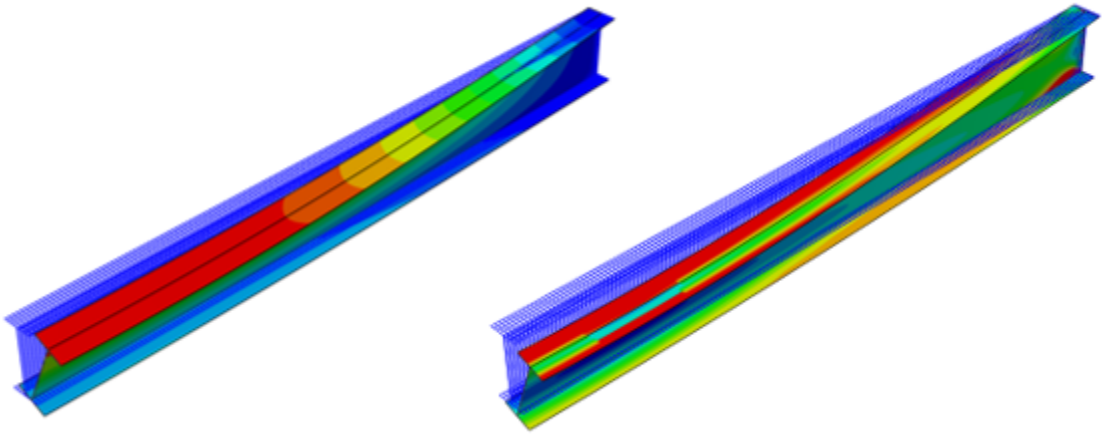

(b) Lowest negative eigen mode (left) and final state of failure (right)

Figure 3.7: Different eigen mode and associated state of failure for WWF-beams (half span only)

Therefore, it is imperative to say that shape of the imperfection may initiate the out-of-plane buckling but only lowest positive eigen mode is sensitive to varying degree of imperfection. Therefore, the selection of appropriate imperfection input is as significant as choosing the accurate boundary conditions. Column strength curves from SSRC (Bjorhovde 1972) were developed using L/1000 as maximum permissible initial out-of-straightness. Moreover, two North American structural steel delivery specifications (e.g., ASTM A6 in the United States; CSA G40.20 in Canada) restrict the magnitude of maximum initial out-of-straightness as a factor of L/1000 (Ziemian 2010). Therefore, in this study, a maximum initial out-of-straightness of L/1000 is assumed as an initial geometric imperfection. This has been introduced by changing the co-ordinates of all nodes based on the scaled eigenvectors which has been obtained from previous eigen value buckling analysis. The scaling has been done in such a way so that the maximum out-of-plane deformation of mid node will have the largest imperfection magnitude of L/1000 as shown in Figure 3.8.

.

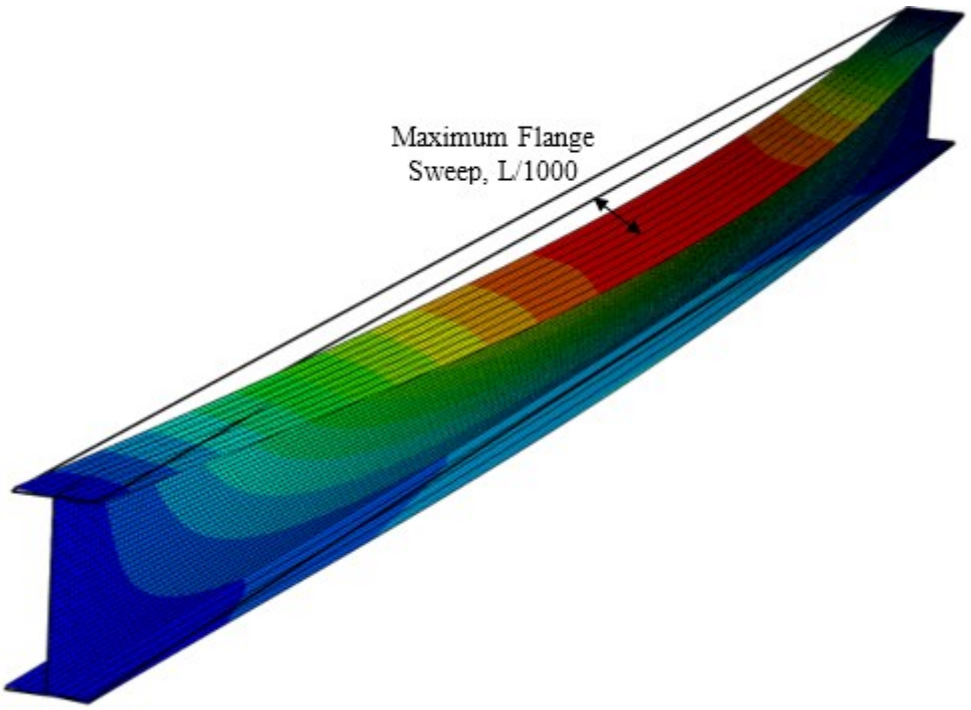

Figure 3.8: Maximum flange sweep of L/1000 for initial imperfection

3.2.7 Residual Stress

Generally, the presence of residual stress in steel member causes premature initial yielding by affecting the stiffness of member which consequently lowers the ultimate strength. Residual stress present in both hot-rolled and built-up members due the effect of differential cooling which usually happens while it manufactured. Therefore, it is very obvious that large variation of residual stress is observed from one member to another. As a result of this, detailed sensitivity analysis and results will be discussed in subsequent chapters. However, in this section, an idealized pattern of residual stress is considered and hence an attempt was made to observe the effect of residual stress application on FE model.

ECCS Technical Committee 8 (1984) recommends a typical pattern of residual stress as shown in Figure 3.9 for hot-rolled I-beams. It should be mentioned that this distribution of residual is only used to see that the application is working or not.

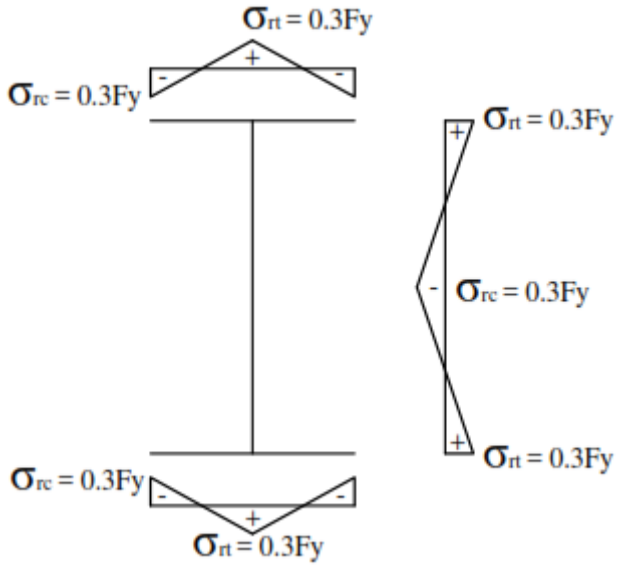

Figure 3.9: Recommended residual stress pattern by ECCS (1984)

Thus, the recommended values of residual stress were applied to the defined element sets of the member as an initial stress field along the perpendicular direction of each element sets. Such application of residual stress converts the model to a non-equilibrium state numerically and hence it is required to create a static step before applying any loads to a model which will consequently let the model to attain its equilibrium state. After this equilibrium step, contour map of stress is captured from finite element model as shown in Figure 3.10.

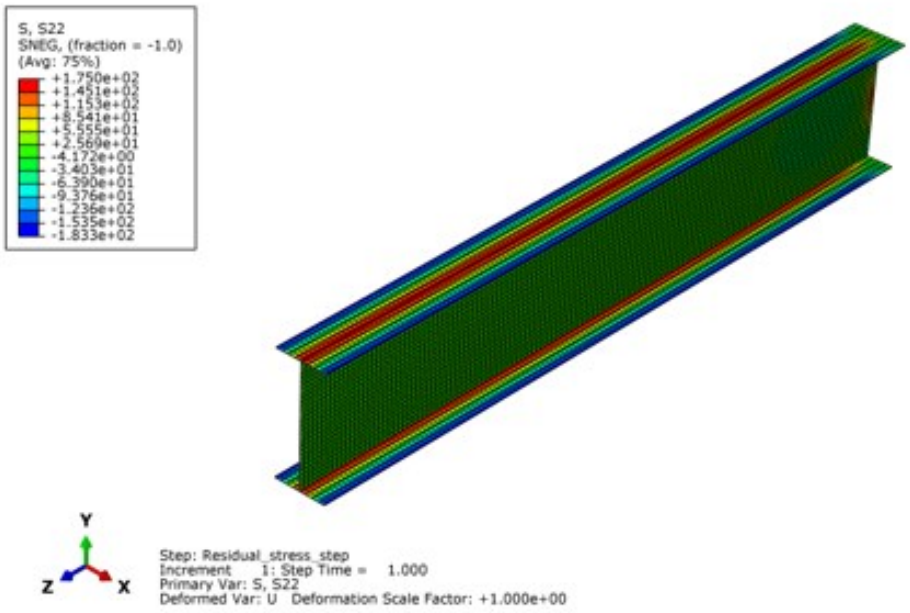

(a) Distribution of residual stress at flange

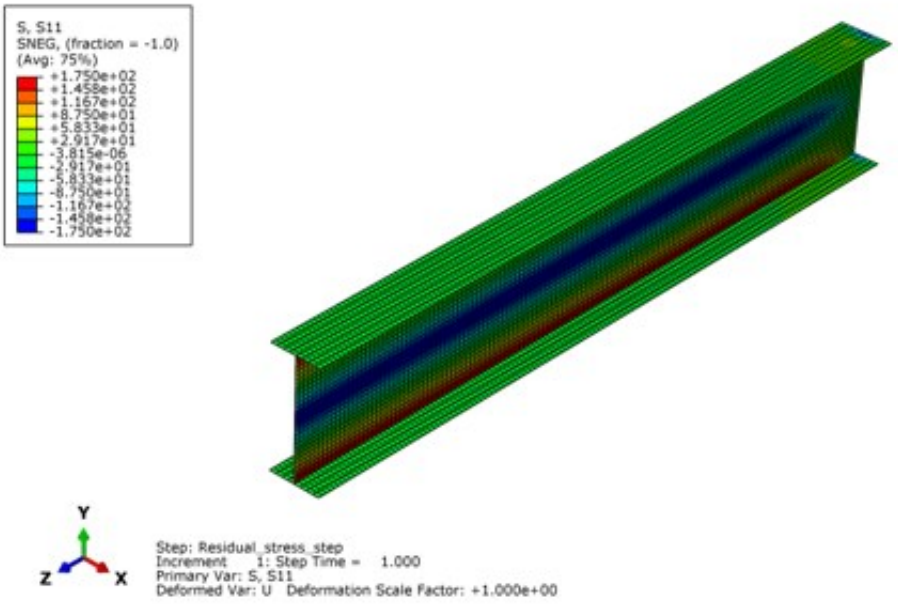

(b) Distribution of residual stress at Web

Figure 3.10: Contour map of applied residual stress in finite element model

From the contour plot in Figure 3.10, it is seen that the stress contours do not extend until the end of beam since it extracted after the commencement of equilibrium step. Therefore, values of residual stress were taken at a certain distance from the end of the beam after finishing of equilibrium step and plotted in figure 3.11, which show the distribution across the flange and web of the model. It is clear that the distributions in figure 3.11 resemble a more accurate model since the stress distributions are non-linear across the elements.

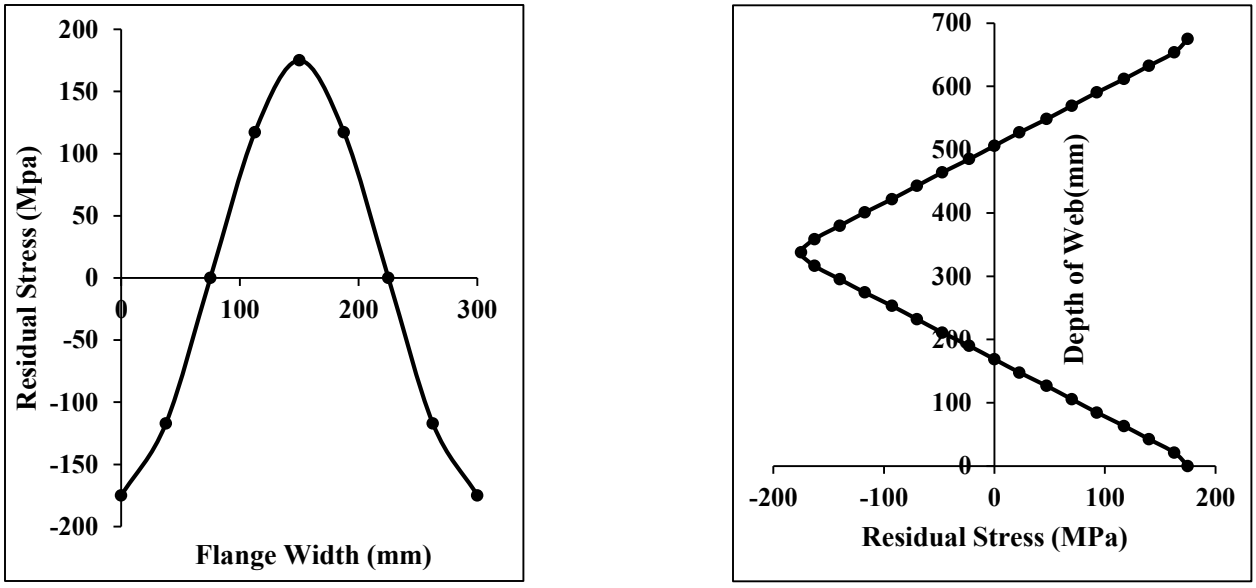

(a) (b)

Figure 3.11: Distribution of residual stress across (a) flange and (b) web from FE model

As mentioned in chapter 2, presence of residual stresses affects the yielding of the member and ultimate load carrying capacity of steel members as well. This reduction in capacity is primarily controlled by both magnitude and distribution of initial stresses in steel member. Detailed sensitivity study will be carried out to investigate the effect of residual stress in next chapter. But, a simple sensitivity analysis was performed on an 8m long beam of WWF-700×175 section to determine the influence of residual stresses for equal end moment only. From results, as shown in

figure 3.12, it can be seen that yielding occurs at an earlier stage with an application of residual stresses (RS) which in turn reduces the ultimate load. This shows that the modelling of residual stresses can have a significant impact on the load capacity of steel beams.

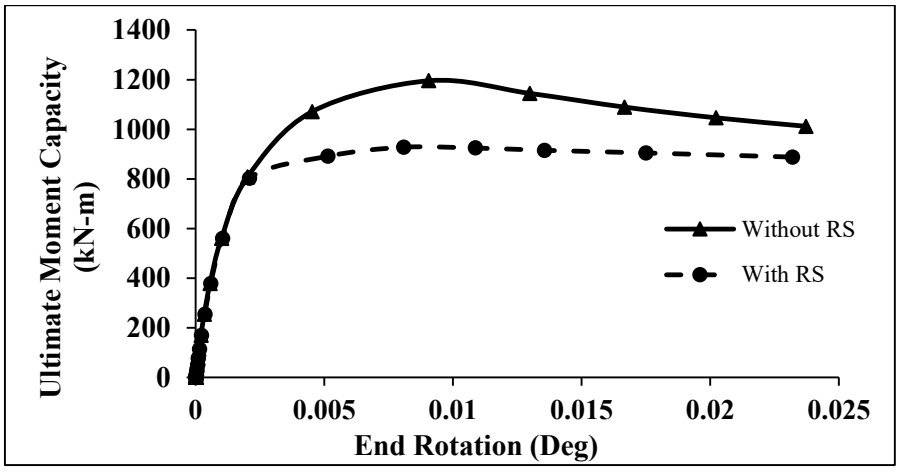

Figure 3.12: Effect of residual stress on LTB capacity of steel beams

3.3 Preliminary Validation

In this section, a preliminary validation is done using the assumptions and modelling considerations mentioned in earlier sections of this chapter. This validation is of utmost importance for the validation of experimental test which will be done in chapter 4. Therefore, a validation was implemented on W-760×185 beam with a wide range of length. This, however, is not the final validation and it includes only the comparison of the results obtained from FE analysis with current LTB resistance curve of CSA, as well as the fundamental elastic buckling as shown in Figure 3.13. In this particular case, the only uniform moment was applied to selected beam with varying range of unbraced length. In addition, FE analysis was performed without considering any residual stress and with a negligible amount of imperfection (i.e. L/10000).

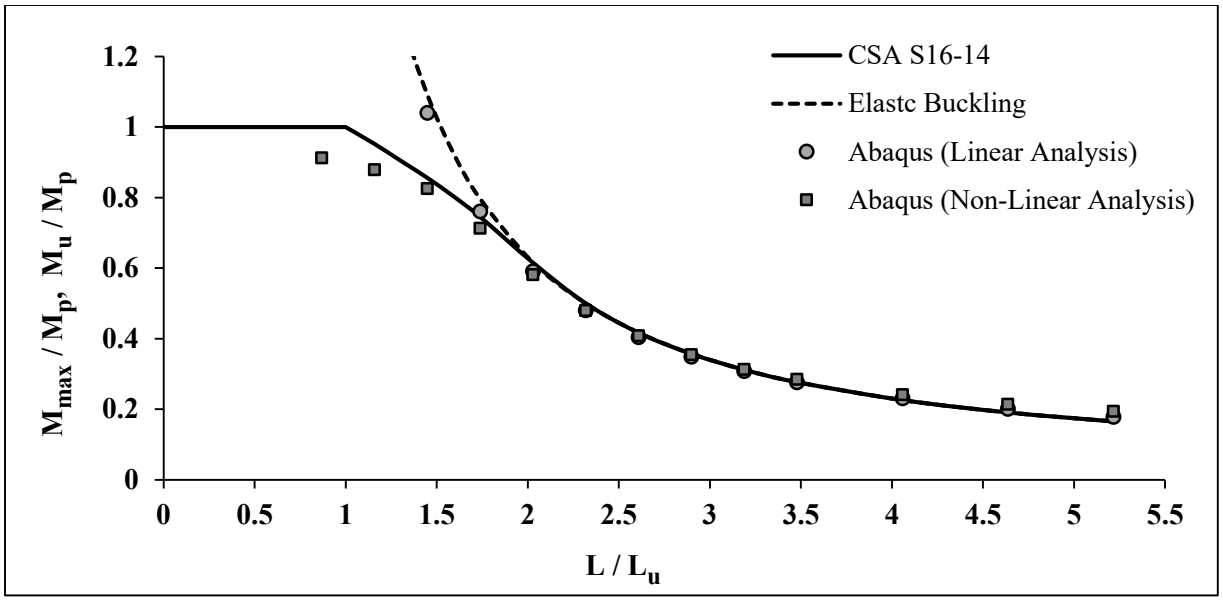

Figure 3.13: Preliminary validation of finite element model

Chapter 4: Lateral Torsional Buckling of Laterally Unsupported WWF-beams Subjected to Uniform Moment

4.1 Introduction

The CAN/CSA S16-14 strength curve is basically developed based on a statistical analysis conducted by Baker and Kennedy (1984) of Dibley's (1969) rolled I-section member tests. However, a recent statistical analysis conducted by MacPhedran and Grondin (2009) showed that current equation tends to overestimate the strength of welded beams. Therefore, this chapter primarily addresses the evaluation of current approach of strength prediction by CSA in the case of welded wide flange shape beams subjected to uniform end moment by finite element analysis.

Current LTB curve for WWF-beams in Canadian standard consists of three different parts: local buckling region, inelastic LTB region, and elastic LTB region. The LTB resistance in local buckling region is taken as a full plastic moment of the section while in other regions the LTB capacity is calculated using the equations as stated earlier in Chapter 2. It has been observed from previous studies that effect of residual stress due to welding on LTB capacity of members is more significant in the inelastic region. Thus, in this chapter, both intermediate and slender beams are analyzed for a uniform moment.

First, the finite element model as developed in chapter 3 is validated against the experimental test conducted by Dibley (1969). In addition, an extensive sensitivity analysis is performed for simply supported beam with uniform end moment considering different residual stress patterns as reported in the literature.

4.2 Validation of Finite Element Model

The FE model as developed in chapter 3 was validated for the test result of rolled I-section which had been conducted by Dibley (1969). In total 30 tests were performed on five universal beam sections with different unbraced length. The beams were tested with loads applied symmetrically at two points to provide a constant moment region and were supported at the reactions and load points to prevent lateral displacement. Since, the basic equation for critical buckling strength of an unsupported span, L was derived for idealized end support conditions and a uniform bending moment loading condition, the span of the beam should be replaced by an effective length, L_e so that the same equation can be used for any loading or support condition. The effective length was determined by the effective length factor, k. Detailed measurements of the deflected shape of test beams were also done to verify the calculated effective length factors. Reported effective length factor was ranging from 0.55 to 0.7. In addition, residual stress was measured on both surfaces of the flanges and web for each of the four sections. Results from the measurement of residual stress showed that these were similar in magnitude and distribution to those occurring in lower strength steel section

In FE model idealized simply supported beam with uniform end moment was assumed. As a result, in FE model the length of each beam section was considered to be equal to effective length as reported in the test. Thus, in total eighteen FE models were developed using the modelling technique as discussed in the previous chapter with a uniform moment of 1 kN-m applied at both ends. Material properties were taken as reported in test i.e. Fy= 516 MPa, E= 206000 MPa and Poisson ratio=0.3. Both elastic and inelastic lateral buckling response were captured from non-linear FE analysis and results were then compared with the experiment results as shown in Table 4.1. It is observed that the FE model is able to predict the LTB capacity of beam satisfactorily. The

maximum difference between test and the predicted lateral torsional buckling capacity was about 5%. A graphical comparison is also done as shown in Figure 4.1.

Table 4.1: Comparison of Finite Element Results with Test Results

Section	Length, L (m)	Effective Length Factor, k	Effective Length, L_e (m)	Plastic Section Modulus, Z_p (cm^3)	Yield Stress, F_y (MPa)	Plastic Moment, M_p (kN-m)	L_e/r_y	M_u (exp) kN-m	M_u (FE) kN-m
8×5¼ UB 17lb/ft	4.99	0.59	2.9441	277	505	139.89	94.5	91	89.16
	5.01	0.59	2.9559	280	505	141.4	94.5	84.5	82.77
	3.77	0.7	2.639	278	505	140.39	84	103.5	100.6
	2.95	0.7	2.065	278	505	140.39	65.9	131.1	127.9
	1.86	0.7	1.302	280	505	141.4	42	138.3	134.8
	5.08	0.59	2.9972	308	309	95.172	94.4	80.3	82.22
8×8 UC 58lb/ft	3.77	0.61	2.2997	1017	457	464.77	42.7	458.2	455.1
	2.15	0.7	1.505	1007	457	460.2	28	464.7	461.6
12×4 UB 19lb/ft	3.77	0.7	2.639	429	516	221.36	125	105.9	102.6
	3.29	0.7	2.303	429	516	221.36	109	118.5	119.9
	2.09	0.7	1.463	427	516	220.33	70	190	192.2
	1.05	0.7	0.735	427	516	220.33	35	217.4	231.1
	1.47	0.7	1.029	427	516	220.33	49	204.6	207.3
6×6 UC 20lb/ft	2.16	0.7	1.512	271	581	157.45	40	153.8	149.2
	4.82	0.61	2.9402	257	462	118.73	77	94.1	93.32
	6.03	0.55	3.3165	258	462	119.2	86.9	84.7	85.5
	4.34	0.58	2.5172	257	468	120.28	65.6	102.5	100.9
	4.33	0.58	2.5114	273	567	154.79	65.6	114.5	111.8

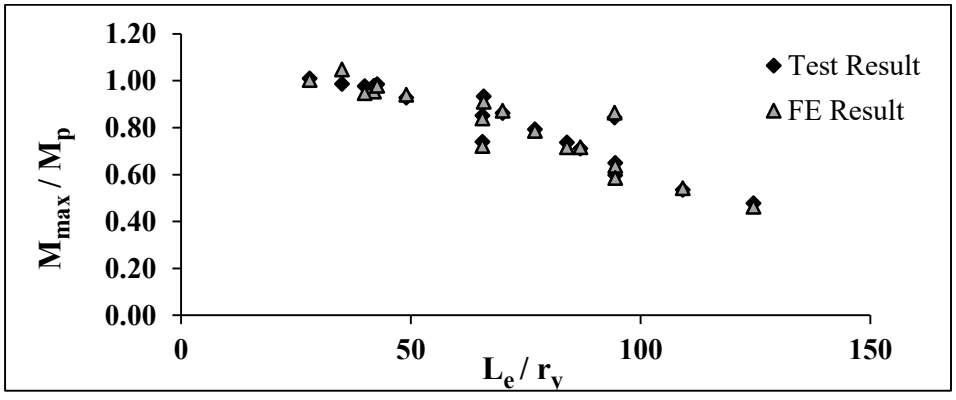

Figure 4.1: Comparison between Finite Element and Test Results

4.3 Simulation Parameters

The validated FE model is then used to perform the parametric study on LTB capacity of WWF-beams under uniform end moment condition. Therefore, this section discusses the details of different parameters such as cross-sectional dimension, initial imperfection and different patterns of residual stress.

4.3.1 Sectional Dimension

For the parametric study, 10 cross sections of WWF-beams with different length were selected with a wide range of dimensionless slenderness ratio so that the beams lie both in the intermediate and slender region. The details of chosen cross-sections are listed below in Table 4.2.

Table 4.2: Details of Cross-section

Section	1800 × 700	1800 × 510	1200 × 263	1100 × 234	1200 × 418	900 × 417	900 × 347	1100 × 458	700 × 245	700 × 175
Flange Width, b (mm)	550	500	300	300	500	550	500	550	400	300
Height, h (mm)	1800	1800	1200	1100	1200	900	900	1100	700	650
Flange Thickness, t (mm)	50	30	25	25	35	40	35	40	30	11
Web Thickness, w (mm)	20	20	16	14	16	11	11	14	11	25

4.3.2 Initial Imperfection

As discussed earlier in section 3.2.6, current Canadian code of practice restricts the amount of initial imperfection as L/1000 which is basically based on column strength curve. However, there is no tolerance limit for initial out-of-straightness in the case of designing beam considering lateral

torsional buckling effect. Therefore, in this research, all the FE analysis was done considering the initial geometric imperfection as L/1000.

4.3.3 Residual Stress

The effect of residual stress on lateral torsional buckling had been studied by several researchers and both magnitude and distribution of residual stress will be considerably different due to welding as reported by various research (Alpsten and Tall 1970; Nethercot 1974; Fukumoto 1981). Therefore, welded beams were found to have a lower lateral buckling strength than rolled beams. This effect is even more evident in the case of inelastic welded beams. Results from different experiments confirmed that residual stress is dependent on few parameters such as manufacturing processes, sectional geometry, fabrication process etc. (McFalls and Tall 1969; Alpsten and Tall 1970). However, weld type and yielding strength of material do not show any significant effect on magnitude and distribution of residual stress (Alpsten and Tall 1970). Typical residual stress patterns had also been suggested by (Chernenko and Kennedy 1991) which were based on a number of experimental measurement of residual stress as presented in the literature. For the purpose of this research, four different residual stress patterns were selected for sensitivity analysis. All of them represent of measured values in several experiments as reported in the literature. The details of selected residual stress are described in subsequent sections.

4.3.3.1 Residual Stress Measured at Lehigh University

Residual stress measured at Lehigh University is a common residual stress pattern employed in North America for various research on rolled I-section members. However, various researchers i.e. Beedle and Tall (1960), Nagaraja Rao and Tall (1961), Estuar and Tall (1963), Tall (1964b), Nagaraja Rao et al. (1964), Alpsten and Tall (1970) etc. measured residual stress for welded shapes

manufactured from mill plate. On the other hand, an attempt was made by McFalls and Tall (1969), Alpsten and Tall (1970), Alpsten (1972a, b), and Bjorhovde et al. (1972) to investigate the strength of welded shape made from flame cut plate. However, all the measured residual stresses correspond to column type sections and summarized by Chernenko and Kennedy (1991) with typical shapes and range of maximum compressive and tensile stresses. Therefore, in this study two types of residual stress pattern i.e. mill plate and flame cut plate with the upper bound of compressive and tensile residual stresses as reported by Chernenko and Kennedy (1991) are considered to examine the sensitivity of LTB curve due to these type of residual stress. Selected residual stress patterns are illustrated in following Figure 4.2.

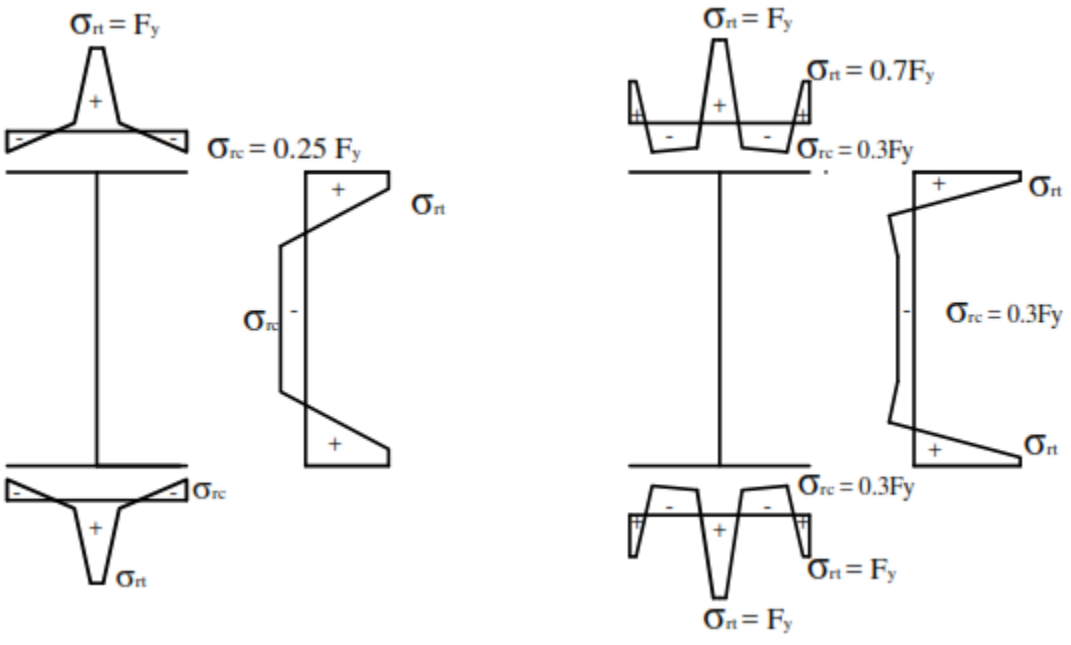

(a) (b)

Figure 4.2: Residual Stress measured (a) mill plate and (b) flame cut type at Lehigh University

4.3.3.2 Residual Stress Measured by Fukumoto and Itoh (1981)

Fukumoto and Itoh (1981) prepared thirty-four nominally identical cross-sections of welded I-250×100×6×8 mm (ordinary mild steel) with a span length of 5.02 m. However, a short beam had been cut out for residual stress measurement. Hence, longitudinal residual stresses were measured by sectioning method on both side of flanges and webs where the optimum mesh sizes of sectioning were even smaller than those for the rolled beams. Reported residual stress patterns in this welded beam-type sections are somewhat different in the flange compared to the patterns for the column-type section (Nagaraja Rao and Tall (1961), McFalls and Tall (1969)) as shown in Figure 4.4. Therefore, the sensitivity of LTB resistance due to this type of residual stress pattern is also evaluated.

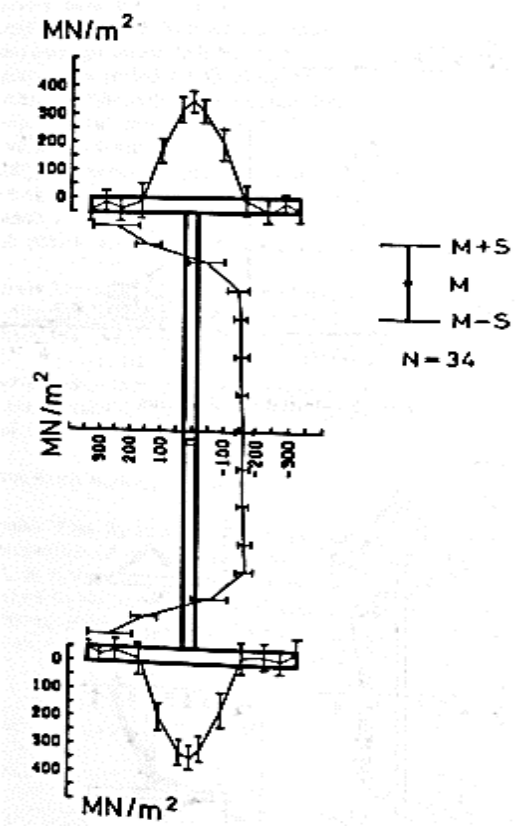

Figure 4.4: Residual Stress Measured by Fukumoto and Itoh (1981)

4.3.3.3 Residual Stress Measured by Dux and Kitipornchai (1983)

Dux and Kitipornchai (1983) made six sets of residual strain measurements following the sectioning method for hot rolled beam. The measurement was done on opposite sides of both flanges and webs. Thus, mean values of residual strain were obtained and using a Young's modulus of 2.099×10^5 MPa the value of residual stress was calculated as shown in Figure 4.5. It should be mentioned that other test programs such as Dibley (1969) also found residual stresses similar to those measured by Dux and Kitipornchai in the case of rolled beams. Hence, the purpose of choosing this residual stress pattern was to investigate the sensitivity of current code equations to this type of residual stress.

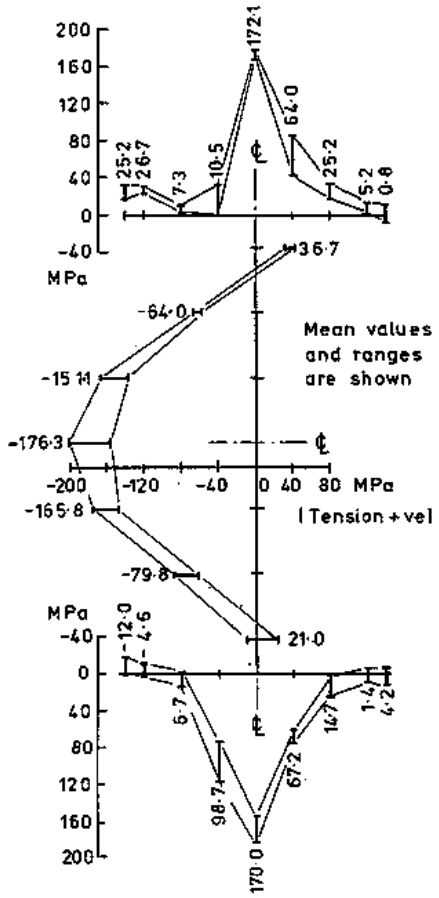

Figure 4.5: Residual Stress Measured by Dux and Kitipornchai (1983)

4.4 Sensitivity Analysis on Welded Beams

In this section, LTB curves are developed from the results of FE analysis for ten welded wide flange shape beams using various residual stress patterns as shown in from Figure 4.3 to Figure 4.5 with an initial geometric imperfection of L/1000. Thus, this sensitivity study aims to find out the influence of various residual stresses pattern on LTB resistance curve. All the members are modelled with simply supported boundary condition using FE program for equal and opposite moments applied at both ends. FE models are developed following the modelling technique as described in chapter 3. Figure 4.6 shows a representative sketch of the FE model used in all simulations.

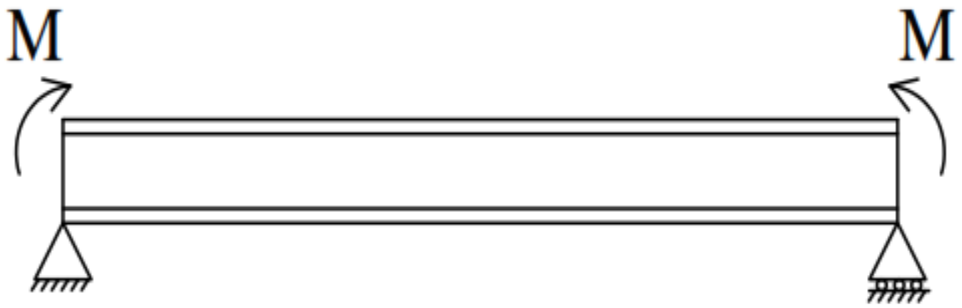

Figure 4.6: Simply Supported Beam with Equal End Moment

Results from FE analysis were non-dimensionalized and plotted along with CSA strength curve. Therefore, maximum moment capacities, M_{max} obtained from FE analysis are non-dimensionalized by plastic moment, M_p of the corresponding section while lengths are non-dimensionalized by minimum unbraced length, L_u of the corresponding section. Thus, M_{max}/M_p vs L/L_u graph is drawn for all those sections as listed in table 4.1. Figure 4.7(a) to Figure 4.7 (j) present the results of FE analysis along with CSA curve for various residual stress pattern. In addition, FE results for zero residual stress with a negligible amount of imperfection (L/20000) are included in these plots to get a clear view on effects of residual stress.

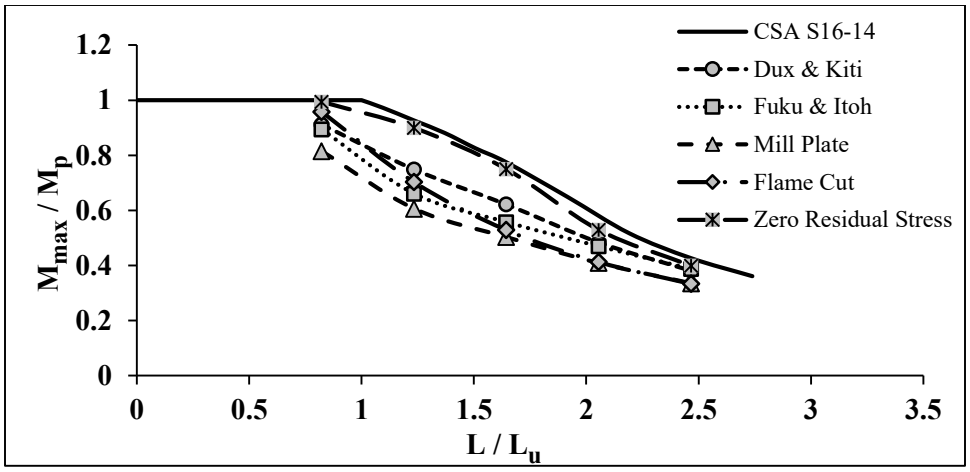

(a) WWF-1800×700

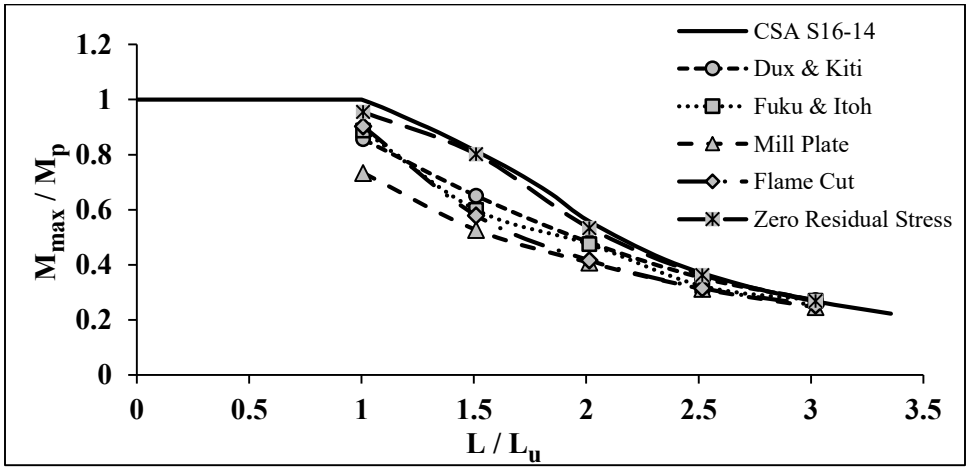

(b) WWF-1800×510

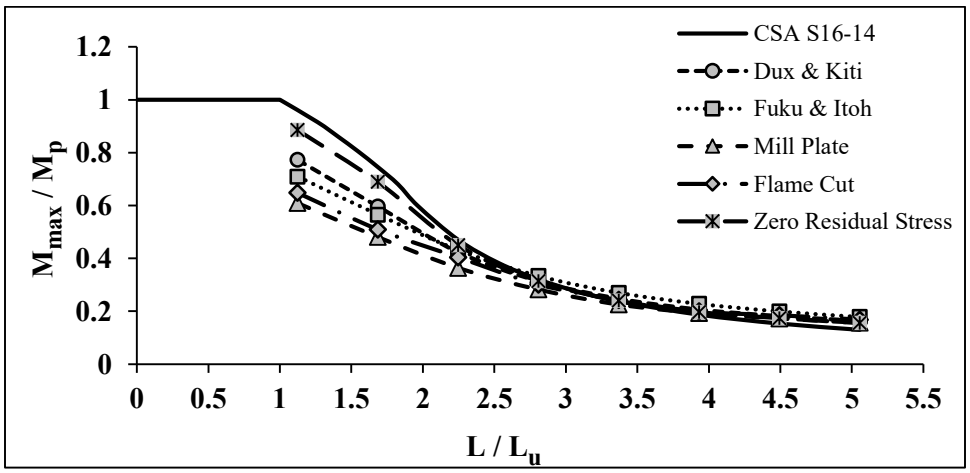

(c) WWF-1200×263

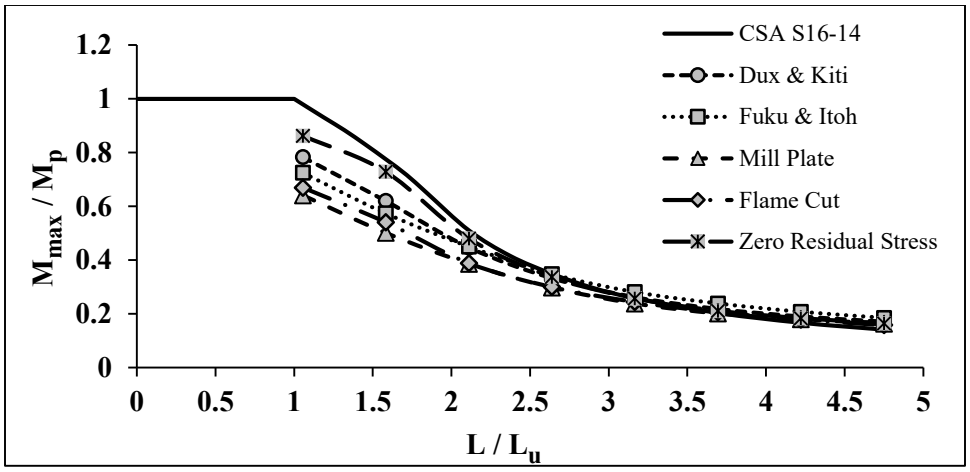

(d) WWF-1100×234

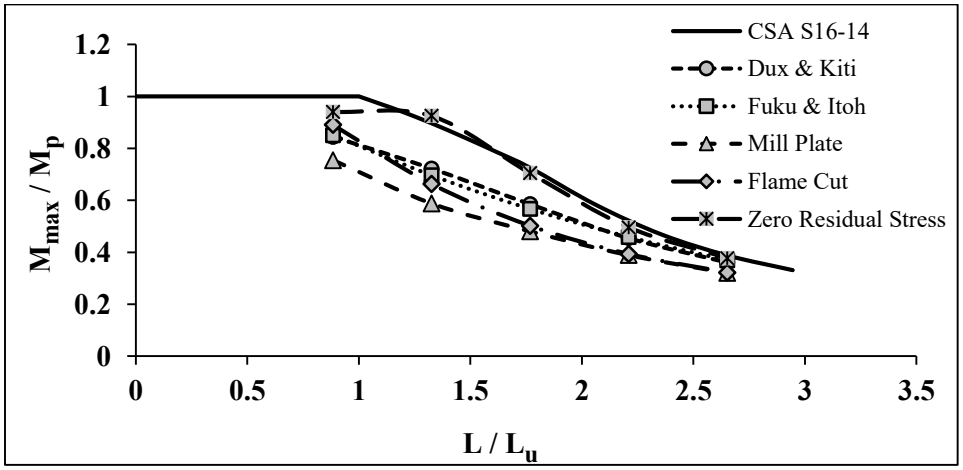

(e) WWF-1200×418

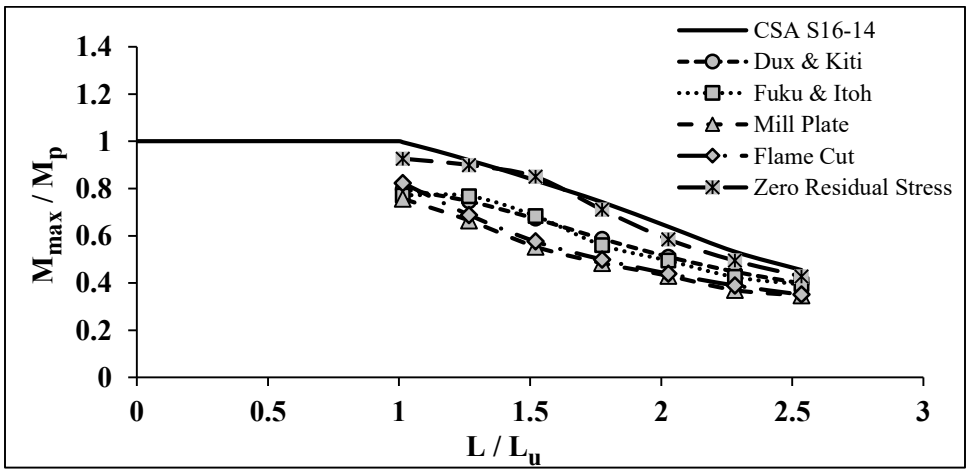

(f) WWF-1100×458

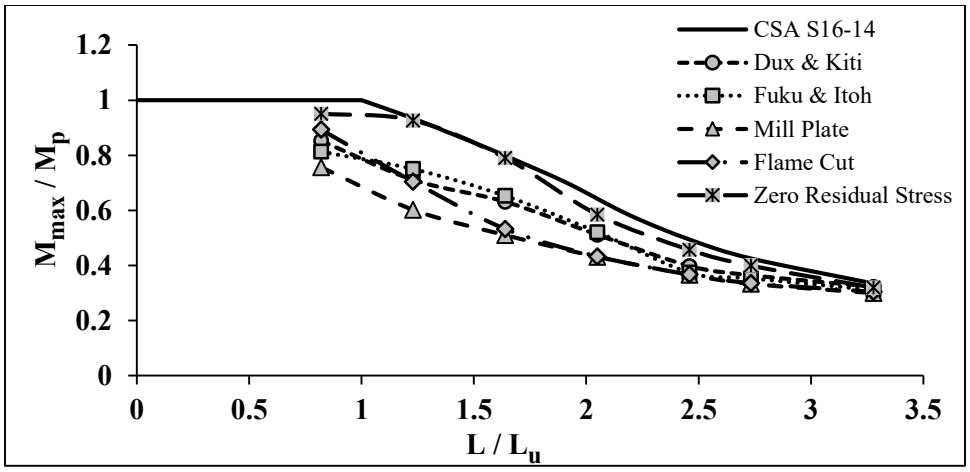

(g) WWF-900×347

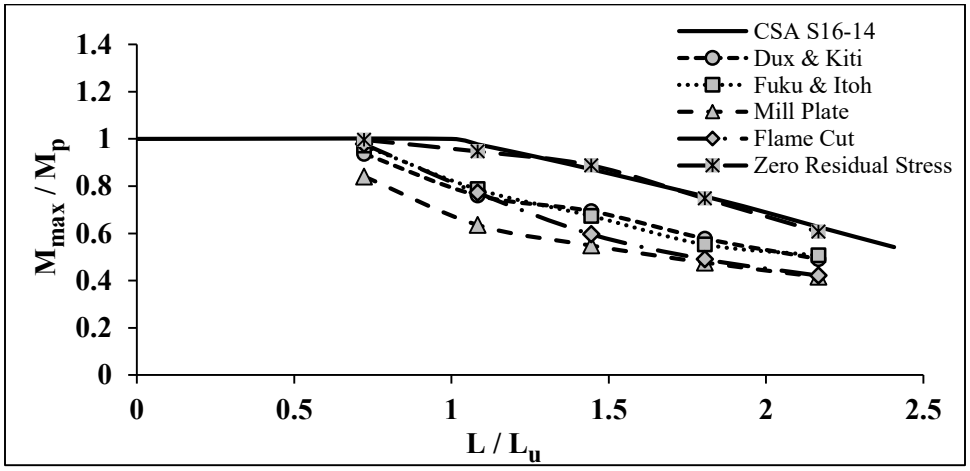

(h) WWF-900×417

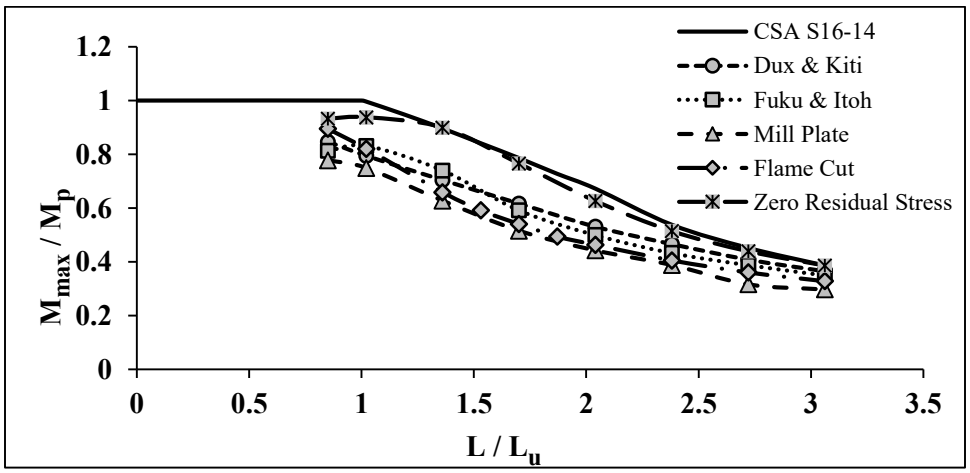

(i) WWF-700×245

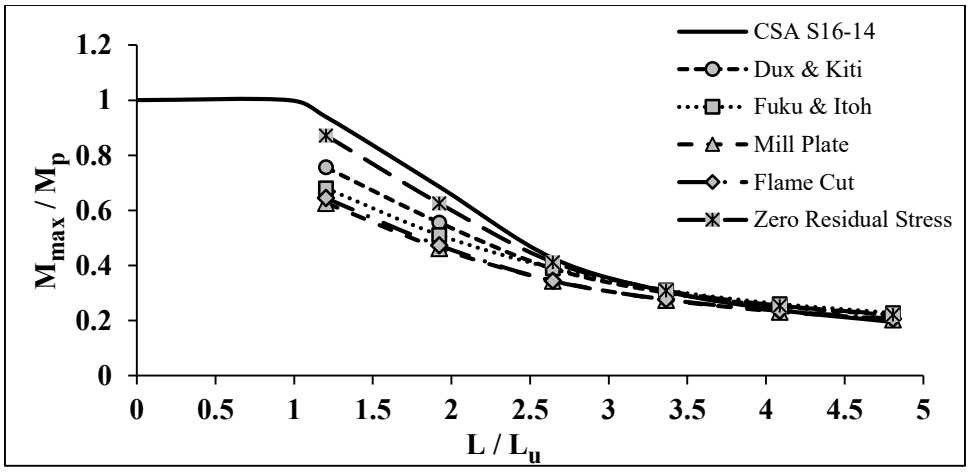

(j) WWF-700×175

Figure 4.4. LTB resistance curves for various WWF-beams with different residual stress pattern

A similar trend (i.e. difference between FE and code results are large in the inelastic range of LTB and becomes small as it goes to the elastic range, more discrepancies in the case of the deep beam than shallow one) has been found from the above plots of all sections considering various residual stress pattern. So, it is imperative to say that sensitivity of member capacities due to welding type residual stress is mostly significant in inelastic LTB region. Moreover, it is clear from the above plots that, FE results which correspond to "Dux and Kiti" type residual stress fit more close with current code than others. This is because of its being rolled-beam type stress distribution. Another significant observation can be made from the plots that, both "Dux and Kiti" and "Fuku and Itoh" type residual stress often gives higher member capacities (i.e. WWF-1200×263, WWF-1100×234, WWF-700×175) than the CSA strength curve particularly in the range of elastic LTB.

Among the three of welding-type residual stresses, "Fuku and Itoh" type predicts higher member capacities than other two. One of the reasons behind this behavior is a measurement of reported residual stress was done for beam type sections. Also, the presence of high tensile residual stress along the flanges facilitates to carry more end moments before lateral buckling occurs. However,

Lehigh pattern which is a common residual stress pattern employed in North America gives the lower resistance throughout the entire analysis. Particularly, mill plate type residual stress gives smallest capacities while flame cut type residual stress gives larger capacities than mill plate type residual stress but smaller than other two. This trend has been observed in all range of LTB region. The reason behind giving higher capacities than mill plate type residual stress by flame cut type is due to the presence of high tensile stress at flange tips which consequently compensate the compressive stress in flanges.

As shown in Figure 4.4 (a) to Figure 4.4 (j), the plastic moment capacity has never been achieved from FE analysis in the case of zero residual stress and a negligible amount of imperfections. However, corresponding FE results of this case show sufficiently close agreement with current strength curve of CSA both in the inelastic and elastic range of LTB. At this point, it is essential to look into the effect of each type of residual stress on LTB capacities of all members individually which can be understood from the graphs shown in Figure 4.8 (a) to Figure 4.8 (e). Therefore, ultimate moment capacity, $M_{ultimate}$ both from code and FE analysis is been non-dimensionalized by dividing it by the plastic moment, M_p of the corresponding section. Also, a modified slenderness ratio, $\lambda = \sqrt{M_p / M_u}$ is also defined where, M_u is the elastic moment capacity of beam calculated from Equation 2.1. Thus, plots, as shown in Figure 4.8, are developed taking $M_{ultimate} / M_p$ and $\sqrt{M_p / M_u}$ along the Y and X axis respectively. In addition to this, proposed equation by MacPhedran and Grondin as discussed in chapter 2 is plotted in these graphs with a recommended value of n=1.9. Moreover, proposed strength curves by different design standard i.e. AISC, EC are plotted to make the comparison. These curves are developed based on the LTB design equation as specified in the corresponding standard which is discussed in Chapter 2.

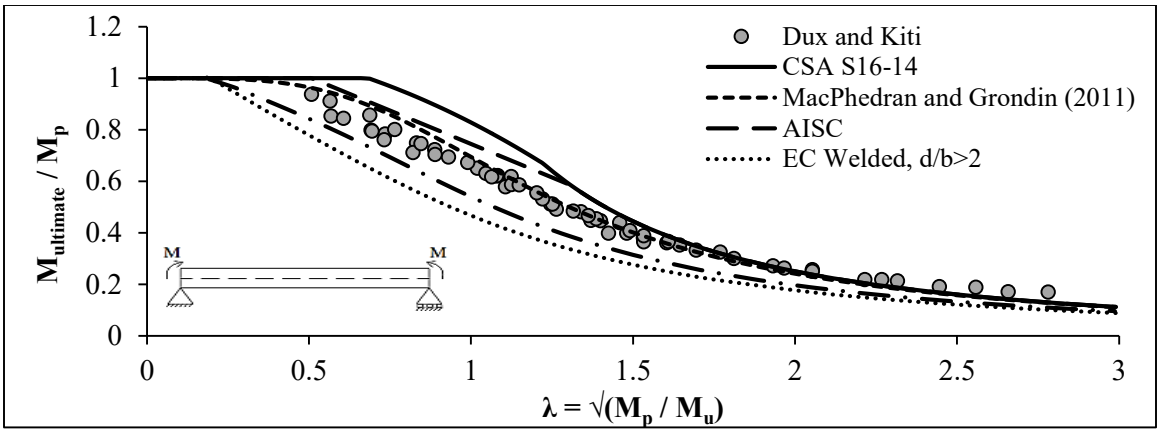
Dux and Kiti
CSA S16-14
MacPhedran and Grondin (2011)
AISC
EC Welded, d/b>2
M
M
$M_{ultimate} / M_p$
$\lambda = \sqrt{(M_p / M_u)}$
0
0.2
0.4
0.6
0.8
1
1.2
0.5
1.5
2
2.5
3

(a)

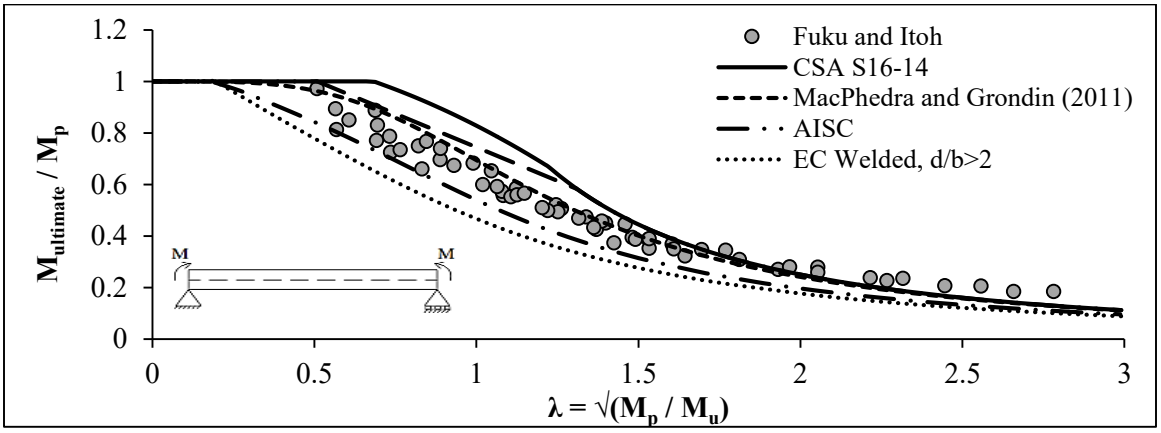
Fuku and Itoh
CSA S16-14
MacPhedra and Grondin (2011)
AISC
EC Welded, d/b>2
M
M
$M_{ultimate} / M_p$
$\lambda = \sqrt{(M_p / M_u)}$
0
0.2
0.4
0.6
0.8
1
1.2
0.5
1.5
2
2.5
3

(b)

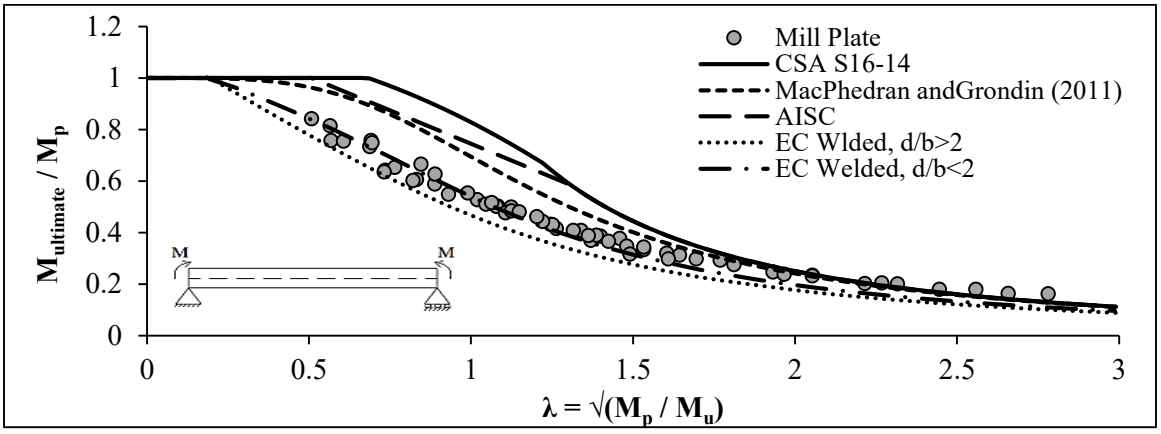
Mill Plate
CSA S16-14
MacPhedran andGrondin (2011)
AISC
EC Wlded, d/b>2
EC Welded, d/b<2
M
M
$M_{ultimate} / M_p$
$\lambda = \sqrt{(M_p / M_u)}$
0
0.2
0.4
0.6
0.8
1
1.2
0.5
1.5
2
2.5
3

(c)

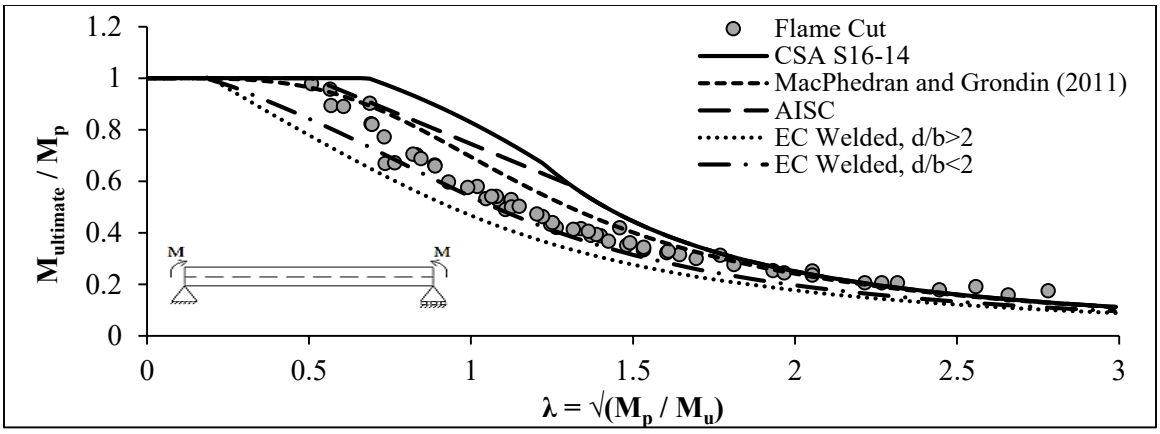

(d)

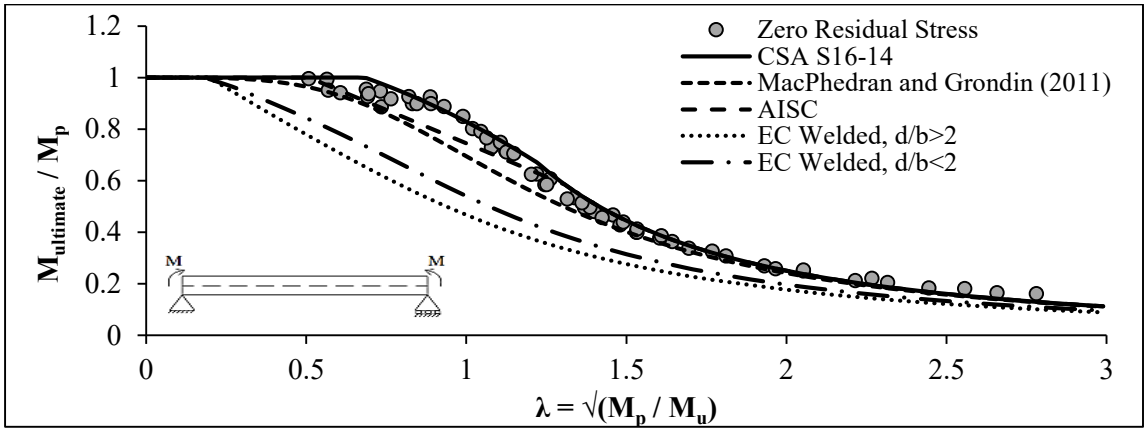

(e)

Figure 4.8: Finite element results vs CSA code values for (a) "Dux and Kiti", (b) "Fuku and Itoh", (c) Mill Plate, (d) Flame Cut and (e) Zero type residual stress

From the demonstration in Figure 4.8 (a) to Figure 4.8 (d), most of the FE results are found under the strength curve of CSA S16-14 in all cases of residual stress. It is interesting to note that, both AISC and CSA overestimate capacities significantly in the inelastic range of LTB while both of the specification predict well in the elastic zone of LTB. But, Eurocode predicts lower capacities almost in every instance and unlike the two north American standards, it predicts the member capacities satisfactorily in the inelastic region of LTB especially in the case of mill plate and flame cut type residual stress. Thus, it can be said that CSA strength curve somewhat overestimates the

LTB capacity of welded beams. But, almost all results for zero residual stress lie on the strength curve of CSA S16-14. To discuss the results quantitatively, all FE results are listed in Table 4.3 as a function of various residual stresses and compared with code values as a percentage.

Table 4.3: Finite Element Results and Comparison with CSA S16-14

Section	Length (m)	M_{code} (kN-m)	FE Analysis Result and Comparison with CSA S16-14									
			Dux and Kiti	% diff	Fuku and Itoh	% diff	Mill Plate	% diff	Flame Cut	% diff	Zero Residu-al Stress	% diff
WWF 1200×263	4	4778	3838	20	3522	26	3127	35	3219	33	4398	7.9
	6	3700	2961	20	2808	24	2388	35	2531	32	3423	7.5
	8	2333	2103	10	2142	8	1809	22	2007	14	2235	4.2
	10	1589	1558	2	1655	-4	1402	12	1496	6	1561	1.8
	12	1178	1228	-4	1339	-14	1121	5	1203	-2	1193	-1.3
	14	927	1024	-11	1132	-22	959	-3	987	-7	980	-5.8
	16	760	901	-19	989	-30	858	-13	917	-21	865	-13.8
	18	642	812	-26	885	-38	778	-21	836	-30	772	-20.2
WWF 1800×700	6	22000	19997	9	19617	11	17883	19	21016	4	21810	0.9
	9	20333	16427	19	14500	29	13302	35	15424	24	19733	3.0
	12	17000	13640	20	12230	28	11035	35	11604	32	16455	3.2
	15	12479	10620	15	10303	17	8969	28	9062	27	11612	6.9
	18	9356	8363	11	8499	9	7354	21	7324	22	8763	6.3
WWF 1800×510	6	14556	12529	14	12998	11	10736	26	13206	9	13972	4.0
	9	11889	9522	20	8770	26	7710	35	8475	29	11730	1.3
	12	8167	7055	14	6948	15	5976	27	6087	25	7814	4.3
	15	5418	5159	5	4725	13	4577	16	4609	15	5310	2.0
	18	3922	3975	-1	3953	-1	3605	8	3694	6	3934	-0.3
WWF 1100×234	4	4100	3290	20	3045	26	2693	34	2813	31	3724	9.2
	6	3256	2605	20	2410	26	2105	35	2271	30	3060	6.0
	8	2144	1879	12	1891	12	1622	24	1633	24	2017	5.9
	10	1467	1399	5	1462	0	1250	15	1260	14	1419	3.3
	12	1087	1102	-1	1180	-9	1002	8	1028	5	1083	0.3
	14	856	918	-7	1002	-17	846	1	866	-1	888	-3.8
	16	702	800	-14	871	-24	757	-8	752	-7	772	-9.9
	18	594	720	-21	777	-31	688	-16	665	-12	693	-16.6

WWF 1200×418	6	8956	7568	15	7624	15	6763	24	7979	11	8431	5.9
	9	8033	6473	19	6239	22	5270	34	5942	26	8292	-3.2
	12	6500	5245	19	5077	22	4309	34	4499	31	6314	2.9
	15	4617	4075	12	4109	11	3488	24	3525	24	4443	3.8
	18	3478	3236	7	3307	5	2872	17	2888	17	3381	2.8
WWF 900x417	6	7278	6825	6	7076	3	6125	16	7125	2	7250	0.4
	9	7111	5539	22	5732	19	4631	35	5623	21	6896	3.0
	12	6344	5052	20	4909	23	3995	37	4344	32	6465	-1.9
	15	5502	4209	24	4027	27	3470	37	3571	35	5447	1.0
	18	4567	3579	22	3691	19	3029	34	3067	33	4421	3.2
WWF 900×347	6	5989	5103	15	4869	19	4531	24	5348	11	5693	4.9
	9	5589	4255	24	4492	20	3604	36	4219	25	5547	0.7
	12	4778	3778	21	3907	18	3054	36	3189	33	4732	1.0
	15	3857	3062	21	3120	19	2582	33	2592	33	3501	9.2
	18	2956	2382	19	2238	24	2192	26	2196	26	2735	7.5
	20	2544	2180	14	2113	17	1996	22	2011	21	2391	6.0
	24	1998	1929	3	1861	7	1793	10	1821	9	1911	4.3
WWF 1100×458	8	9444	7573	20	7311	23	7181	24	7809	17	8788	7.0
	10	8722	7080	19	7283	17	6306	28	6527	25	8530	2.2
	12	7911	6378	19	6484	18	5251	34	5461	31	8060	-1.9
	14	7044	5574	21	5317	25	4593	35	4740	33	6742	4.3
	16	6056	4849	20	4693	23	4082	33	4169	31	5544	8.4
	18	5056	4251	16	4037	20	3509	31	3697	27	4692	7.2
	20	4322	3779	13	3743	13	3289	24	3330	23	4059	6.1
WWF 700×245	5	3222	2730	15	2621	19	2507	22	2885	10	3010	6.6
	6	3211	2561	20	2681	17	2415	25	2647	18	3023	5.9
	8	2889	2270	21	2386	17	2023	30	2125	26	2900	-0.4
	10	2533	1989	21	1908	25	1663	34	1744	31	2468	2.6
	12	2167	1712	21	1611	26	1427	34	1494	31	2019	6.8
	14	1733	1504	13	1396	19	1252	28	1307	25	1658	4.3
	16	1456	1318	9	1251	14	1021	30	1163	20	1417	2.6
	18	1244	1179	5	1129	9	959	23	1058	15	1246	-0.1
WWF 700×175	5	2056	1656	19	1489	28	1372	33	1411	31	1908	7.2
	8	1500	1217	19	1117	26	1012	33	1035	31	1368	8.8
	11	932	850	9	853	8	754	19	753	19	902	3.2
	14	668	658	1	678	-2	602	10	605	9	675	-1.1
	17	520	549	-6	569	-9	508	2	515	1	555	-6.7
	20	426	479	-12	497	-17	447	-5	452	-6	484	-13.6

From the above Table 4.3, it is observed that FE simulation gives up to 37% smaller capacities than CSA strength equation in the inelastic region of LTB for WWF-900×417 at an unbraced length of 12m and 15m for mill plate type residual stress. However, current CSA equation is found to be conservative by 1.9% at 12m length and only 1% un-conservative at the length of 15m for the same section without considering any residual stress. In addition, current equation never appears to be conservative in the region of inelastic LTB of any section considering any of the four residual stresses while it overestimates for some cases (i.e. WWF-700×175, WWF-1100×234 and WWF-1200×263) in the region of elastic LTB particularly for "Dux and Kiti" and "Fuku and Itoh" type residual stress. FE simulation predicts up to 38% higher capacities than CSA equation in this region for WWF-1200×263 at an unbraced length of 18m taking "Fuku and Itoh" type residual stress. Moreover, FE results for zero residual stress and a negligible amount of initial imperfection almost match with CSA equation as shown in Figure 4.8 (e) with a maximum under prediction of 9.2% for WWF-1100×234 at a length of 4m which is very close to its maximum limit of unbraced length.

A similar trend (i.e. difference of FE result and CSA equation is more at a close length of the plastic region of LTB) has also been observed for other sections considering zero residual stress.

4.5 Summary

In this chapter, detailed sensitivity study has been performed for welded shape beams considering various types of residual stress pattern using the validated finite element model. All the FE analyses are done for simply supported beam subjected to equal end moment. In addition, analyses are done without considering any residual stress to get a clear view about the effect of various residual stress on LTB resistance. After that, CAN/CSA S16-14 strength curve for LTB has been evaluated based

on the findings from FE analysis. It has been observed that current equation overestimates the LTB resistance capacities of welded shape beams in case of simply supported beam with equal end moment. At this stage, it is required to evaluate the current strength curve for other moment gradient which will be discussed in next chapters.

Chapter 5: Lateral Torsional Buckling of Laterally Unsupported WWF-beams Subjected to Linear and Non-linear Moment Gradient

5.1 Introduction

In Chapter 4, current LTB resistance equation is evaluated for uniform moment gradient along the length of the beam. It has been observed that current approach overestimates the member capacities for all type residual stress especially significant amount of overestimation has been found for mill plate type residual stress. However, uniform moment condition is considered as a severe condition that may not come in a practical situation. Therefore, it is essential to evaluate the performance of current approach for other load configuration. CSA S16-14 accounts for moment gradient by applying an LTB moment modification factor, ω_2 on the resistance equations for a uniform moment. The modifier, ω_2 is taken equal to 1.0 for a uniform moment. However, a general equation has been provided to use for any moment distribution which was introduced by Wong and Driver (2010). The solution is given as

$$\omega_2 = \frac{4\,M_{max}}{\sqrt{M_{max}^2 + 4\,M_a^2 + 7M_b^2 + 4M_c^2}} \leq 2.5 \qquad [5.1]$$

where M_{max}, M_a, M_b, M_c represent absolute values of maximum, first, second and third quarter moment along the unbraced length of a section for a given load configuration.

This chapter evaluates the current CSA curve of LTB for welded beams by FEA considering various moment gradient loadings. Additionally, FE results are compared with other strength curves recommended by various design standards such as AISC, Eurocode etc. as well as by other

researchers i.e. MacPhedran and Grondin. Thus, all the results including different strength curves are non-dimensionalized in the same way as it is done in Chapter 4. It should be noted that all FE simulations are performed considering mill plate type residual stress and initial imperfection of L/1000.

5.2 Evaluation of CSA Strength Curve for Welded Beams Subjected to Linear Moment Gradient

Ten welded beams listed in Table 4.2 are studied here for linear moment diagrams, as shown in Figure 5.1. This section evaluates the performance of current LTB equation of CSA considering moment gradients with β = 0.5, 0 and -1, which returns values of ω_2 equal to 1.3, 1.75 and 2.3 from Equation 5.1 respectively.

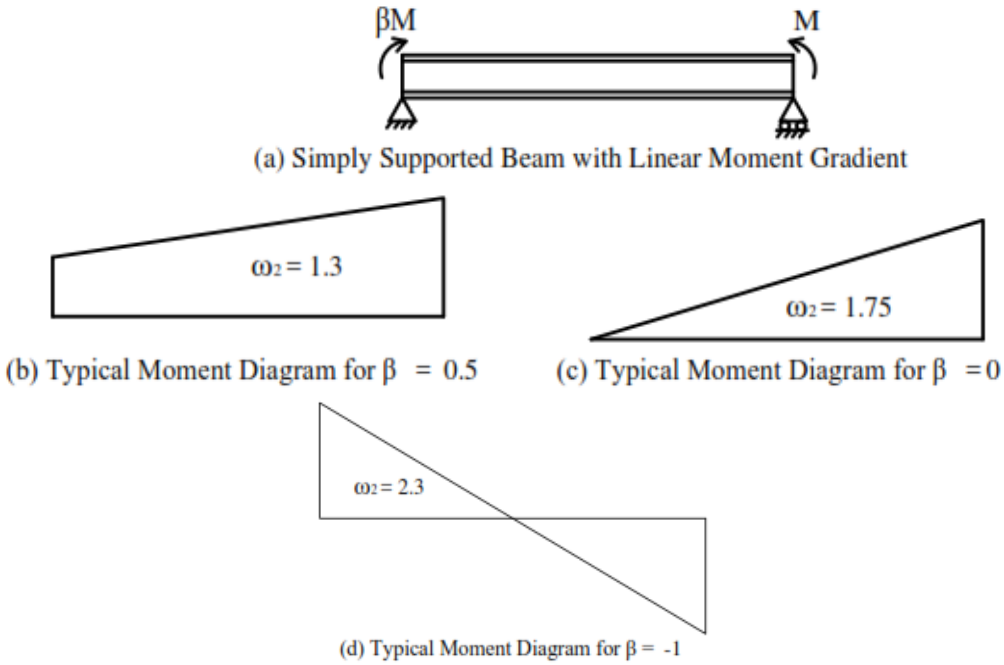

Figure 5.1: Typical moment diagram for different moment gradient

Finite element results for different linear moment gradient as summarized in APPENDIX B are non-dimensionalized following the same way as followed earlier in Chapter 4. Thus, Figure 5.2

(a), (b) and (c) show the comparison of FE results and CSA S16-14 strength considering various linear type moment gradient in which $M_{ultimate}/M_p$ is in ordinate and $\lambda = \sqrt{M_p/M_u}$ is in abscissa. Different strength curves are also plotted for comparison.

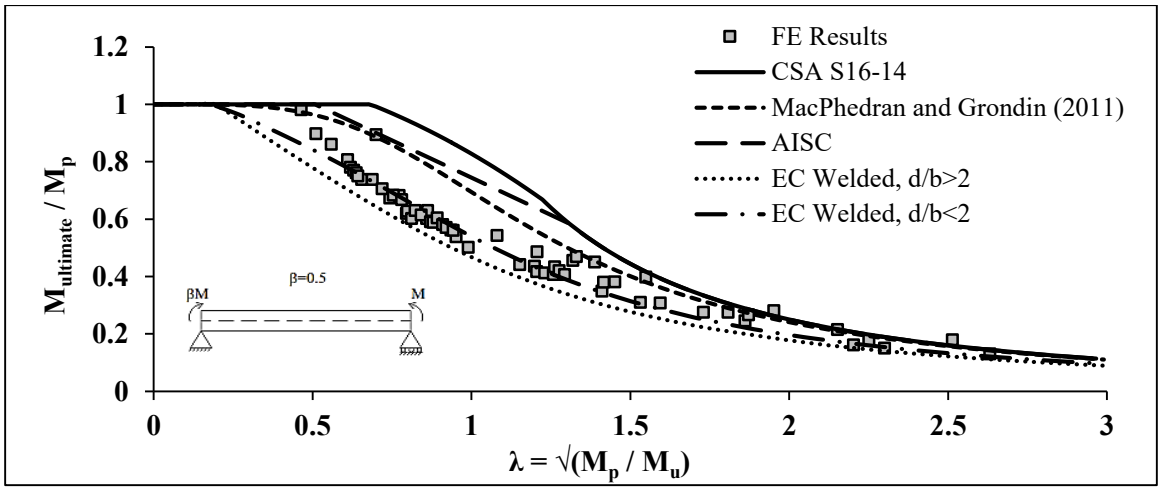

(a) $\omega_2 = 1.3$

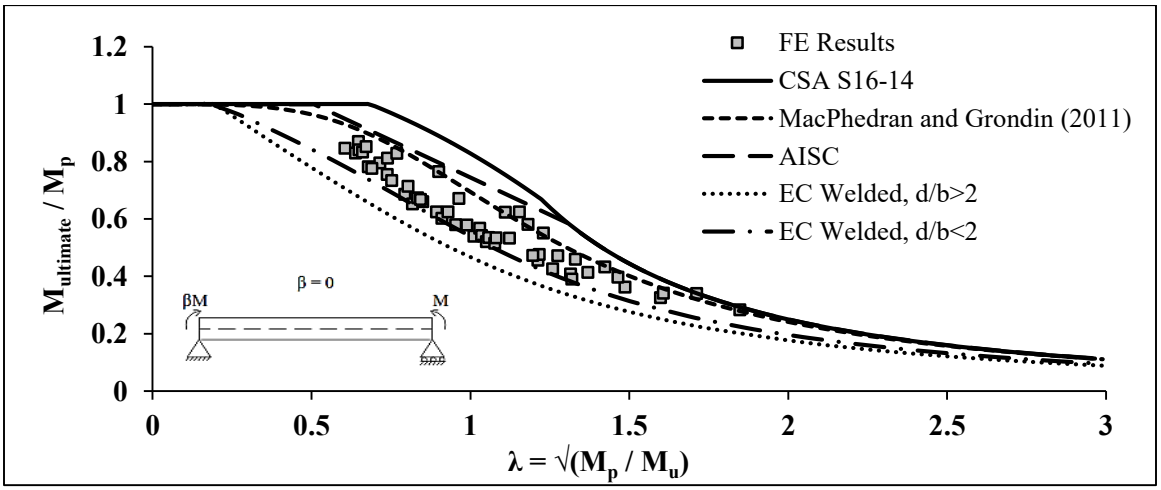

(b) $\omega_2 = 1.75$

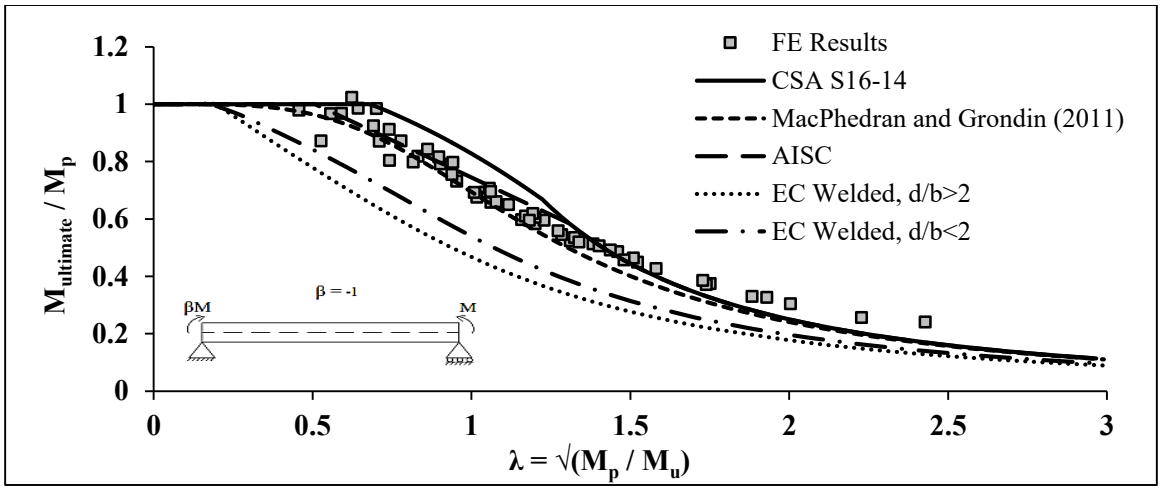

(c) $\omega_2 = 2.3$

Figure 5.2: Moment gradient LTB curves for (a) ω_2 = 1.3, (b) ω_2 = 1.75 and (c) ω_2 = 2.3

The followings can be assembled from Figure 5.2 (a) to Figure 5.2 (c):

1. In all graphs, a significant difference is observed in the region of inelastic LTB while less amount of difference is found in the elastic region of LTB. This trend is similar to the results found in cases for constant moment gradient. However, the difference between simulation results and code values are less in all these cases (i.e. linear moment gradient) compared to constant moment gradient. The maximum overestimation is observed as 40.1 % for WWF- 900×417 beam with 18m length in case of $\omega_2 = 1.3$. Also, simulation results are higher than strength predicted by CSA specification in many cases and the maximum underestimation is found as 42% for WWF- 1100×234 beam with 30m length in case of $\omega_2 = 2.3$.
2. Current CSA S16-14 strength curve overestimates significantly in cases of both $\omega_2 = 1.3$ and $\omega_2 = 1.75$ while it essentially coincides with FE results for cases with $\omega_2 = 2.3$. Full plastic capacity has never been achieved by FE analysis for $\omega_2 = 1.75$, whereas

it has been achieved or shows less difference with specification for $\omega_2 = 1.3$ in local buckling region. However, the highest difference has been observed within the inelastic region of LTB in cases of $\omega_2 = 1.3$ (40.1%) compared to $\omega_2 = 1.75$ (34.57 %). But, FE results fits more closely to current strength curve within the elastic range for $\omega_2 = 1.3$ than $\omega_2 = 1.75$. It is also seen that; FE analysis gives larger resistance than predicted strength by current specification in few cases for $\omega_2 = 1.3$ within this range of buckling. On the other hand, FE results for $\omega_2 = 2.3$ show sufficiently good agreement with current specification although some discrepancies can be observed within the inelastic region. Most of the cases the plastic capacity of a member is been attained or found very close to code values in local buckling region. In addition, very few FE results are found to lie beneath the strength curve within the elastic zone of buckling.

3. A significant difference has been observed between FE results and current specification in the inelastic range of buckling for all three bending cases. This is because, while ω_2 yields a higher elastic buckling strength, the inelastic LTB strength in the inelastic region becomes higher. Since current code calculates inelastic buckling capacities of member considering the modified elastic buckling for non-uniform moment gradient.
4. It is also interesting to note that current specification is found conservative within elastic buckling region, unlike the inelastic zone. This is particularly evident for bending case with $\omega_2 = 2.3$. This is because, the uniform moment gradient factor ω_2, that is currently calculated in the specifications for various moment gradient (equation 5.1) represents a lower bound to the actual value. This is clear from the above Figure 5.2 (c) where the FE results are found higher in most cases than the resistance equations in the zone of elastic buckling.

5. Unlike the other codes, Eurocode shows sufficiently good agreement with FE results in all three cases (i.e. closely match with FE result for $\omega_2 = 1.3$, slightly underestimates for $\omega_2 = 1.75$ and highly underestimates for $\omega_2 = 2.3$).

From the above discussions, it can be observed that current approach of predicting LTB resistance of WWF-beams by Canadian code is not as much severe in the case of linear moment gradient as it is for a constant moment. Hence, it is important to evaluate the performance of current strength curve for other loading configuration.

5.3 Validation of FE model for Non-linear Moment Gradient

In order to assess the performance of current strength curve for LTB, it is necessary to validate the FE model with experiment test values in the case of non-linear moment gradient. The similar modeling technique as used in the previous analysis has been adopted for validation except the load application scheme. Thus, the concentrated load is applied on a small area of top flange, centroid and bottom flange at mid-span of the beam to avoid premature local buckling and undesirable stress concentration at supports. The magnitude of each concentrated load is selected in a way so that the total amount of load remains as 1kN. On the other hand, for uniformly distributed load, a series of concentrated load are applied to the middle line of top flange, centroid, and bottom flange of the beam as shown in Figure 5.3. In this case, the magnitude of each concentrated load is set to apply a uniform load of 1kN/m. This section describes the test configuration for selected experiments and thus compares the FE results with those test results considering concentrated load applied at mid-span of the beam.

5.3.1 Fukumoto et al (1980)

Fukumoto et al (1980) performed an experimental investigation of laterally unsupported beams from statistical consideration. Twenty-five 7m long members having the nominally identical cross-section of rolled I-200 mm × 100 mm × 5.5 mm × 8 mm were prepared for this test. From each of those members, three groups of the beam with a span length of 2.6 m, 2.0 m, and 1.5 m were cut out. Thus, in total 75 beams were tested under a concentrated load applied vertically at the mid-span of the top flange. All the tested beams were simply supported and restrained at their supports against torsion but not against warping. Two short beams were also cut out from each of the members for tensile coupon test and as well as for residual stress measurement. Figure 5.4 illustrates the test beams and the mean value of measured residual stresses.

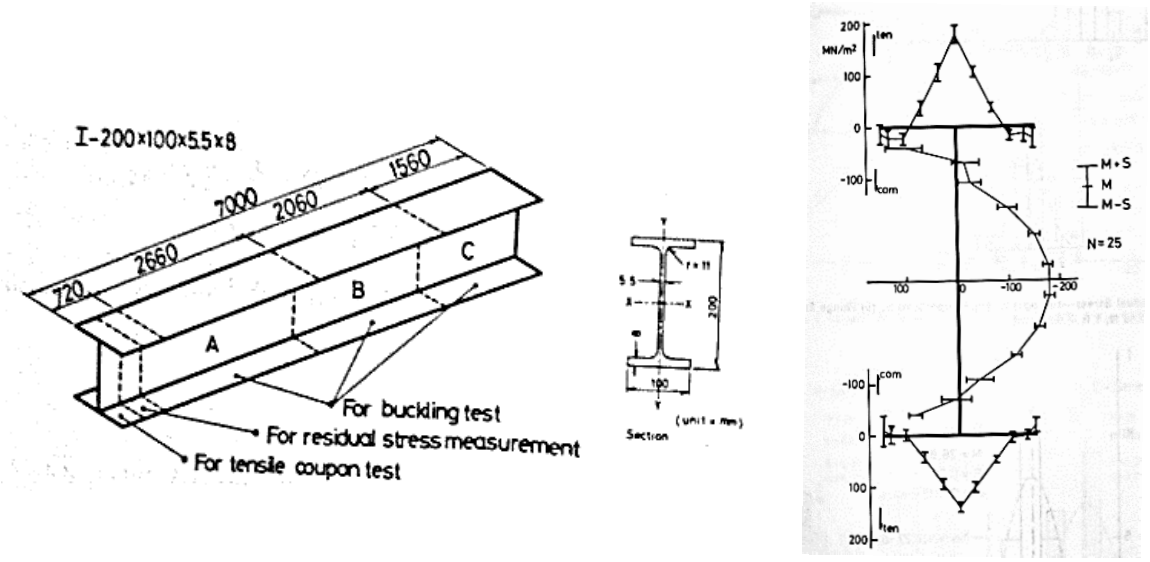

Figure 5.4: Test configuration and measured residual stress by Fukumoto et al (1980)

From the lateral buckling test, ultimate strength P_{max} of all beams were reported. Moreover, all results were categorized into three groups with mean and standard deviation. Therefore, validation of FE model is done for each group of the beam and hence FE results are compared with the

corresponding mean value of ultimate strength. It should be mentioned that; results of tension coupon test were presented by histograph with mean values. Therefore, mean values of yield stress and modulus of elasticity of tested member are taken into account in FE model. Also, the measured mean residual stresses are applied as an initial stress in FE model. Table 5.1 lists the mean value of yield stress and modulus of elasticity along with the comparison of FE result and test result.

Table 5.1: Mean values of material properties and comparison of FE result with test result

Section	Length, L (m)	Yield Stress, F_y (MPa)		Modulus of Elasticity, E (GPa)	Ultimate Strength, P_{max} (kN)		% Difference
		Flange	Web		Test Result	FE Result	
I-200×100×5.5×8	2.6	252	287.4	201.7	68.5	61.67	-9.97
	2				87.5	87.81	0.35
	1.5				120	109.8	-8.52

From the above table, it is observed that FE result show sufficient agreement with test result particularly for the 2m length of the I-200×100×5.5×8 section. Also, load-horizontal deflection and load-vertical deflection curves at the mid-span of the beam were also presented for one of the members of each group. Therefore, finding from finite element analysis can also be compared with experimental values which are illustrated in Figure 5.5 to 5.7.

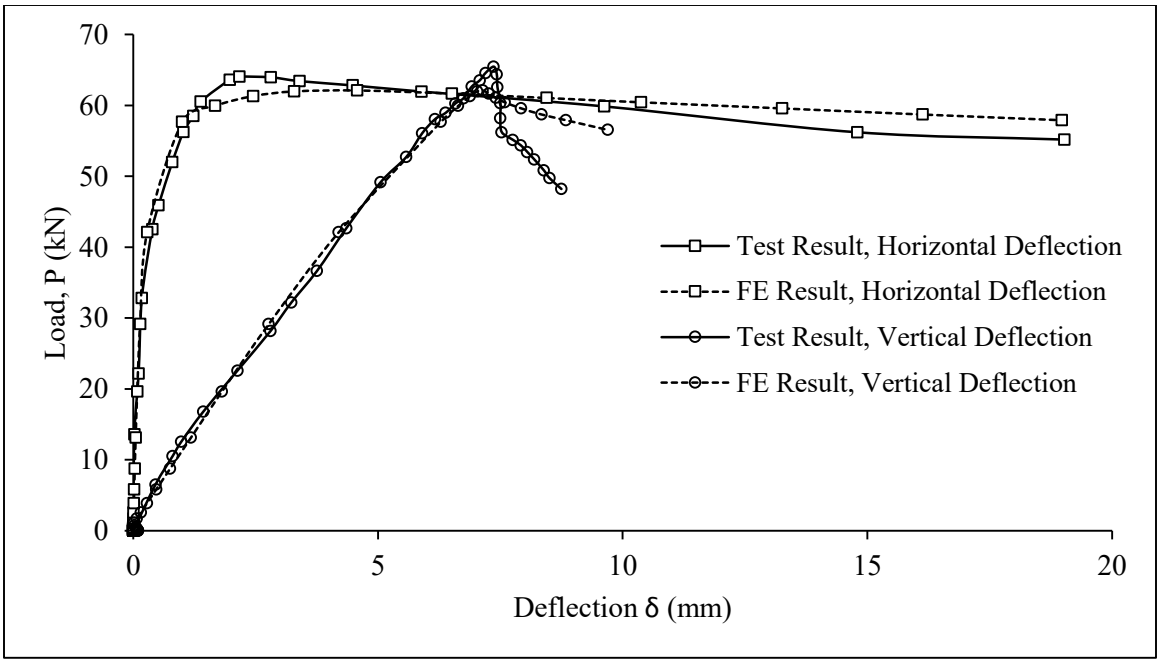

Figure 5.5: Load vs Deflection curve for 2.6 m long beam

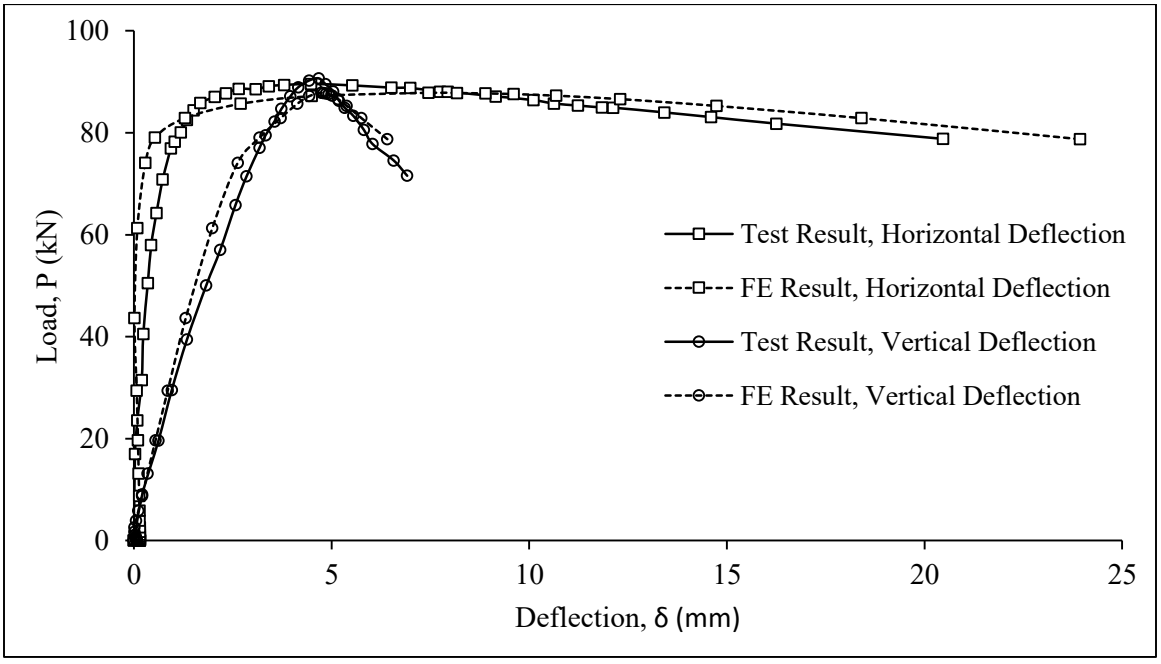

Figure 5.6: Load vs Deflection curve for 2.0 m long beam

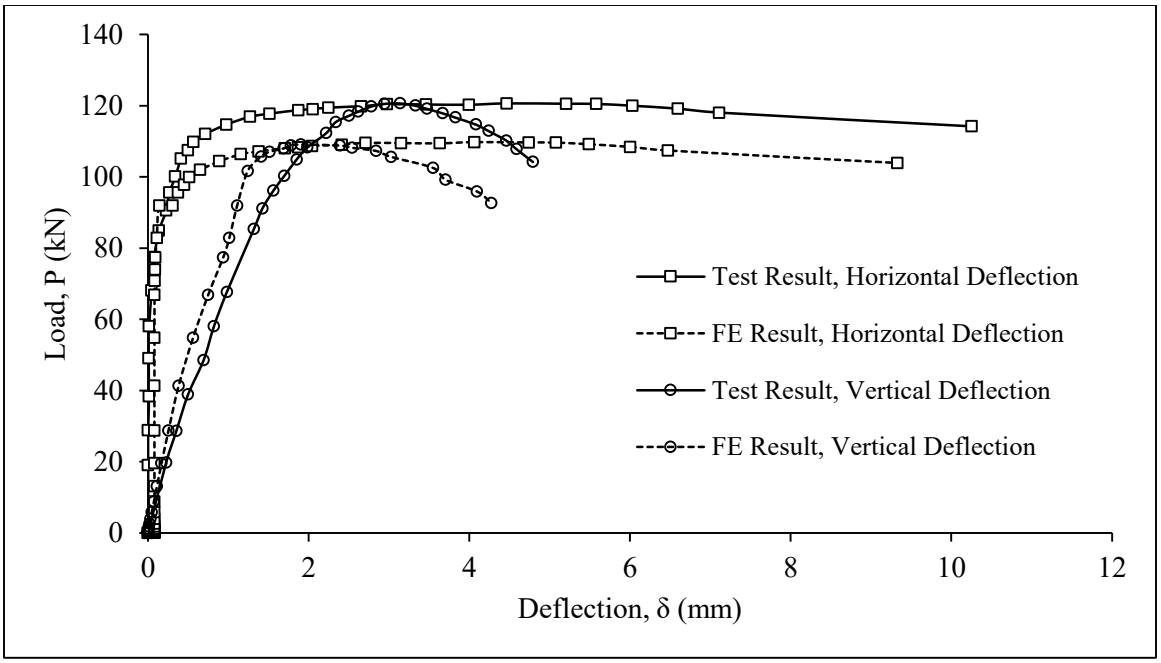

Figure 5.7: Load vs Deflection curve for 1.5 m long beam

It can be observed from above figures that; FE results provide good agreement with test result along the entire path of curve especially for 2.6 m and 2.0 m length of selected beam in both cases of deflection. FE analysis predicts almost equal ultimate strength (i.e. 0.35% difference) in the case of 2.0 m length beam while it under predicts almost 10% of ultimate strength in case of 2.6 m long beam. In spite of some discrepancies with the test result, the initial part of load vs horizontal curve from FE analysis almost matches with test curve in case of 1.5 m length of the beam with an underestimation of 8.52% in ultimate strength.

5.3.2 Fukumoto and Itoh (1981)

Fukumoto and Itoh (1981) performed an experimental investigation on laterally-unsupported welded beams. In this test, thirty-four nominally identical welded I-250×100×6×8 beams with a length of 5.02 m were prepared and two different beams with a span length of 1.8m and 2.6m were cut out from the batch. Thus, in total 68 beams were tested under the same loading and support

configuration as followed by Fukumoto et al (1980). Both tension coupon test and measurement of residual stress were done for each of the 34 members. Mean values of these measurements were reported which were then selected to apply into FE model. Figure 5.8 demonstrates the test setup and mean value of measured value of residual stress.

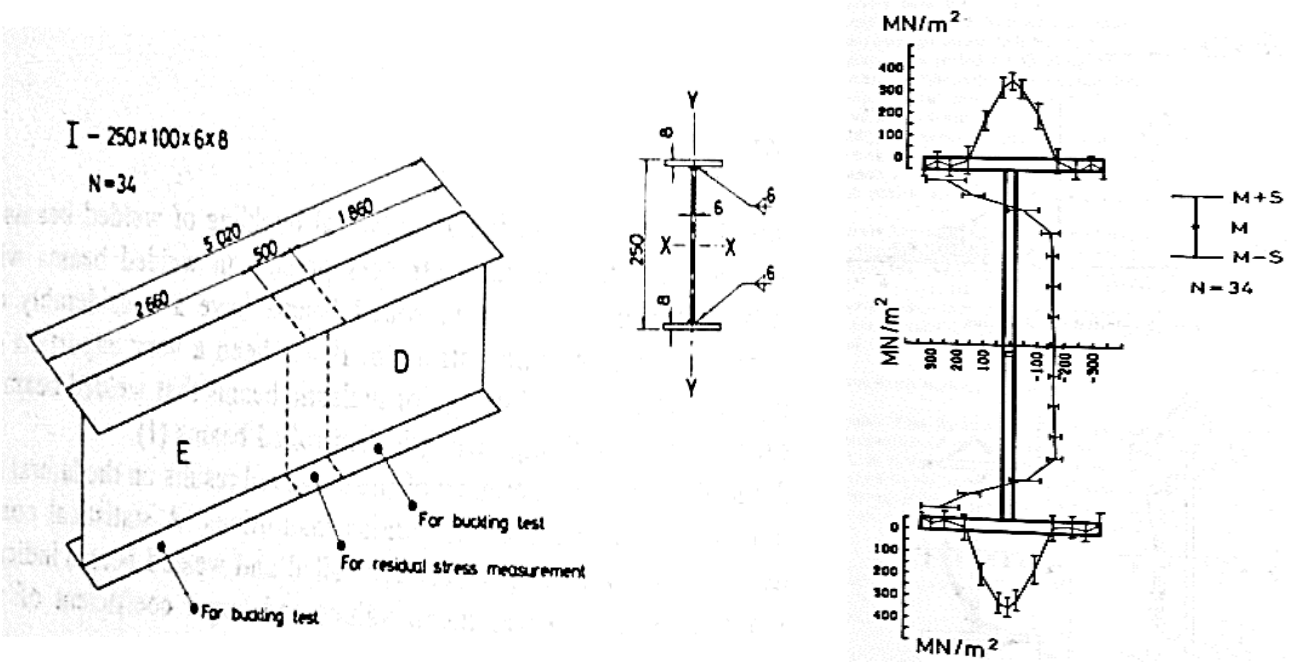

(a) (b)

Figure 5.8: Test configuration and measured residual stress by Fukumoto and Itoh (1981)

The values of ultimate strength P_{max} as found from the experiment for all beams were summarized into two groups with mean and standard deviation. Hence, one FE model is developed for each group of the beam and compared with the corresponding mean value of ultimate strength from the test. Table 5.2 lists the material property and also shows the comparison of FE result with the test. From Table 5.2, it can be gleaned that FE model predicts ultimate strength of beam very closely to experiment in the case of lateral torsional buckling.

Table 5.2: Mean values of material properties and comparison of FE result with test result

Section	Length, L (m)	Yield Stress, F_y (MPa)		Modulus of Elasticity, E (GPa)	Ultimate Strength, P_{max} (kN)		% Difference
		Flange	Web		Test Result	FE Result	
I-250×100×6×8	2.6	292.58	337.23	209.2	88.2	86.65	-1.76
	1.8				149.8	156.74	4.63

5.3.3 Dux and Kitipornchai (1983)

Dux and Kitipornchai (1983) conducted a series of an experiment on the buckling of nine simply supported prismatic beams with three different moment gradient as shown in Figure 5.9. For each configuration, three beams with different lengths are tested. In this study, only case (a) is chosen for the validation of FE model. Table 5.3 shows the dimensions of the test specimen with unbraced length of each beam.

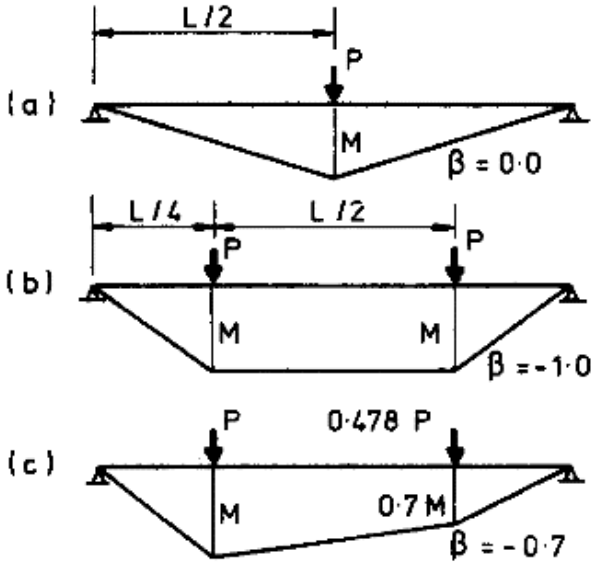

Figure 5.9: Test Loading Configuration

Table 5.3: Dimension of test specimen and measured value of initial out-of- straightness

Length (m)	Top Flange Thickness, T_t (mm)	Bottom Flange Thickness, T_b (mm)	Web Thickness, T_w (mm)	Top Flange Width, B_t (mm)	Bottom Flange Width, B_b (mm)	Depth, D (mm)	Initial out-of-straightness
11	10.57	10.55	6.58	147.34	148.89	256.24	L/10000
9	10.77	10.57	6.82	147.43	147.85	256.35	L/5000
8	10.65	10.53	6.58	148.78	148.28	256.14	L/4000

In total 25 tension coupon test were done, 17 for flanges and 8 for webs to determine the yield stress of selected beams. The mean value of measured yield stress and modulus of elasticity were then reported. In addition, initial bow at the elastic shear center was obtained by measuring the deviation of flange tips from a straight line passing through the two ends of the beam which is listed in Table 5.3. Residual stresses were also measured which has already been discussed in section 4.3.3.3. These experimental measurements are then included into finite element model and the findings are compared with the experimental result which is listed in Table 5.4.

Table 5.4: Mean values of material properties and comparison of FE result with test result

Section	Length, L (m)	Yield Stress, F_y (MPa)		Modulus of Elasticity, E (GPa)	Ultimate Strength, P_{max} (kN)		% Difference
		Flange	Web		Test Result	FE Result	
250UB37	11.0	285	321	209.9	47.1	45.85	2.65
	9.0				62.6	60.53	3.31
	8.0				71.0	67.11	5.48

5.4 Evaluation of CSA Strength Curve for Welded Beams Subjected to Non-Linear Moment Gradient

The aim of this study is to determine the LTB behavior of welded beams subjected to transverse loading. Therefore, same cross-sections as studied earlier are analyzed for two types of non-linear moment gradient i.e. concentrated load applied at mid-span of the beam and uniformly distributed load (UDL) along the length of the beam. In addition, the effect of load height is studied in these cases by changing the position of load at the top flange, centroid and bottom flange. Figure 5.10 illustrates the configuration and position of load.

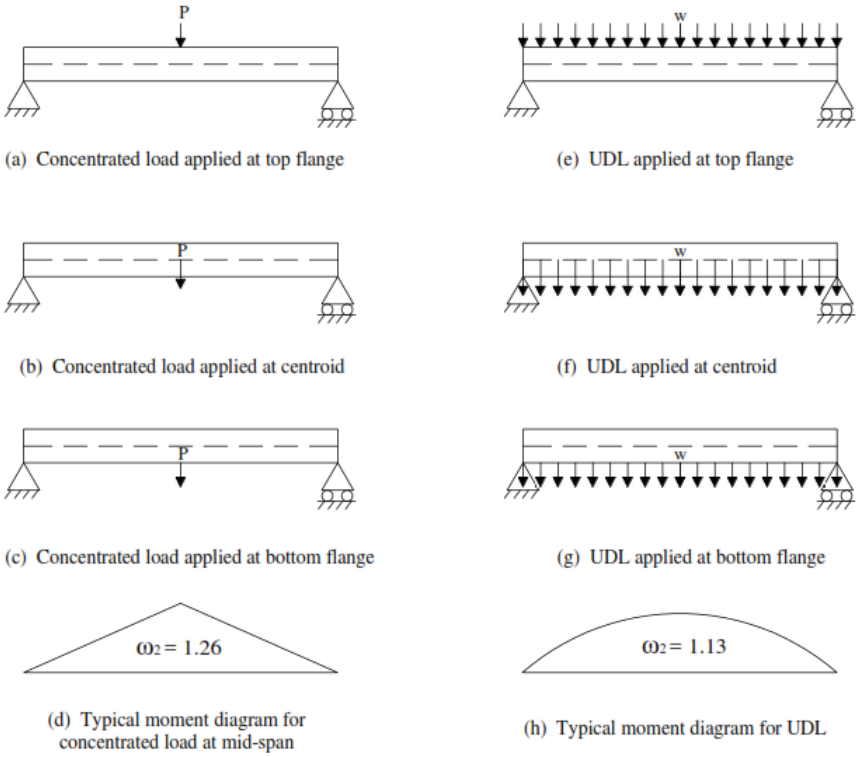

Figure 5.10: Simply supported beam under concentrated load at mid-span and uniformly distributed load acting at (a) (e) top flange, (b) (f) centroid, (c) (g) bottom flange, (d) typical moment diagram for concentrated load and (e) moment diagram for uniformly distributed load

5.4.1 Welded Beams Subjected to Concentrated Load at Mid-Span

Similar to linear moment gradient, all FE simulations are performed considering mill plate type residual stress with an initial imperfection of L/1000 for ten different WWF-shape beams with varying length. All results of FE analysis are then non-dimensionalized as it is done in Chapter 4 and the numerical values of all data points are summarized in APPENDIX B. Thus, CSA strength curve for LTB is plotted along with other strength curves and FE results in Figure 5.11 for concentrated load applied at various height of section which evaluates the performance of current LTB curve and also highlights the effect of load position.

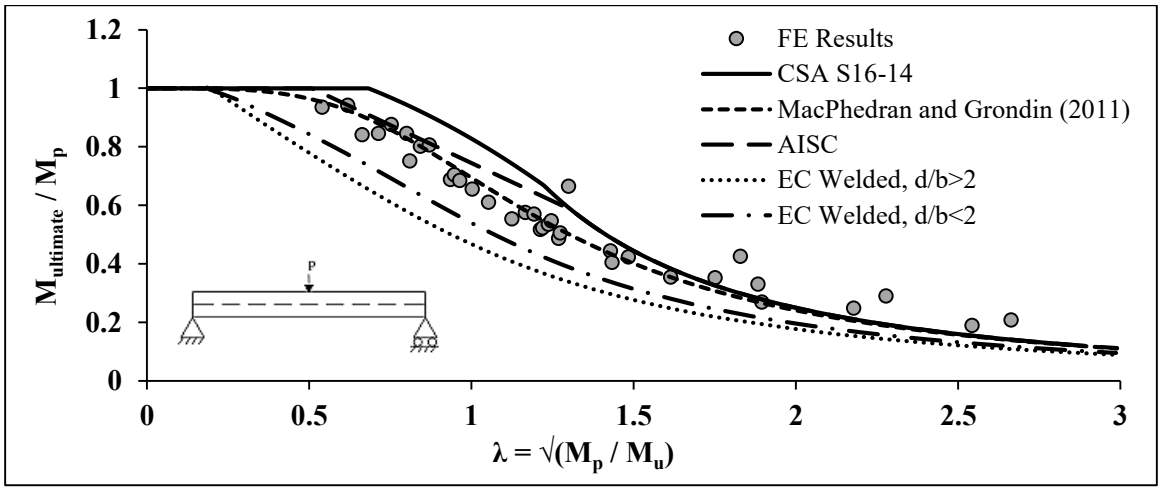

(a)

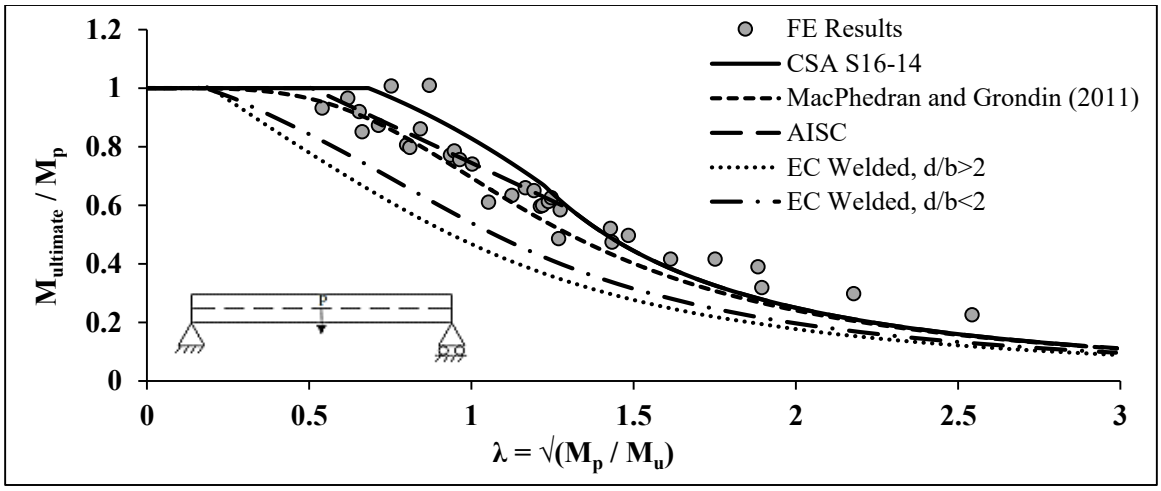

(b)

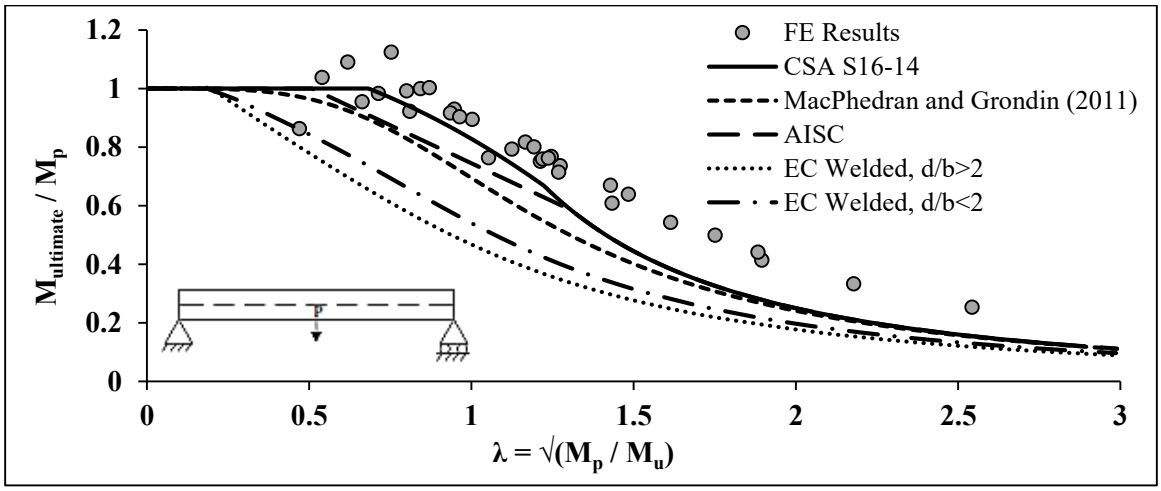

(c)

Figure 5.11: CSA strength curve for LTB and FE results for concentrated load applied at (a) top flange, (b) centroid and (c) bottom flange

From Figure 5.11 (a) to 5.11 (c), the following observations can be made.

1. When the concentrated load is applied to the top flange of the beam, the critical moment decreased and inversely, when it is applied on the bottom face, the critical moment increased.

2. It should also be noted that, in every case, the FE result fall above the strength curve within the elastic range of LTB.
3. Current design equation overestimates slightly in case of concentrated load applied at top flange of welded beams as much as 17 % for WWF 900×417 beam with 18m of unbraced length whereas FE results almost coincide with current strength curve for beams subjected to concentrated load applied at centroid (shear center for doubly symmetric section). Since the current equation is developed considering the position of the load at shear center, it can be said that current design equation is well for the concentrated load. Another positive observation is; it underestimates the LTB capacity of beams for the concentrated load applied at bottom flange as high as 64 % for WWF 1100×234 with 20m of length.
4. It is also significant to note from Figure 5.11 (a) to 5.13 (c) that, in all cases proposed equation by MacPhedran and Grondin underestimates the LTB capacity of welded beams.

5.4.2 Welded Beams Subjected to Uniformly Distributed Load

In this section, FE analysis is performed for distributed load applied at the different position i.e. top flange, centroidal axis (shear center for doubly symmetric section) and bottom flange along the length of the member as shown in Figure 5.10. Similar to previous analysis in this chapter, all FE models are developed using mill plate type residual stress and initial imperfection of L/1000. APPENDIX B summarizes the numerical values of FE results. However, to evaluate the CSA strength curve for this type of load condition, all FE results are non-dimensionalized similar to other analysis. Thus, all data points from FE analysis are plotted along with the CSA strength curve which is developed using the equivalent moment factor, ω_2 for distributed load in Figure 5.12(a) to (c). Since current expression for calculating ω_2 doesn't take account the effect of load height,

all strength curve in Figure 5.12 is same. In addition to this, proposed curve by MacPhedran and Grondin is plotted in these graphs to compare the FE results only.

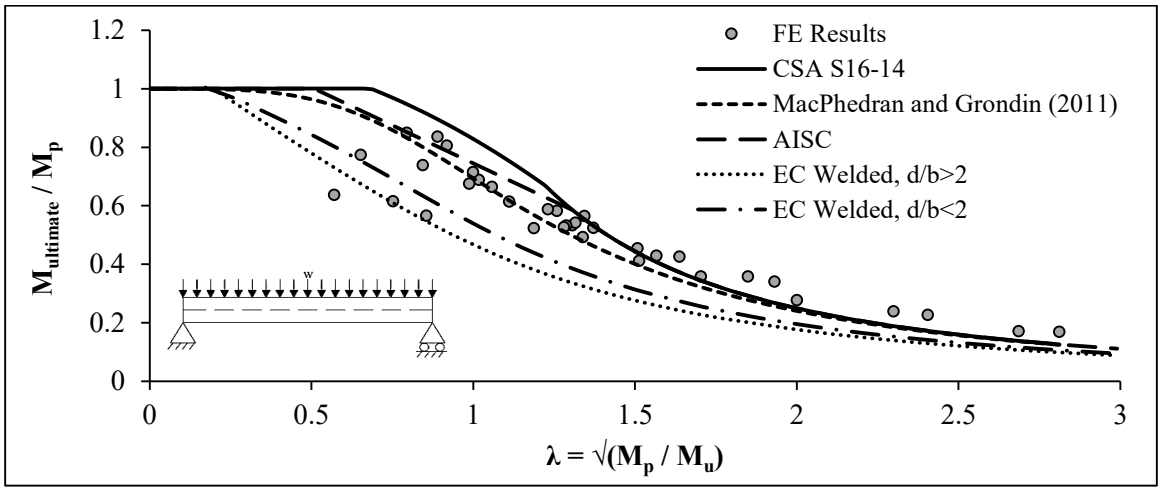

(a)

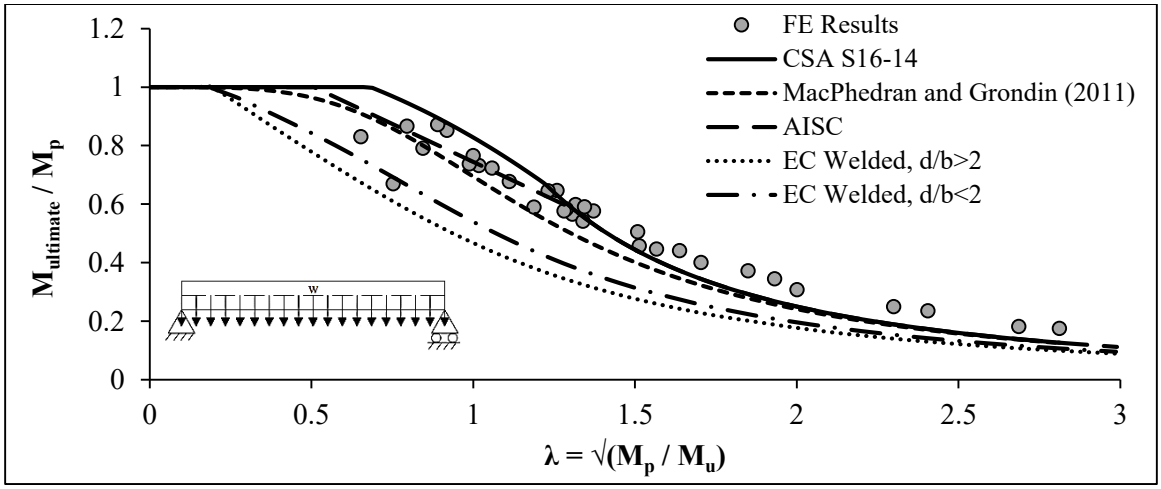

(b)

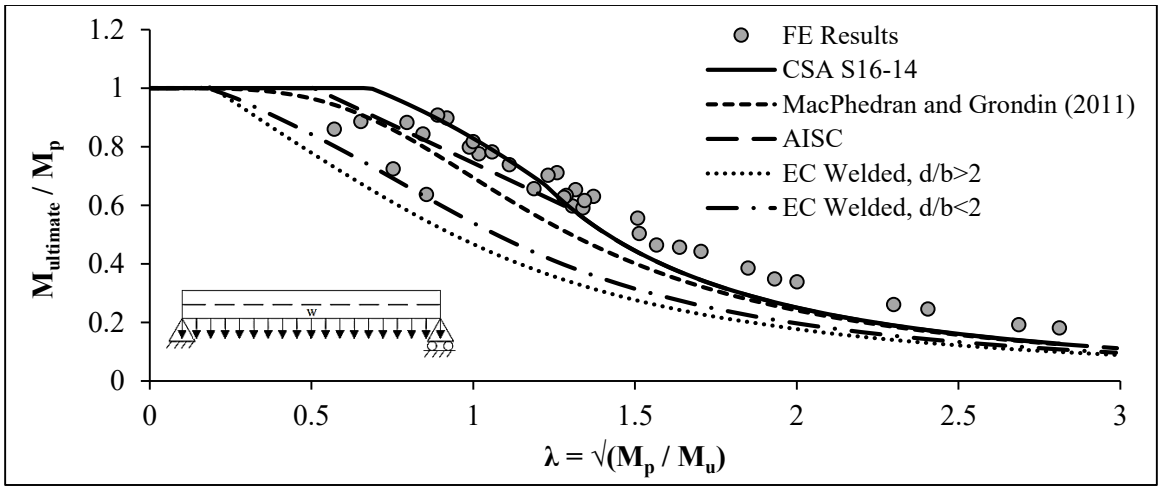

(c)

Figure 5.12: CSA strength curve for LTB and FE results for uniformly distributed load applied at (a) top flange, (b) centroid and (c) bottom flange

From Figure 5.12 (a) to 5.12 (c), the following observations can be made.

1. It is evident that LTB capacity of member increases as the position of distributed load changes from top to bottom flange of a section similar to concentrated load.
2. From results, it is significant to note that, current design specification makes a good prediction in the elastic zone of LTB, especially in the case of distributed load applied at bottom flange as shown Figure 5.12 (c).
3. It is also apparent from the FE analysis that, present LTB resistance curve overestimates within the inelastic region of lateral buckling. This overestimation is more for members with an unbraced length close to its limiting value of length particularly in the case of top flange loading. The maximum discrepancy is found as 33% for WWF 1800×510 with a length of 8m whereas FE result almost matches for distributed load applied at centroidal axis (shear center) of the member. Also, it underestimates the LTB capacity of welded beams for distributed load applied at bottom flange of the member as high as 44 %

considering WWF 1200×263 beam with a length of 20m. So, it can be said that current LTB equation behaves satisfactorily for this type of load condition.

4. It is interesting to note from Figure 5.11 (a) to 5.13 (c) that, in all cases proposed equation by MacPhedran and Grondin underestimates the LTB capacity of welded beams similar to concentrated load.

From the above analyses done for transverse loading condition, it is clear that current approach of predicting LTB capacity by CSA is satisfactory. However, it overestimates inelastic LTB capacity of welded beams, particularly when loads are applied at top flange. Unlike current CSA curve, proposed equation by MacPhedran and Grondin fits very well with the FE results. In addition, the effect of load height is not considered in the current expression for determining ω_2. Therefore, the following section will evaluate the equivalent moment factor, ω_2 for WWF-beams.

5.5 Equivalent moment factor, ω_2 for WWF-beams subjected to moment gradient

CSA S16-14 determines the LTB capacity of a member which is subjected to non-uniform moment gradient by introducing a factor, ω_2 on the resistance equations for a uniform moment. This modifier, ω_2 is known as equivalent moment factor and taken equal to 1.0 for uniform moment gradient. For any other moment gradient, this factor can be calculated by equation 5.1 proposed by Wong and Driver (2010). Equivalent moment factor equation (Equation 5.1) is developed for a wide variety of moment distributions based on the numerical data available in the literature. However, it is significant to note that, referred values which were used for evaluating the proposed equation, are mostly based on rolled beam.

Since, the current equation used in CSA to determine the equivalent moment factor, ω_2 is derived based on elastic buckling solutions, and represents the ratio of the elastic buckling moment under

any moment gradient to the elastic buckling moment under a uniform moment. Therefore, this section addresses the evaluation of equivalent moment factor, ω_2 for welded beams within the elastic range of buckling. Thus, FE results which correspond to elastic buckling solution are considered herein.

5.5.1 Equivalent moment factor, ω_2 for WWF-beams subjected to linear moment gradient

This section evaluates equivalent moment factor, ω_2 based on the FE analysis done for welded beams with various moment gradient as shown in Figure 5.1. Five welded shape beams are chosen for this purpose with an unbraced length of 16m and 18m. All the results from FE analysis and the corresponding calculations of results for various load configuration as shown in Figure 5.1 are presented in Table 5.5. It also lists the comparison of ω_2 values calculated from FE analysis and CSA design equations with mean value and COV. From table 5.5, it is apparent that current Equation 5.1 is un-conservative by 7% and 11% for $\omega_2 = 1.3$ and $\omega_2 = 1.75$ respectively. However, it overestimates only 1.3% for $\omega_2 = 2.3$. Also, the coefficient of variation is satisfactory for this case while the coefficient of variation for $\omega_2 = 1.3$ and $\omega_2 = 1.75$ is found to be as 0.16 and 0.17 respectively. In conclusion, the proposed equation of Wong and Driver (2010) is seemed to be slightly un-conservative for welded beams at least for the load cases considered in this section.

Table 5.5: Equivalent moment gradient, ω_2 for linear moment gradient and comparison with CSA

Section	Length (m)	M^*_{code}	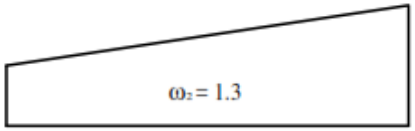				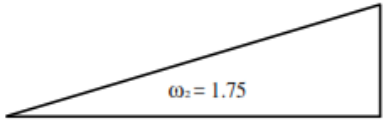				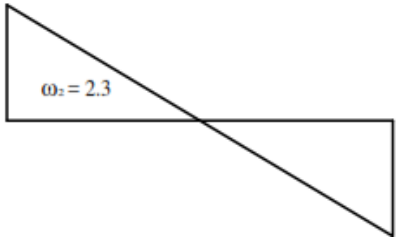			
			M^*_{FE}	Uniform moment factor, ω_2	Mean	Coefficient of variation	M^*_{FE}	Uniform moment factor, ω_2	Mean	Coefficient of variation	M^*_{FE}	Uniform moment factor, ω_2	Mean	Coefficient of variation
WWF 1800x510	16	4826	4525	0.94	1.21	0.16	5964	1.24	1.55	0.17	9611	1.99	2.27	0.09
	18	3922	3581	0.91			4309	1.10			8162	2.08		
WWF 1100x234	16	702	901	1.28			1184	1.69			1706	2.43		
	18	595	818	1.37			1028	1.73			1571	2.64		
WWF 1200x263	16	760	1023	1.35			1348	1.77			1709	2.25		
	18	642	928	1.45			1173	1.83			1463	2.28		
WWF 700x175	16	561	645	1.15			843	1.50			1247	2.22		
	18	484	582	1.20			745	1.54			1098	2.27		

*Units are in kN-m

5.5.2 Equivalent moment factor, ω_2 for WWF-beams subjected to transverse loading

5.5.2.1 Welded Beams Subjected to Concentrated Load at Mid-Span

In this section, equivalent moment factor, ω_2 is calculated for WWF-beams subjected to concentrated load at mid-span. FE results of seven welded beams are selected with different unbraced length and equivalent moment factor is calculated considering the different position of load with respect to shear center i.e. top flange, shear center and bottom as shown in Table 5.6. It also compares the calculated factors in terms of mean and coefficient of variation. In addition to this, modified equivalent moment factor as calculated following the proposed equation [2.26] by Helwig et al. (1997).

From Table 5.6, the following observations can be made.

1. Mean value of ω_2 for top flange loading is only 3% less than that of calculated value by Equation 5.1 whereas it is at least 13% and 28% more in the case of loading at shear center and bottom flange.
2. The COV in all three cases is almost same ranging from 0.12 to 0.15.
3. However, the calculated value is 36% and 13% more than the values as obtained from the recommended expression by Helwig et al. for top flange and shear center loading respectively while being at least 9% less in case of bottom flange loading.

Although, Helwig et al. (1997) provided the expression in order to take account the effect of load position i.e. lower value for top flange loading and higher value for bottom flange loading, but considering the above observations, it is recommended to use the value of $\omega_2 = 1.26$ for concentrated load applied at mid-span (calculated for shear center loading) instead of taking account the extra benefits for bottom flange loading.

Table 5.6: Equivalent moment gradient, ω_2 for concentrated load at mid-span

Section	Length (m)	M_u*	Top Flange		Shear Center		Bottom Flange	
			M_{FEA}*	Uniform Moment Factor, ω_2	M_{FEA}*	Uniform Moment Factor, ω_2	M_{FEA}*	Uniform Moment Factor, ω_2
WWF 1800x510	20	3271	5366	1.64	6344	1.94	6455	1.97
WWF 1800x700	16	11366	13027	1.15	14936	1.31	16730	1.47
	20	7905	10319	1.31	12116	1.53	14026	1.77
WWF 900x347	18	2950	3235	1.10	3559	1.21	4278	1.45
WWF 1100x458	18	5047	5511	1.09	6319	1.25	7201	1.43
WWF 1200x418	18	3483	4423	1.27	5188	1.49	6005	1.72
WWF 700x245	14	1730	1852	1.07	2136	1.23	2424	1.40
	18	1245	1449	1.16	1697	1.36	1961	1.58
WWF 700x175	10	1072	1229	1.15	1422	1.33	1614	1.51
	14	667	862	1.29	1013	1.52	1188	1.78
			Mean	1.22		1.42		1.61
			COV	0.14		0.15		0.12
			Helwig§	0.90		1.26		1.76

*Units are in kN-m

§ Helwig et al. (1997)

5.5.2.2 Welded Beams Subjected to Uniformly Distributed Load

Equivalent moment factor, ω_2 is determined for six WWF-beams for uniformly distributed load applied at different location with respect to shear center i.e. top flange, shear center, bottom flange. The calculated of values of ω_2 for different unbraced length is listed in Table 5.7 along with the mean and coefficient of variation. A comparison between the obtained results and calculated values from Helwig's expression is shown.

Table 5.7: Equivalent moment gradient, ω_2 for uniformly distributed load

Section	Length (m)	M_u*	Top Flange		Shear Center		Bottom Flange	
			M_{FEA}*	Uniform Moment Factor, ω_2	M_{FEA}*	Uniform Moment Factor, ω_2	M_{FEA}*	Uniform Moment Factor, ω_2
WWF 1800x510	16	4827	6218	1.29	6453	1.34	6688	1.39
WWF 1800x700	16	11366	11693	1.03	12398	1.09	13103	1.15
	20	7905	10319	1.31	12173	1.54	14026	1.77
WWF 1100x458	18	5047	5045	1.00	5529.5	1.10	6014	1.19
WWF 1200x418	14	5226	5263	1.01	5780	1.11	6297	1.20
WWF 700x245	14	1730	1695	0.98	1859	1.07	2022	1.17
	18	1245	1326	1.07	1474	1.18	1622	1.30
WWF 700x175	10	1072	1238	1.15	1294	1.21	1350	1.26
	14	667	784	1.18	877	1.31	969	1.45
			Mean	1.11		1.22		1.32
			COV	0.11		0.13		0.15
			Helwig§	0.81		1.13		1.58

*Units are in kN-m

§ Helwig et al. (1997)

The following observations can be made from the Table 5.7:

1. The mean value of ω_2 is found to be only 2% less than the value calculated from equation 5.1 for top flange loading while it is almost as much high as 8% and 17% in the case shear center and bottom flange loading respectively.
2. Almost linear variation of the values of COV is observed ranging from 0.11 to 0.15 for the specified position of loading.
3. The computed ω_2 values from FE analysis are found to be 37% and 8% more comparing with the values as calculated from the proposed equation of Helwig er al. (1997) in the case

of top flange and shear center loading while it is 16% conservative from the proposed equation of Helwig et al. (1997) for the case of bottom flange loading.

Under the consideration of above investigations, it is recommended to use the value of $\omega_2 = 1.13$ in this case without utilizing the benefits for bottom flange loading.

Chapter 6 Conclusions and Recommendations

6.1 Summary

The primary objective of this research was to investigate the lateral torsional buckling behavior of welded wide flange shape beams and asses the performance of current strength equation of CSA S16-14 for LTB. The basis of this study is in the form of a parametric study conducted by a FE model which is able to simulate the realistic beam behavior. The FE model has been validated by the results of three different experimental tests. Summary of the all studies conducted in this research are given below.

1. A detailed finite element was developed considering material and geometric non-linearities. The developed FE model was initially validated for W-shape beams with current CSA S16-14 equations for LTB of W-shape beams.
2. Further in depth validation of FE model was performed against the experimental results of Dibley's (1969) test in Chapter 4.
3. An extensive sensitivity analysis was conducted for ten simply supported WWF-beams of varying unbraced length considering various types of residual stress taken from different experimental measurements. In total, 320 FE models were developed for this analysis and the individual effect of each residual stress pattern was also assessed and presented in Chapter 4.
4. In Chapter 5, the FE model is validated for three more experiments. A detailed parametric study was then performed on ten welded sections subjected to linear and non-linear moment gradient with the severe residual stress pattern as discussed. In total 123 FE model was developed for linear moment gradient while 228 FE model was analyzed for transverse

loading which corresponds two types of non-linear moment gradient. The analyses conducted for transverse loading take account the effect of loading height.

5. The equivalent moment gradient factor was calculated for selected WWF-sections and thus compared with the recommended values by CSA S16-14.

Section 6.2 of this final chapter provides a summary of the key findings and conclusions that can be drawn from this research. The recommendations for future work presented in Section 6.3 include a summary of the other contributing factors that were not considered in this study as well as important aspects that are found to be valuable during this investigation.

6.2 Conclusions

The main findings of this research can be divided into several parts as follows.

Concerning the FE modelling of beam, the following findings can be listed:

- The sensitivity analysis conducted on the initial geometric imperfections confirmed that the final mode of failure of the beam was independent of the imperfection shape and magnitude. However, the ultimate failure load was found sensitive to imperfection shape of 1st eigenmode with varying magnitude. Therefore, the first eigenmode was used to incorporate the initial imperfection in form of a predefined deflected shape with a magnitude of L/1000: recommended tolerance limit of initial out-of-straightness by CSA.
- Typical residual stress pattern as recommended in ECCS Technical Committee 8 (1984) was applied in a W-beam. The residual stress pattern applied in FE model was in non-linear nature and applied values of residual stress satisfactorily resembled with recommended values. This investigation also showed that, it imposes an adverse effect on LTB by reducing the strength of the beam at least 10% using that residual stress pattern.

- The non-linear analysis showed a satisfactory agreement with the code results, fortifying the necessity of including residual stresses in FE model to observe the realistic non-linear behavior of a beam.

The following observations can be made from the validation of FE model:

- The results of FE model presented an excellent correlation with the test results of Dibley (1969). In total, 30 FE model was developed similar to test program and the maximum moment capacity of each member was captured. A maximum of 5% difference was found between test and FE results.
- Validation of FE model with Fukumoto et al. (1980**)** experimental results provided a close agreement while comparing the load-deflection behavior. FE model was capable to predict the ultimate strength of beams very accurately (i.e. 8.52%, 0.35% and 10% difference between FE and test results were obtained in case of 1.5m, 2.0m and 2.6m beams respectively).
- The validation of FE model was also done against the test result of Fukumoto and Itoh (1981) and once again it performed reasonably well. Only 1.76% underestimation was observed considering 2.6m welded beams while 4.63% overestimation was found in case of 1.8m welded beam.
- A maximum of 5.48% underestimation was found while validating the FE model against the test result as obtained by Dux and Kitipornchai (1983) considering a universal beam section of 8.0m length.

The following conclusions can be made from the sensitivity analysis:

- Sensitivity of member capacities due to the presence of welding type residual stress was mostly significant in inelastic LTB region since more difference between FE results and code values was observed in this region of buckling as opposed to elastic region of LTB.
- "Dux and Kiti" type residual stress referred a typical hot rolled type residual stress distribution and obtained FE results using this pattern fitted more close with current code than others. Moreover, in some instances both "Dux & Kiti" and "Fuku & Itoh" type residual stress gave higher member capacities (i.e. WWF-1200×263, WWF-1100×234, WWF-700×175) than the CSA strength curve particularly in the range of elastic LTB.
- Among the three types of welding-type residual stresses, "Fuku & Itoh" type predicted higher member capacities than other two due to the presence of high amount of tensile residual stress along the flanges. Using this pattern up to 38% higher capacities than CSA equation was obtained for WWF-1200×263 at an unbraced length of 18m.
- However, Lehigh pattern which is a common residual stress pattern employed in North America provided the lower resistance throughout the entire analysis. Particularly, mill plate type residual stress gives smallest capacities (i.e. up to 37% lower capacity was obtained for WWF-900×417 beam at an unbraced length of 12m and 15m) while flame cut type residual stress provided larger capacities than mill plate type residual stress but smaller than other two.
- The plastic moment capacity was never achieved from FE analysis considering zero residual stress and a negligible amount of imperfections.

- Eurocode provides lower capacities almost in every instance and unlike the two North American standards, it predicted the member capacities satisfactorily in the inelastic region of LTB especially in the case of mill plate and flame cut type residual stress.

From the parametric study the following findings can be drawn:

- Current CSA S16-14 strength curve overestimated significantly in cases of both $\omega_2 = 1.3$ and $\omega_2 = 1.75$ while it essentially coincided with FE results for cases with $\omega_2 = 2.3$.
- However, the highest difference had been observed within the inelastic region of LTB in cases of $\omega_2 = 1.3$ (40.1%) compared to $\omega_2 = 1.75$ (34.57 %). But, FE results fits more closely to current strength curve within the elastic range for $\omega_2 = 1.3$ than $\omega_2 = 1.75$.
- FE results for $\omega_2 = 2.3$ show sufficiently good agreement with current specification although some discrepancies can be observed within the inelastic region. Most of the cases the plastic capacity of a member has been attained or found very close to code values in local buckling region. In addition, very few FE results are found to lie beneath the strength curve within the elastic zone of buckling.
- Unlike the other codes, Eurocode shows sufficiently good agreement with FE results in all three cases (i.e. closely match with FE result for $\omega_2 = 1.3$, slightly underestimates for $\omega_2 = 1.75$ and highly underestimates for $\omega_2 = 2.3$).

From the parametric study done for transverse loading, the following observations are made:

- Current design equation overestimated slightly in case of concentrated load applied at top flange of welded beams as much as 17 % for WWF 900×417 beam with 18m of unbraced length.

- FE results almost coincided with current strength curve for beams subjected to concentrated load applied at centroid (shear center for doubly symmetric section).
- However, current resistance equation of beams underestimated the LTB capacity of beams in most of the cases considering the concentrated load applied at bottom flange as high as 64 % for WWF 1100×234 with 20m of length.
- Similar to the concentrated load, LTB capacity of member subjected to uniformly distributed load along its length increased as the position of load changed from top to bottom flange.
- It was observed that current LTB resistance curve overestimated within the inelastic region of buckling for uniformly distributed load particularly for members with an unbraced length close to its limiting value of unbraced and subjected to top flange loading (i.e. 33% lower capacity was obtained for WWF 1800×510 with a length of 8m).
- FE result almost matched for distributed loads applied at centroidal axis (shear center) of the member.
- Also, current code equation underestimated the LTB capacity of welded beams for distributed load applied at bottom flange of the member as high as 44 % considering WWF 1200×263 beam with a length of 20m.

From the evaluation of uniform moment gradient factor, the following conclusions can be made:

- Mean value of ω_2 for concentrated load applied at top flange was only 3% less than that of recommended value by CSA S16-14 whereas it was at least 13% and 28% more in the case of loading at shear center and bottom flange respectively.

The COV in all three cases was almost same ranging from 0.12 to 0.15 in the case of concentrated loading applied at various height of a section.

- However, the obtained value of ω_2 was 36% & 13% more than the values calculated from the recommended expression by Helwig et al. (1997) for concentrated load applied at top flange and shear center respectively while being at least 9% less in case of bottom flange loading.
- The mean value of ω_2 was found to be only 2% less in case of uniformly distributed load than the recommended values by CSA S16-14 when the load was applied at top flange. However, it was almost as much high as 8% and 17% in the case shear center and bottom flange loading respectively.

  Almost linear variation of the values of COV is observed ranging from 0.11 to 0.15 for uniformly distributed loading applied at various positions.
- The computed ω_2 values from FE analysis were found to be 37% and 8% more comparing with the values as calculated from the proposed equation of Helwig et. al. (1997) in the case of uniformly distributed load applied at top flange and shear center while it was 16% conservative from the proposed equation of Helwig et al. (1997) for the case of bottom flange loading.

6.3 Recommendations for Future Work

Based on the findings and results obtained during this investigation the following recommendations can be made while designing a WWF-beam subjected to LTB.

- Different combination of residual stress and initial imperfection must be considered in further study.

- A detailed reliability analysis based on the FE results is needed before criticizing of current approach of strength calculation.
- Other contributing factor of LTB i.e. support height, various moment gradient, effective length, stiffener between supports etc. should be taken into consideration in future investigation.

REFERENCES

Abaqus. (2010). "Abaqus standard user's manual, 6.11." Dassault Systèmes.

AISC (2010a). "Specifications for Structural Steel Buildings, ANSI/AISC 360-10", American Institute of Steel Construction, Chicago, IL

Alpsten, G. A. (1972a). "Prediction of thermal residual stresses in hot-rolled plates and shapes of structural steel." 9th IABSE Congress, Final Report, Amsterdam, The Netherlands, pp. 1- 13.

Alpsten, G. A. (1972b)."Residual stresses, yield strength and column strength of hot-rolled and roller-straightened steel shapes." Colloquium on Column Strength, Paris, France, pp. 39-59.

Alpsten, G., and Tall, L. (1970). "Residual stresses in heavy welded shapes." Welding Journal Research Supplement, 49(3), 93s- 105s.

Amin Mohebkhah, and Chegeni, B. (2012). "Local–global interactive buckling of built-up I-beam sections." Thin-Walled Structures, 33-37.

AS 4100. (1998). "Standards Association of Australia", Sydney, Australia.

Baker, K. A. (1984). "Resistance Factors for Laterally Unsupported. " Can. J. Civil Eng., 1008 1019.

Beedle, L. S., and Tall, L. (1960). "Basic column strength. " ASCE Journal of the Structural Division, 86(ST7): 139- 173.

Bjorhovde, R. (1972). "Deterministic and Probabilistic Approaches to the Strength of Steel Columns. " Ph.D. dissertation, Lehigh University, Bethlehem, PA.

Bleich, F. (1952), Buckling Strength of Metal Structures, McGraw-Hill, New York.

Canadian Standards Association, (CSA). (2014). "Limit States Design of Steel Structures." CAN/CSA-S16-14: Toronto, Ontario, Canada.

Chernenko, D. E., and Kennedy, D. J. (1991). "An Analysis of the Performance of Welded Wide Flange Columns." Can. J. Civil Eng., Vol. 18, pp. 537–555.

Cook, R. D. and D. S. Malkus (2002). "Concepts and applications of finite element analysis." Ed. by W. Anderson. John Wiley & Sons Inc.

Dibley, J. E. (1969). "Lateral Torsional Buckling of I-Sections in Grade 55 Steel." Proc. Inst. Civil Eng., 599–627.

Dux, P.F., and Kitipornchai, S. (1983), "Inelastic Beam Buckling Experiments," Journal of Constructional Steel Research, Vol. 3, No. 1, 3-9

ECCS (1984)."Ultimate limit state calculation of sway frames with rigid joints". Technical Committee 8 33, p. 20

Estuar, F. R., and Tall, L. (1963)."Experimental investigation of welded built-up columns." Welding Journal, Research Supplement, 42(4): 164s- 176s.

Eurocode 3. (2005). EN 1993-1-1 Eurocode 3: "Design of steel structures - Part 1–1: general rules and rules for buildings." European Committee for Standardization (CEN), Brussels, Belgium

Fukumoto Y. (1976). "Lateral buckling of welded beams and girders in HT 80 steel." IABSE congress report, 403-408

Fukumoto, Y., and Itoh, Y. (1981)."Statistical Study of Experiments on Welded Beams." Journal of Structural Division, ASCE, 107 (ST1): 89-103

Fukumoto, Y., and Kubo, M. (1977)."An experimental review of lateral buckling of beams and girders." International Colloquium on Stability of Structures Under static and Dynamic Loads, ASCE, 541-562.

Fukumoto, Y., Itoh, Y., and Kubo, M. (1980)."Strength Variation of Laterally Unsupported Beams." Journal of Structural Division, ASCE, 106 (ST1): 165-181.

Galambos, T. (1968)."Structural Members and Frames." Prentice-Hall, Upper Saddle River, N.J.

Greiner, R. and Kaim, P. (2001)."Comparison of LT-Buckling Design Curves with Test Results." ECCS TC 8 Report 23. European Convention for Constructional Steelwork, Brussels, Belgium

Hassan, R. (2013)."Distortional Lateral Torsional Buckling Analysis for Beams of Wide Flange Cross-Sections." M.A.Sc dissertation, Department of Civil Engineering, Faculty of Engineering, University of Ottawa, Canada.

Helwig, T. A., Frank, K. H., and Yura, J. A. (1997)."Lateral-torsional Buckling of Singly Symmetric I -Beams." Journal of Structural Engineering 123(9), 1172-1179.

Hibbitt Karlsson, Sorensen. (2011). "ABAQUS/Standard User's Manual. Version 6.11. " RI: HKS Inc., Pawtucket; 2011.

Kennedy, D.J.L., and Gad Aly, M. (1980). "Limit states design of steel structures-performance factors." Canadian Journal of Civil Engineering, 7(1): 45–77.

Kim, Y.D. (2010). "Behavior and Design of Metal Building Frames Using General Prismatic and Web-Tapered Steel I-Section Members." Doctoral Dissertation, School of Civil and Environmental Engineering, Georgia Institute of Technology, Atlanta, GA.

Kirby, P. A. and D. A. Nethercot (1979). "Design for structural stability. " Ed. by M. R. Horne. Granada Publishing Limited

MacPhedran, I., and Grondin, G. (2011). "A Proposed Simplified Canadian Beam Design. " Can. J. Civ. Eng. 38: 141-143.

McFalls, R. K., and Tall, L. (1969). "A study of welded columns manufactured from flame-cut plates." Welding Journal Research Supplement, 48(4), 141s- 153s.

Nagaraja Rao, N. R., and Tall, L. (1961). " Residual stresses in welded plates." Welding Journal, Research Supplement, 40(10): 468s -480s.

Nagaraja Rao, N. R., Estuar, F. R., and Tall, L. (1964). " Residual stresses in welded shapes." Welding Journal, Research Supplement, 43(7): 294s -306s.

NCCI (2008)."Elastic critical moment for lateral torsional buckling." SN003a-EN-EU. Steel Construction Institute. Berkshire

Nethercot, D. (1974). "Buckling of welded beams and girders." IABSE publications, 107-121.

Nethercot, D. A. and K. C. Rockey (1971). "A unified approach to the elastic lateral buckling of beams". The structural engineer 49, pp. 321–330

Peraza, D. B. (Feb. 2008). Avoiding Structural failures during construction. url: http://www.structuremag.org/article.aspx?articleID=527

Saatcioglu M, Humar J (2003). "Dynamic analysis of buildings for earthquake resistant design." Can J Civ Eng;30:338–59.

Salvadori, M. G. (1955). "Lateral Buckling of I-beams. " American Society of Civil Engineers 120, pp. 1165–1177

Sharifi, S. T. (2015). " Inelastic lateral-torsional buckling capacity of corroded web opening steel beams using artificial neural networks. " The IES Journal Part A: Civil & Structural Engineering, 24-40.

Simulia (2013). "ABAQUS/Standard Version 6.12-1", Simulia, Inc. Providence, RI

Subramanian L. and White D.W. (2015), " Evaluation of Lateral Torsional Buckling Resistance Equations in AISC and AASHTO. " Proceedings of the Annual Stability Conference, Structural Stability Research Council.

Tall, L. (1964b). " Residual stresses in welded plates. " Welding Journal, Research Supplement, 43(1): 10s-23s.

Timoshenko, S. P., and Gere, J. M. (1961). " Theory of Elastic Stability, 2nd ed. " McGraw-Hill, New York

Trahair, N. S. (1993). " Flexural-Torsional buckling of structures. " CRC Press, Boca Raton, FL.

Vlasov, V. Z. (1961). " Thin- Walled Elastic Beams. " Israel Program for Scientific Translations, Jerusalem

Wong, E., and Driver, R.G., (2010). " Critical evaluation of equivalent moment factor procedures for laterally unsupported beams. " Engineering Journal, AISC, 2010(Q1). pp. 1–20

Xiao, Q. (2014, April). " Lateral Torsional Buckling of Wood Beams. " M.A.Sc dissertation, Departments of Civil Engineering, University of Ottawa, Canada

Ziemian, Ronald D., Editor. (2010). " Guide to Stability Design Criterion for Metal Structures." Hoboken, New Jersy: John Wiley & Sons, Inc.

APPENDIX A

Derivation of the Elastic Critical Moment

In figure A.1, a beam is considered to be subjected to arbitrary loads applied in the YZ plane: plane of maximum rigidity. If a small lateral deflection occurs due to this application of load, we can easily find the critical values of the loads by forming the differential equations of equilibrium for that deflected beam. For this purpose, we have to define the fixed coordinate axes X, Y, Z as illustrated in the figure A.1 (Timoshenko et al., 1961).

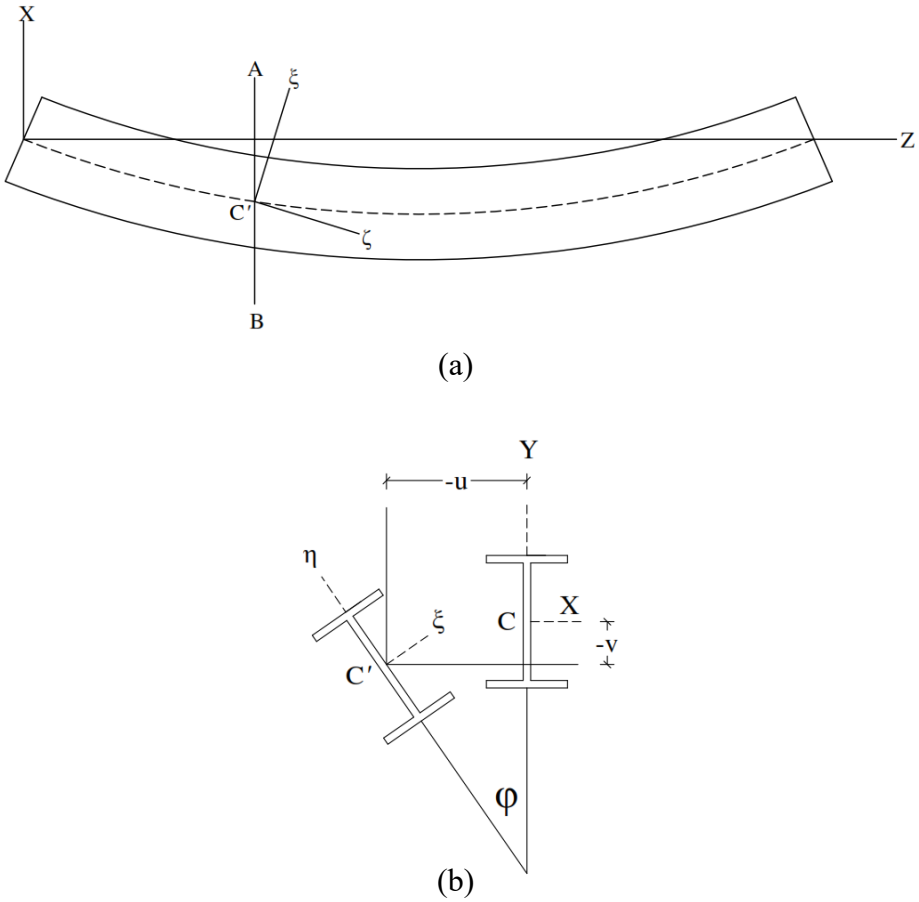

Figure A.1: Beam subjected to arbitrary loads in YZ plane (a) top view (b) section A-B

At any section A-B, the coordinate axes ξ, η, ζ are taken at the centroid of the cross section as shown in figure A.1. The axes ξ and η refer axes of symmetry and considered as principal axes of the cross section, whereas ζ is in the direction of the tangent to the deflected axis of the beam after buckling. The deflection of the beam is defined by the displacement of the centroid of the cross section in X and Y axis which can be represented by u and v respectively and by the angle of rotation Φ of the cross section (Timoshenko et al., 1961).

The right-hand rule is followed while defining the sign of angle. Thus, the angle of rotation Φ is taken positive about the Z axis. The component u and v are taken positive along the direction of corresponding axes. Thus, the displacement u and v of point C in figure A.1 are shown negative. Considering the quantities u, v, Φ very small, the cosines of the angles between coordinate axes X, Y, Z and ξ, η, ζ can be calculated as given in Table A.1 (Timoshenko et al., 1961).

Table A.1: Cosines of angles between axes

Axes	X	Y	Z
ξ	1	Φ	$-\frac{du}{dz}$
η	$-\Phi$	1	$-\frac{dv}{dz}$
ζ	$\frac{du}{dz}$	$\frac{dv}{dz}$	1

Now, the curvatures of the deflected axis of the beam in the ZX and YZ planes can be taken as $\frac{d^2u}{dz^2}$ and $\frac{d^2v}{dz^2}$ respectively, for small deflections. For small angles of twist Φ, the curvatures in the $\xi\zeta$ and $\eta\zeta$ planes can be assumed to have the same values. Thus the differential equations for bending of the beam become:

$$EI_{\xi}\frac{d^2v}{dz^2} = M\xi \qquad [A.1]$$

$$EI_{\eta}\frac{d^2u}{dz^2} = M\eta \qquad [A.2]$$

In these equations I_{ξ} and I_{η} are the moments of inertia of the cross section about the ξ and η axes, respectively whereas M_{ξ} and M_{η} represent the bending moments about the same axes, with assumed positive directions. The equation for twisting of the buckled bar is

$$C\frac{d\Phi}{dz} - C_1\frac{d^3\Phi}{dz^3} = M\zeta \qquad [A.3]$$

where $C = GJ$ is the torsional rigidity and $C_1 = EC_{\omega}$ is the warping rigidity. Equation A.3 is valid for a beam of thin-walled open cross section, such as the I-beam in figure A.1. Equation A.1, A.2 and A.3 represent the three differential equations of equilibrium for the buckled beam.

Now, let us consider an I-beam to be subjected to end moments M_0 as shown in figure A.2. So, the bending and twisting moments at any cross section of this beam can be obtained by taking the components of M_0 about the ξ, η and ζ axes.

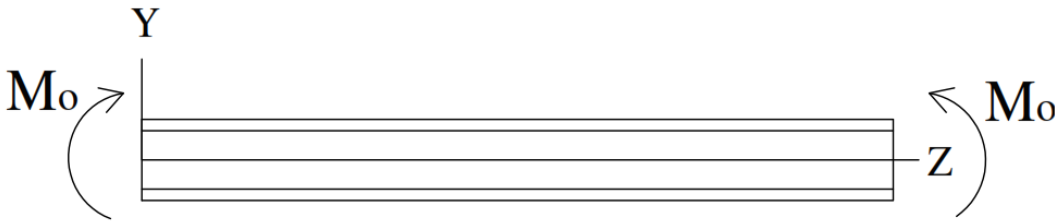

Figure A.2: I-beams subjected to end moments Timoshenko et al., 1961

Thus, using the values given in the first column of table A.1, and also considering the positive directions of the moments, we obtain

$$M_{\xi} = M_o \quad M_{\eta} = \Phi M_o \quad M_{\zeta} = -\frac{du}{dz}M_o \qquad [A.4]$$

Substituting these values into equations A.1, A.2 and A.3, we obtain the following equations for u, v and Φ:

$$EI_{\xi}\frac{d^2v}{dz^2} - M_o = 0 \qquad [A.5]$$

$$EI_{\eta}\frac{d^2u}{dz^2} - \Phi M_o = 0 \qquad [A.6]$$

$$C\frac{d\Phi}{dz} - C_1\frac{d^3\Phi}{dz^3} + \frac{du}{dz}M_o = 0 \qquad [A.7]$$

By differentiating equation A.7 with respect to z, and eliminating $\frac{d^2u}{dz^2}$ and also by combining with equation A.6, we obtain the following equation for the angle of twist Φ (Timoshenko et al., 1961):

$$C_1\frac{d^4\Phi}{dz^4} - C\frac{d^2\Phi}{dz^2} - \frac{{M_0}^2}{EI_{\eta}}\Phi = 0 \qquad [A.8]$$

or

$$\frac{d^4\Phi}{dz^4} - 2\alpha\frac{d^2\Phi}{dz^2} - \beta\Phi = 0 \qquad [A.9]$$

where

$$\alpha = \frac{C}{2C_1} \qquad \beta = \frac{{M_o}^2}{EI_{\eta}C_1} \qquad [A.10]$$

The general solution of equation A.9 is

$$\Phi = A_1 \sin mz + A_2 \cos mz + A_3 e^{nz} + A_4 e^{-nz} \qquad [A.11]$$

in which m and n are positive, real quantities defined by the relations:

$$m = \sqrt{-\alpha + \sqrt{\alpha^2 + \beta}} \quad n = \sqrt{\alpha + \sqrt{\alpha^2 + \beta}} \qquad [A.12]$$

The constants of integration A_1, A_2, A_3 and A_4 must be determined using the end of the beam. Assuming that the ends of the beam cannot rotate about the Z axis, figure A.1, but are free to warp, we find that the conditions at the ends are (Timoshenko et al., 1961):

$$\Phi = \frac{d^2\Phi}{dz^2} = 0 \text{ at } z = 0 \text{ and } z = l \qquad [A.13]$$

From the conditions at z = 0 we conclude that

$$A_2 = 0 \qquad A_3 = -A_4 \tag{A.14}$$

and therefore the angle of twist φ can be represented in the form

$$\Phi = A_1 \sin mz - 2A_4 \sinh nz \tag{A.15}$$

Now using the conditions at $z = l$ we obtain the equations

$$A_1 \sin ml - 2A_4 \sinh nl = 0 \tag{A.16}$$

$$A_1 m^2 \sin ml + 2A_4 n^2 \sinh nl = 0 \tag{A.17}$$

Setting the determinant of these equations equal to zero yields

$$(\sin ml)(n^2 \sinh nl + m^2 \sinh ml) = 0 \tag{A.18}$$

Since m and n are positive nonzero quantities, we conclude that

$$\sin ml = 0 \tag{A.19}$$

and from equations A.16 and A.17 we also obtain $A_4 = 0$. Therefore, the form of buckling is given by the equation A.20 and the beam buckles in the shape of a sine wave (Timoshenko et al., 1961).

$$\Phi = A_1 \sin mz \tag{A.20}$$

The smallest value of m satisfying equation A.19 is

$$m = \frac{\pi}{l} \tag{A.21}$$

or, using the expressions in equation A.12

$$\frac{\pi^2}{l^2} = -\alpha + \sqrt{\alpha^2 + \beta} \tag{A.22}$$

Substituting expressions (A.7, A.9, A.10) and solving for the critical value of the moment M_0 from the last equation, we find

$$M_{cr} = \frac{\pi}{L}\sqrt{EI_\eta C(1 + \frac{C_1}{C}\frac{\pi^2}{L^2})} \tag{A.23}$$

APPENDIX B

FE Results of WWF-beams Subjected to End Moment with $\omega_2 = 1.3$

Section	Length (m)	M_{code} (kN-m)	M_{FE} (kN-m)	%Difference
1800×510	16	6226	4525	-27.32
	20	4221	3581	-15.16
1800×700	8	21945	16182	-26.26
	12	18819	11800	-37.30
1100×234	12	1401	1153	-17.70
	16	906	901	-0.55
	20	664	752	13.25
1200×263	8	3033	2673	-11.88
	12	1531	1410	-7.91
	16	988	892	-9.72
900×417	10	7207	4968	-31.07
	14	6368	3954	-37.91
	18	5474	3279	-40.10
900×347	10	5985	3771	-36.99
	14	4796	2907	-39.39
	18	3806	2382	-37.41
1100×458	6	9485	9302	-1.93
	10	9216	6388	-30.69
	14	7910	4756	-39.87
	18	6465	3951	-38.89
1200×418	6	8960	8013	-10.57
	10	8169	5397	-33.93
	14	6469	3958	-38.82
	18	4493	3124	-30.47
700×245	6	3223	2602	-19.27
	10	2797	1812	-35.22
	14	2215	1404	-36.61
	18	1606	1224	-23.79
700×175	6	2029	1373	-32.33
	10	1383	892	-35.50
	14	861	674	-21.72
	18	625	582	-6.88

FE Results of WWF-beams Subjected to End Moment with $\omega_2 = 1.75$

Section	Length (m)	M_{code} (kN-m)	M_{FE} (kN-m)	%Difference
1800×510	12	12000	7877	-34.36
	16	8446	5964	-29.39
	20	5726	4752	-17.01
1800×700	12	20506	14287	-30.33
	16	17441	11412	-34.57
	20	13835	9316	-32.66
1100×234	8	2145	2245	4.66
	12	1086	1518	39.78
	16	702	984	40.17
1200×263	8	4083	3712	-9.09
	12	2061	2011	-2.43
	16	1330	1362	2.41
900×417	10	7280	6157	-15.43
	14	6895	4982	-27.74
	18	6236	4214	-32.42
900×347	10	5985	4672	-21.94
	14	5345	3734	-30.14
	18	4649	3079	-33.77
1100×458	10	9660	7864	-18.59
	14	8698	6248	-28.17
	18	7634	5131	-32.79
1200×418	10	8730	6759	-22.58
	14	7477	5182	-30.69
	18	6063	4079	-32.72
700×245	10	3036	2297	-24.34
	14	2607	1828	-29.88
	18	2171	1533	-29.39
700×175	6	2159	1739	-19.45
	10	1696	1169	-31.07
	14	1168	904	-22.60
	18	848	745	-12.15

FE Results of WWF-beams Subjected to End Moment with $\omega_2 = 2.3$

Section	Length (m)	M_{code} (kN-m)	M_{FE} (kN-m)	%Difference
1800×510	10	14221	11758	-17.32
	14	11945	9875	-17.33
	18	9020	8162	-9.51
	22	6413	6786	5.82
	26	4895	5641	15.24
	30	3926	4770	21.50
1800×700	14	20514	17510	-14.64
	18	18031	15191	-15.75
	22	15350	13052	-14.97
	26	12239	11404	-6.82
	30	10004	10035	0.31
1100×234	6	4146	3658	-11.77
	10	3141	2727	-13.18
	14	1968	2039	3.61
	18	1368	1571	14.84
	22	1045	1276	22.11
	26	846	1077	27.30
	30	712	1011	41.99
1200×263	8	5367	5309	-1.07
	12	2709	2816	3.95
	16	1748	1919	9.78
900×417	10	7280	6342	-12.88
	14	7248	6729	-7.16
	18	6747	5957	-11.71
	22	6237	5320	-14.70
	26	5729	4786	-16.46
	30	5224	4345	-16.83
900×347	10	5985	5794	-3.19
	14	5713	5214	-8.73
	18	5183	4519	-12.81
	22	4643	3950	-14.93
	26	4103	3487	-15.01
	30	3478	3135	-9.86
1100×458	10	9485	9169	-3.33
	14	9227	8651	-6.24
	18	8416	7508	-10.79
	22	7573	6574	-13.19
	26	6719	5782	-13.95
	30	5745	5168	-10.04

1200×418	10	8960	8826	-1.50
	14	8153	7548	-7.42
	18	7077	6328	-10.58
	22	5924	5330	-10.03
	26	4678	4588	-1.92
	30	3861	4023	4.20
700×245	6	3224	3156	-2.11
	10	3196	3174	-0.69
	14	2870	2631	-8.33
	18	2538	2241	-11.70
	22	2209	1950	-11.72
	26	1834	1726	-5.89
	30	1559	1583	1.54
700×175	6	2191	2243	2.37
	10	1893	1745	-7.82
	14	1513	1355	-10.44
	18	1114	1108	-0.54
	22	876	935	6.74
	26	724	812	12.15
	30	617	722	17.02

FE Results of WWF-beams Subjected to Concentrated Load at Mid Span

Section	Length (m)	M_{code} (kN-m)	FE Analysis Result and Comparidon with CSA S16-14					
			Top Flange	% diff	Centorid	% diff	Bottom Flange	% diff
WWF 1800x510	8	13727	12209	11	12967	6	13492	2
	12	10122	9260	9	10573	-4	11719	-16
	20	4123	5366	-30	6344	-54	6455	-57
WWF 1800x700	8	21945	20509	7	20765	5	20958	4
	12	18666	16697	11	18433	1	19831	-6
	16	14321	13027	9	14936	-4	16730	-17
	20	9961	10319	-4	12116	-22	14026	-41
WWF 1100x234	8	2703	2550	6	2920	-8	3224	-19
	12	1369	1645	-20	1944	-42	2098	-53
	16	885	1157	-31	1392	-57	1397	-58
	20	649	883	-36	1052	-62	1065	-64
WWF 1200x263	8	2942	3539	-20	3619	-23	3645	-24
	12	1485	2264	-52	2295	-55	2326	-57
	16	957	1545	-61	1572	-64	1596	-67
	20	701	1104	-58	1185	-69	1207	-72

WWF 900x417	10	7179	6838	5	7062	2	7158	0
	14	6320	5564	12	6242	1	6678	-6
	18	5405	4474	17	5123	5	5775	-7
WWF 900x347	4	5985		100	4556	24	4556	24
	10	5647	5622	0	5366	5	5936	-5
	14	4747	4058	15	4058	15	4572	4
	18	3718	3235	13	3235	13	4278	-15
WWF 1100x458	6	9485		100	8183	14	8186	14
	10	9175	9225	-1	10619	-16	10664	-16
	14	7839	6901	12	7812	0	8493	-8
	18	6360	5511	13	6319	1	7201	-13
WWF 1200x418	6	8960	9307	-4	9282	-4	9300	-4
	10	8118	8025	1	10049	-24	8990	-11
	14	6378	5731	10	6567	-3	7322	-15
	18	4389	4423	-1	5188	-18	6005	-37
WWF 700x245	6	3224	3373	-5	3460	-7	3516	-9
	10	2775	2522	9	2813	-1	2998	-8
	14	2180	1852	15	2136	2	2424	-11
	18	1568	1449	8	1697	-8	1961	-25
WWF 700x175	6	2018	1951	3	2097	-4	2190	-9
	10	1351	1229	9	1422	-5	1614	-20
	14	841	862	-3	1013	-20	1188	-41
	18	610	655	-7	775	-27	907	-49

FE Results of WWF-beams Subjected to Uniformly Distributed Load

Section	Length (m)	M_{code} (kN-m)	FE Analysis Result and Comparison with CSA S16-14					
			Top Flange	% diff	Centroid	% diff	Bottom Flange	% diff
WWF 1800×510	8	13372	8281	38	8975	33	9317	30
	12	9223	8516	8	9652	-5	10410	-13
	16	5454	6218	-14	6582	-21	6688	-23
WWF 1800×700	8	21771	10782	50	10997	49		100
	12	17910	15095	16	16380	9	17023	5
	16	12844	11693	9	12646	2	13103	-2
	20	8933	9410	-5	9990	-12	10178	-14
WWF 1100×234	8	2424	2276	6	2561	-6	2746	-13
	12	1228	1503	-22	1593	-30	1621	-32
	16	794	1000	-26	1068	-35	1095	-38

	20	582	717	-23	776	-33	805	-38
WWF 1200×263	8	2639	2602	1	2924	-11	3131	-19
	12	1332	1692	-27	1746	-31	1731	-30
	16	859	1124	-31	1194	-39	1218	-42
	20	628	839	-34	888	-41	902	-44
WWF 900×417	10	7041	4477	36	4973	29	5275	25
	14	6084	4912	19	5472	10	5818	4
	18	5064	3807	25	4379	14	4779	6
WWF 900×347	6	5985	3047	49	3479	42	3774	37
	10	5505	4416	20	4828	12	5052	8
	14	4501	3675	18	4130	8	4424	2
	18	3334	2946	12	3305	1	3534	-6
WWF 1100×458	6	9485	4829	49	5666	40	6282	34
	10	8976	8050	10	8377	7	8375	7
	14	7486	6297	16	6997	7	7424	1
	18	5713	5045	12	5640	1	6014	-5
WWF 1200×418	6	8960	5702	36	6838	24	7707	14
	10	7866	7210	8	7782	1	8050	-2
	14	5905	5263	11	5895	0	6297	-7
	18	3936	4071	-3	4617	-17	4982	-27
WWF 700×245	6	3264	2494	24	2728	16	2856	13
	10	2668	2304	14	2518	6	2633	1
	14	1964	1695	14	1896	3	2022	-3
	18	1407	1326	6	1504	-7	1622	-15
WWF 700×175	6	1960	1832	7	1948	1	1989	-1
	10	1211	1238	-2	1320	-9	1350	-11
	14	754	784	-4	894	-19	969	-29
	18	547	608	-11	688	-26	741	-35